To the Graduate Council:

I am submitting herewith a thesis written by Xiaolin Luo entitled "Time-varying Autoregressive Modeling of Nonstationary Signals". I have examined the final electronic copy of this thesis for form and content and recommend that it be accepted in partial fulfillment of the requirements for the degree of Master of Science, with a major in Electrical Engineering.

Mohammed Ferdjallah
Major Professor

We have read this thesis
and recommend its acceptance:

Michael J. Roberts

Seddik M. Djouadi

Accepted for the Council:

Anne Mayhew
Vice Chancellor and
Dean of Graduate Studies

(Original signatures are on the file with official student records.)

TIME-VARYING AUTOREGRESSIVE MODELING OF NONSTATIONARY SIGNALS

A Thesis

Presented for the

Master of Science

Degree

The University of Tennessee, Knoxville

Xiaolin Luo

May, 2005

Copyright © 2005 by Xiaolin Luo
All rights reserved.

ACKNOWLEDGEMENTS

I would like to express my gratitude to all those who helped me complete my Master of Science degree in Electrical Engineering. In particular, I am indebted to my advisor, Dr. Mohammed Ferdjallah, for his guidance and effort in helping me write this thesis. His advices are always very helpful to me, and it has been a great pleasure working with him. I would like to give my sincere thank to Dr. Michael J. Roberts for teaching me the knowledge on the signal and system. I also would like to thank Dr. Seddik M. Djouadi for serving on my committee.

I am very grateful to my dear parents and good friends, whose consistent support give me encouragement to tackle the problems met in my study and life.

ABSTRACT

Nonstationary signal modeling is a research topic of practical interest. In this thesis, we adopt a time-varying (TV) autoregressive (AR) model using the basis function (BF) parameter estimation method for nonstationary process identification and instantaneous frequency (IF) estimation. The current TVAR model in direct form (DF) with the blockwise least-squares and recursive weighted-least-squares BF methods perform equivalently well in signal modeling, but the large estimation error may cause temporary instabilities of the estimated model.

To achieve convenient model stability monitoring and pole tracking, the TVAR model in cascade form (CF) was proposed through the parameterization in terms of TV poles (represented by second order section coefficients, Cartesian coordinates, Polar coordinates), where the time variation of each pole parameter is assumed to be the linear combination of BFs. The nonlinear system equations for the TVAR model in CF are solved iteratively using the Gauss-Newton algorithm. Using the CF, the model stability is easily controlled by constraining the estimated TV poles within the unit circle. The CF model shows similar performance trends to the DF model using the recursive BF method, and the TV pole representation in Cartesian coordinates outperforms all other representations. The individual frequency variation can be finely tracked using the CF model, when several frequency components are present in the signal.

Simulations were carried on synthetic sinusoidal signals with different frequency variations for IF estimation. For the TVAR model in DF (blockwise), the basis dimension (BD) is an important factor on frequency estimation accuracy. For the TVAR model in DF (recursive) and CF (Cartesian), the influences of BD are negligible. The additive white noise in the observed signal degrades the estimation performance, and the the noise effects can be reduce by using higher model order. Experiments were carried on the real electromyography (EMG) data for frequency estimation in the analysis of muscle fatigue. The TVAR modeling methods show equivalent performance to the conventional Fourier transform method.

TABLE OF CONTENTS

CHAPTER I Nonstationary Signal Modeling and Analysis……..……...1

1.1 Introduction……..1

1.2 Nonparametric Approaches…….2

1.3 Parametric Approaches……3

1.4 Motivations for Time-varying AR Model in Cascade Form…….……..5

1.5 Thesis Outline…….…….6

CHAPTER II Time-varying Autoregressive Modeling in Direct Form……..7

2.1 Stochastic Process Modeling……...7

2.1.1 Modeling Essentials……7

2.1.2 Model of Nonstationary Process…….8

2.2 Time-varying AR Model in Direct Form…….……..10

2.2.1 Modeling in Direct Form…….…….10

2.2.2 Time-varying Model Parameterization…….11

2.3 Time-varying AR Parameter Estimation in Direct Form……...11

2.3.1 Prediction Error Identification in Direct Form…….....…….....11

2.3.2 Blockwise Least-Squares Basis Function Method……...…….12

2.3.3 Recursive Weighted-Least-Squares Basis Function Method……....15

2.4 Time-varying Spectrum and Instantaneous Frequency Estimation……...18

2.5 Model Order and Basis Function Selection……...19

2.5.1 Model Order……..19

2.4.2 Basis Function……...19

2.6 Performances of Time-varying AR Model in Direct Form……...……20

2.6.1 Simulations on Synthetic Data……..20

2.6.2 Performance Measures……..20

2.6.2.1 Parameter Estimation Error…….……...20

2.6.2.2 Prediction Gain…….....22

2.6.2.3 Frequency Estimation Error……...22

2.6.2.4 Pole Trajectory……...22
2.6.3 Results and Discussions……23
2.7 Chapter Summary……..30

CHAPTER III Time-varying Autoregressive Modeling in Cascade Form……...32
3.1 Motivations for Cascade Formulation……...32
3.2 Time-varying AR Model in Cascade Form…….....33
3.2.1 Modeling in Cascade Form..…….....33
3.2.2 Time-varying Parameterization in Cascade Form...…….34
3.2.2.1 Parameterization in terms of Time-varying Pole……...…34
3.2.2.2 Parameterization using Second-order Section Representation…..35
3.2.2.3 Parameterization using Cartesian Coordinate Representation…...36
3.2.2.4 Parameterization using Polar Coordinate Representation (r,θ)...36
3.2.2.5 Parameterization using Polar Coordinate Representation (α,β)..37
3.3 Time-varying AR Parameter Estimation in Cascade Form……...38
3.3.1 Prediction Error Identification in Cascade Form…..……38
3.3.2 Error Gradient Generation in Cascade Form……39
3.3.2.1 General Error Gradient Generating Process……..…….....39
3.3.2.2 Error Gradient for Second-order Section Representation……..40
3.3.2.3 Error Gradient for Cartesian Coordinate Representation.....……..41
3.3.2.4 Error Gradient for Polar Coordinate Representation (r,θ)……...42
3.3.2.5 Error Gradient for Polar Coordinate Representation (α,β)……..43
3.3.3 Basis Coefficients Calculation in Cascade Form……..44
3.4 Performances of Time-varying AR Model in Cascade Form…….....46
3.4.1 Test1: Single Pole Pair Case……46
3.4.2 Test2: Double Pole Pairs Case……..51
3.5 Chapter Summary……..55

CHAPTER IV Instantaneous Frequency Estimation via Time-varying Autoregressive Modeling……..56

4.1 Instantaneous Frequency…….56
4.2 Simulations on Sinusoidal Signals with Time-varying Frequencies …….57
4.2.1 Time-varying AR Model for Sinusoidal Signals……..…….57
4.2.2 Instantaneous Frequency Estimates ……...…...59
4.2.3 Effects of Different Basis Functions……..67
4.2.4 Influences of Additive White Noise……..……....72
4.3 Experiments on Electromyography Data……...…….76
4.3.1 Experiment Procedures……..77
4.3.1.1 Data Preprocessing……..77
4.3.1.2 Mean Frequency Estimation……...78
4.3.2 Results and Discussions…….79
4.4 Chapter Summary……...83

CHAPTER V Thesis Summary and Further Research……...85
5.1 Thesis Summary…….……..85
5.2 Further Research……..87

REFERENCES…….89

APPENDIXES……..96

VITA……...104

LIST OF TABLES

Table 4.1: $\overline{FE}$ of the *signal 3* via the TVAR modeling (model order $p = 2$) in direct form (blockwise and recursive) and cascade form (Cartesian) at different signal-to-noise ratios (0,5,10,20dB)……...…..…….74

Table 4.2: $\overline{FE}$ of the *signal 3* via the TVAR modeling (model order $p = 4$) in direct form (blockwise and recursive) and cascade form (Cartesian) at different signal-to-noise ratios (0,5,10,20dB) ……..…….....76

LIST OF FIGURES

Figure 2.1: Stochastic process modeling…..……...8

Figure 2.2: Time-varying AR model in direct form……..10

Figure 2.3: Time-varying linear prediction in direct form……...……..12

Figure 2.4: Power time functions $f_j(n)$ ($j = 0$ to 8)……..……...21

Figure 2.5: The *expected path* of parameter estimates of the TVAR model in direct form using blockwise and recursive basis function methods with basis dimension $q = 4$ …24

Figure 2.6: $\sum_i MSE_{c_i}(n)$ ($i = 1,2$) of the TVAR model in direct form using blockwise and recursive basis function methods with various basis dimensions ($q = 0,2,4,8$) ...25

Figure 2.7: $\overline{PG}$ via the TVAR modeling in direct form using blockwise and recursive basis function methods with various basis dimensions ($q = 0$ to 8)……..……...26

Figure 2.8: The *expected path* of frequency estimates $\bar{f}(n)$ via the TVAR modeling in direct form using blockwise and recursive basis function methods with basis dimension $q = 4$ ……28

Figure 2.9: $\overline{FE}$ via the TVAR modeling in direct form using blockwise and recursive basis function methods with various basis dimensions ($q = 0$ to 8)…….....28

Figure 2.10: The average estimated pole trajectories of the TVAR model in direct form using blockwise and recursive basis function methods with basis dimension $q = 4$ ...29

Figure 2.11: $\overline{N}_{unstable}$ of the TVAR model in direct form using blockwise and recursive basis function methods with various basis dimensions ($q = 0$ to 8) ……...…….30

Figure 3.1: Time-varying AR model in cascade form…….……..34

Figure 3.2: Time-varying linear prediction in cascade form…….……38

Figure 3.3: Error gradient generating process for the time-varying AR model in cascade form……...…40

Figure 3.4: The average estimated pole trajectory of the TVAR model in cascade form using the pole representation in Cartesian coordinate with basis dimension $q = 4$ in test1……...47

Figure 3.5: $\overline{PG}$ via the TVAR modeling in direct form (blockwise and recursive) and cascade form (four forms of pole representation) with various basis dimensions ($q = 0$ to 8) in test 1…..…….....47

Figure 3.6: The *expected path* of parameter estimates of the TVAR model in direct form (blockwise and recursive) and cascade form (Cartesian) with basis dimension $q = 4$ in test1……...49

Figure 3.7: $\overline{FE}$ via the TVAR modeling in direct form (blockwise and recursive) and cascade form (four forms of pole representation) with various basis dimensions ($q = 0$ to 8) in test1……...……50

Figure 3.8: The *expected path* of frequency estimates $\bar{f}(n)$ via the TVAR modeling in direct form (blockwise and recursive) and cascade form (Cartesian) with basis dimension $q = 4$ in test1……...……50

Figure 3.9: The average estimated pole trajectories and expected paths of frequency estimates via the TVAR modeling in direct form (blockwise and recursive) and cascade form (Cartesian) with basis dimension $q = 4$ in test2……..…52

Figure 3.10: $\overline{PG}$ via the TVAR modeling in direct form (blockwise and recursive) and cascade form (four forms of pole representation) with various basis dimensions ($q = 0$ to 8) in test2……...……...…….....53

Figure 4.1: Spectrograms of four sinusoidal signals with time-varying frequencies……60

Figure 4.2: Instantaneous frequency estimates of the *signal 1* via the TVAR modeling in direct form (blockwise and recursive) and cascade form (Cartesian) with various basis dimensions ($q = 1,4,7,10$)……..61

Figure 4.3: Instantaneous frequency estimates of the *signal 2* via the TVAR modeling in direct form (blockwise and recursive) and cascade form (Cartesian) with various basis dimensions ($q = 1,4,7,10$)……..62

Figure 4.4: Instantaneous frequency estimates of the *signal 3* via the TVAR modeling in direct form (blockwise and recursive) and cascade form (Cartesian) with various basis

dimensions ($q = 1,4,7,10$)……..63

Figure 4.5: Instantaneous frequency estimates of the *signal 4* via the TVAR modeling in direct form (blockwise and recursive) and cascade form (Cartesian) with various basis dimensions ($q = 1,4,7,10$)…….....64

Figure 4.6: $\overline{FE}$ of four sinusoidal signals via the TVAR modeling in direct form (blockwise and recursive) and cascade form (Cartesian) with various basis dimensions($q = 0$ to 10)……...66

Figure 4.7: Three types of basis functions ($j = 0$ to 10)...……..……...68

Figure 4.8: $\overline{FE}$ of four sinusoidal signals via the TVAR modeling in direct form (blockwise) using different basis functions with various basis dimensions ($q = 0$ to 10)…….……..……...70

Figure 4.9: $\overline{FE}$ of four sinusoidal signals via the TVAR modeling in cascade form (Cartesian) using different basis functions with various basis dimensions ($q = 0$ to 10)…….. …….....71

Figure 4.10: Instantaneous frequency estimates of the *signal 3* via the TVAR modeling (model order $p = 2$) in direct form (blockwise and recursive) and cascade form (Cartesian) at different signal-to-noise ratios (0,5,10,20dB)…....……..……73

Figure 4.11: Instantaneous frequency estimates of the *signal 3* via the TVAR modeling (model order $p = 4$) in direct form (blockwise and recursive) and cascade form (Cartesian) at different signal-to-noise ratios (0,5,10,20dB)…...…….....75

Figure 4.12: The EMG signal after down sampling and bandpass filtering (20s)…….77

Figure 4.13: Frequency spectrum and instantaneous frequency estimates of the EMG signal in one interval (0.5s)……..…….80

Figure 4.14: Frequency spectrum via Fourier transform and probability distributions of instantaneous frequency estimates via the TVAR modeling in direct form and cascade form over the entire EMG data interval (20s)……...81

Figure 4.15: Time course of the mean frequency estimates via short-time Fourier transform and the TVAR modeling in direct form and cascade form……..….82

LIST OF ABBREVIATIONS

AR	Autoregressive
ARMA	Autoregressive Moving Average
AWN	Additive White Noise
BF	Basis Function
BC	Basis Coefficient
BD	Basis Dimension
CF	Cascade Form
DF	Direct Form
DPSS	Discrete Prolate Spheroidal Sequence
EMG	Electromyography
FE	Frequency Estimation Error
IF	Instantaneous Frequency
LS	Least Squares
PG	Prediction Gain
PSD	Power Spectral Density
MA	Moving Average
MNF	Mean Frequency
MSE	Mean Squared Error
SNR	Signal-to-Noise Ratio
STFT	Short Time Fourier Transform
TF	Time Frequency
TIV	Time Invariant
TV	Time Varying
TVAR	Time Varying Autoregressive
WLS	Weighted Least Squares

CHAPTER I

Nonstationary Signal Modeling and Analysis

1.1 Introduction

Nonstationary signal modeling is a research topic of practical interest, because most temporal signals encountered in real applications, such as speech, biomedical, seismic and radar signals, have time-varying statistics. The problem of time dependency was usually circumvented by assuming local stationarity over a relatively short time interval, in which stationary system identification and analysis techniques are applied. However, this assumption is not always suitable, and methods for nonstationary processes are needed.

Nonstationary signal analysis methods can be categorized into *nonparametric* and *parametric*. The *nonparametric* approaches are based on time-dependent spectral representations, and include the short-time Fourier transform [FG1992], the time-frequency distribution [LC1989], and the evolutionary spectrum [MBP1988]. Due to the *uncertainty principle* [SJO1996], one can not get both high time and frequency resolutions using these *nonparametric* methods. The *parametric* approaches are based on time-varying (TV) linear predictive models, including autoregressive (AR), moving average (MA) and autoregressive moving average (ARMA). As with the time-invariant case, more parsimonious representation of signals and higher resolution of time-frequency spectra can be obtained using *parametric* methods. Moreover, the *parametric* approaches can be used to track relatively fast TV dynamics, which can not be achieved by the *nonparametric* approaches. The model parameters can be estimated using gradient-based adaptive algorithms, Kalman filtering and basis function methods [MN2000].

1.2 Nonparametric Approaches

Presently, three main *nonparametric* approaches, namely the short-time Fourier transform, time-frequency distribution and evolutionary spectrum, are used to analyze the time-dependent spectrum of a nonstationary signal.

The short-time Fourier transform (STFT) [FG1992] is the most common technique for computing a time-varying (TV) spectrum, which is based on the assumption that the signal can be considered stationary in a short time interval. In this approach, the signal is divided into small segments fitting into a sliding window, the Fourier transform of the windowed signal is used to obtain the energy distribution v.s. frequency at a given time corresponding to the center of the window (*spectrogram*). Since the window length affects the time and frequency resolutions in an opposite manner, the joint time-frequency resolutions of the STFT are inherently limited. Specifically, improving the time resolution by using a short window results in a loss of frequency resolution, and vice versa. To alleviate this trade-off problem, the use of TV window was proposed to achieve desired frequency resolution at different times [DT1990].

The time-frequency (TF) distribution [LC1989], which devises a *bilinear distribution* to describe the energy or intensity of a nonstationary signal simultaneously in time and frequency, has been widely used and yields higher TF resolutions than the STFT since the signal is not windowed. The three dimensional TF distribution plot gives a more revealing picture of the temporal localization of a signal's spectral components and enables the analysis of frequency variations with time [FG1992]. Depending on the specific kernel function used for the bilinear transformation, various TF distributions have been proposed. In particular, the Wigner distribution has received more attention as a convenient tool for the analysis of signals with single TF component. However, in the case of signals with several TF components, the *bilinear distribution* suffers from artifacts such as cross-terms, which makes the energy distribution difficult to interpret. Moreover, the positivity of the spectral density is not guaranteed. The cross-term can be reduced by the use of smoothing kernels [HW1989] [YLI1990].

The evolutionary spectrum [MBP1988] was proposed to define a meaningful time-varying (TV) spectrum, which avoids many of the pitfalls of the *bilinear distribution*. In the evolutionary spectral theory, nonstationary signals are represented using sinusoids with slowly varying amplitudes (*oscillatory processes*) and the spectrum is defined on this representation. It assumes that at each frequency the TV amplitudes of a signal can be represented by a set of orthonormal expansion functions, so the time-frequency resolutions can be manipulated by changing the number of expansion functions. Although it is mathematically well grounded, it has suffered from a shortage of estimators. The evolutionary *periodogram* [AAL1994] and the data-adaptive evolutionary spectrum [AAL1995] were proposed to provide better spectral estimates.

1.3 Parametric Approaches

The *parametric* approaches are based on the linear time-varying (TV) model, in which a nonstationary process is represented using an AR, MA or ARMA model with parameters changing with time. The TV spectrum can be estimated from the TV model parameters, and the *instantaneous frequency* [BB11992] of the nonstationary signal can be extracted. In contrast with *nonparametric* approaches, good accuracy in signal representation and high frequency resolution in spectral estimation can be obtained by using *parametric* approaches even for short data sequences. To estimate the TV model parameters, some assumptions need to be made on the time variations, and the adaptive algorithms, Kalman filtering and basis function methods can be used.

When the time evolution of the model parameters is relatively slow, a gradient-based adaptive algorithm, such as steepest decent, least mean squares (LMS) or recursive least squares (RLS) [SH1986], can be used to update the TV parameters based on the local gradient estimation. These adaptive algorithms work reasonably well for slow time variations, but they are sensitive to noise due to the local estimation. The sensitivity may be reduced by increasing the step size, but the convergence rate will be decreased too. If

the TV parameters change relatively fast, compared to the algorithm's convergence speed, the common adaptive algorithms will fail to track the parameter's time evolution.

Identification of fast-varying nonstationary process can be handled successfully only in the case of *structured* nonstationarity, where an *explicit* mathematical description of model parameter variations is adopted. Based on the assumption of *stochastic* or *deterministic* parameter changes, the Kalman filtering [SH1996] or the basis function method [MN2000] can be used correspondingly. Generally, the faster the model parameters change with time, the more detailed should be the *prior* knowledge on their variations to guarantee good estimation results.

Kalman filtering imposes a probabilistic structure on a parameter trajectory and regards it as a *stochastic* process (i.e. random walk). Because of its recursive structure, Kalman filtering allows on-line processing even of huge data sets, which avoid interval-related computations [MWHRC1998]. However, it is not an appropriate model when parameter changes do not fit into a probabilistic structure, and the proper state transition matrix is also difficult to estimate.

The basis function (BF) method assumes that the parameter variations can be approximated by a linear combination of known BFs, which allows relatively fast parameter evolution in a somewhat *deterministic* way, and the estimation is the calculation of those unknown basis coefficients. The BF method was pioneered by Rao [TSR1970] and Liporace [LAL1975]. Previous studies on the BF methods were reported in [FK1977] [MAA1983] [YG1983] [KB1984] [ML1985] [RMGJ1987] and [MN1988], and some current research has been presented in [MG1993] [AL1994] [JP1996] [JFADF1998] [RHK2003]. The parameters can be obtained by either the blockwise processing of all the data at one time or the recursive processing of each datum sequentially [GMJ1986] [MN1987]. Each data block can be of any length, provided that computational complexity and time are not restricted. Various types of BFs can be used, such as power time functions, Fourier series and Legendre polynomials [CD1974],

selecting suitable BFs partially depends on the dynamics of a nonstationary signal and no uniform rule exists. Proper basis dimensions also need to be chosen, which influence the accuracy and robustness of parameter estimates.

1.4 Motivations for Time-varying AR model in Cascade Form

In this study, we concentrate on the time-varying (TV) AR model using the basis function (BF) method to identify a nonstationary process and estimate the instantaneous frequency.

One of the problems with the TVAR model is the possible temporary instability [MAA1983], that is, the TV poles of the estimated model are not guaranteed to remain inside the unit circle on the z-plane. The TV *synthesis* filter, which is obtained from the unstable model, is usually of no practical value as its impulse response becomes excessively large [SJO1996]. To monitor the pole locations, the transfer function denominator of the TV filter in direct form (DF) needs to be factorized using a computationally demanding root-finding algorithm, which is generally impractical for real-time processing. In addition, the parameters of a TVAR model in DF may not provide the most convenient information for some applications, where the TV poles contain the physical information of the system. Moreover, the parameterization of a TVAR model in terms of polynomial coefficients is not a natural representation for the frequency variations over time.

The time-invariant (TIV) filter in cascade form (CF) has been studied in [LS1978] [SL1986] [YPY1987], and the parameterization of the TIV model in terms of poles and zeros has also been explored in [SL1986][AD1990]. Using the CF, the poles or zeros can be estimated directly from the data and the constraints can be easily imposed during the estimation. In order to achieve convenient stability monitoring and better frequency estimation, we propose to formulate the TVAR model in CF through the parameterization in terms of TV poles.

1.5 Thesis Outline

The rest of the thesis is organized as follows. Chapter II provides a review on the current time-varying (TV) AR model in direct form using the blockwise and recursive basis function parameter estimation methods and demonstrates their performances through simulations on synthetic data. Chapter III presents the proposed TVAR model in cascade form, with different forms of TV pole representation, using the BF method. Performances of the TVAR model in cascade form are evaluated via simulations on synthetic data and compared with those of the TVAR model in direct form. Chapter IV explores the performance characteristics of the instantaneous frequency estimation via the TVAR modeling in direct form and cascade form through simulations on synthetic sinusoidal signals with different frequency variations. Experiments are also carried on real surface electromyography (EMG) data for frequency estimation in the analysis of muscle fatigue. Chapter V summaries the work in this thesis and provides suggestions for further research.

CHAPTER II

Time-varying Autoregressive Modeling in Direct Form

In this chapter, the stochastic process modeling is described firstly. Then, the time-varying (TV) AR model in direct form using blockwise and recursive basis function parameter estimation methods are briefly reviewed. Finally, the performance characteristics of TVAR modeling in direct form are illustrated via simulations on synthetic data.

2.1 Stochastic Process Modeling

2.1.1 Modeling Essentials

Wold's decomposition theorem [SH1996] states that any stationary discrete-time stochastic process can be decomposed into the sum of a *linear predictable process* and a *general linear process* $x(n) = x_p(n) + x_g(n)$, with the two components uncorrelated with each other. The first component $x_p(n)$ is *deterministic*, which can be calculated from infinitely many of its previous values $x_p(n) = -\sum_{i=1}^{\infty} c_i x_p(n-i)$ with zero prediction variance. The second component $x_g(n)$ is *nondeterministic*, which can be estimated as $x_g(n) = \sum_{i=0}^{\infty} h_i v(n-i)$, where $h_0 = 1, \sum_{i=0}^{\infty} h_i^2 < \infty$ and $v(n)$ denotes a white noise sequence.

According to the *Wold's decomposition*, any wide-sense stationary process $\{x(n)\}$ can be regarded as a result of passing a series of statistically independent random inputs $\{v(n)\}$, such as white Gaussian noise, through a linear causal time-invariant filter with $H(z) = \sum_{i=0}^{\infty} h_i z^{-i}$, where $\sum_{i=0}^{\infty} h_i^2 < \infty$ [SH1996], as shown in Figure 2.1. Here, $v(n)$ is an innate part of the model, and gives rise to the random nature of the observed process.

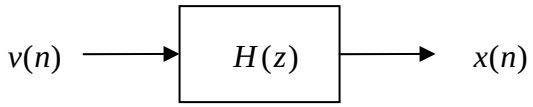

Figure 2.1: Stochastic process modeling.

The filter postulated by the *Wold's decomposition* is characterized using infinitely many coefficients, which is not suitable for practical system modeling. The parsimonious representation of a stochastic model may be expressed as [SH1996]

$$x(n) + \sum_{i=1}^{N_a} a_i x(n-i) = v(n) + \sum_{j=1}^{N_b} b_j v(n-j) \tag{2.1}$$

where a_i and b_j are time-invariant model parameters. According to the manner in which the linear combinations indicated in (2.1) are formulated, three types of linear stochastic models can be categorized as follows [SH1996]:

- AR: no past values of the model input are used ($b_j = 0, 1 \le j \le N_b$).
- MA: no past values of the model output are used ($a_i = 0, 1 \le i \le N_a$).
- ARMA: both past values of the model input and output are used ($a_i \ne 0, b_j \ne 0$).

In system identification, the presence of poles in an AR or ARMA model can give better performance than an MA model, but the main drawback is the possible instability. In addition, an AR model is more popular than an MA or ARMA model for computational reasons. Specifically, the computation of the AR parameters involves a set of linear equations, while the computation of the MA and ARMA parameters require solving sets of nonlinear equations and are thus more complicated.

2.1.2 Model of Nonstationary Process

A nonstationary stochastic process has the probability distribution that is not time shift invariant. A practical nonstationary process comprises signals with time-varying (TV) mean $\mathrm{E}[x(n)] = m_x(n)$ and/or TV covariance $\mathrm{E}[(x(n) - m_x(n))(x(n-i) - m_x(n-i))] = r_x(n,i)$. In practice, the TV mean can be

eliminated from the signals by subtracting the local average. Here, we concentrate on zero-mean nonstationary covariance processes.

Similar to the stationary case, the *Cramer-Wold's decomposition* [HC1961] states that a purely nondeterministic second-order, zero-mean nonstationary covariance process $\{x(n)\}$ possesses a one-sided linear representation

$$x(n) = \sum_{i=0}^{\infty} h_i(n) v(n-i)\,, \tag{2.2}$$

where $v(n)$ denotes white noise and $\sum_{i=0}^{\infty} h_i^2(n) < \infty\,,\ \forall n$.

According to (2.2), the nonstationary process can be viewed as a result of passing white noise through a causal filter with the time-varying (TV) transfer function $H(n,z) = \sum_{i=0}^{\infty} h_i(n) z^{-i}$. Since the noise shaping filter is characterized in terms of infinitely many impulse response coefficients, the *Cramer-Wold's decomposition* can not be used for practical modeling. Similar to the stationary case, one can obtain a finite-order stochastic model for a nonstationary process as [MN2000]

$$x(n) + \sum_{i=1}^{N_a} a_i(n) x(n-i) = v(n) + \sum_{j=1}^{N_b} b_j(n) v(n-j)\,, \tag{2.3}$$

where $a_i(n)$ and $b_j(n)$ are the TV model parameters. The corresponding TV system transfer function in direct form can be represented as

$$H(n,z) = \frac{1 + \sum_{j=1}^{N_b} b_j(n) z^{-j}}{1 + \sum_{i=1}^{N_a} a_i(n) z^{-i}}\ . \tag{2.4}$$

A general framework of modeling nonstationary signals through time-dependent ARMA model has been presented in [YG1983].

2.2 Time-varying AR Model in Direct Form

Considering the advantages and simplicity of the AR model, the time-varying (TV) AR model is adopted for the nonstationary signal modeling and analysis in our study.

2.2.1 Modeling in Direct Form

The nonstationary process $x(n)$ can be represented by a TVAR model as (shown in Figure 2.2)

$$x(n) = -\sum_{i=1}^{p} c_i(n)x(n-i) + v(n)\,, \tag{2.5}$$

where $c_i(n)$ are the TVAR model parameters, p is the model order and $v(n)$ is the input white Gaussian noise with zero mean and variance σ_v^2.

The signal generating system, can be considered as a linear all-pole time-varying filter with the transfer function in direct form

$$H(n,z) = \frac{1}{1+\sum_{i=1}^{p} c_i(n)z^{-i}} = \frac{1}{P(n,z)}\,. \tag{2.6}$$

It is assumed that $H(n,z)$ has all the poles within the unit circle on the z-plane, which guarantees it is a stable filter. Without this assumption, $x(n)$ given by (2.5) will not be a valid description of the signal [MN2000].

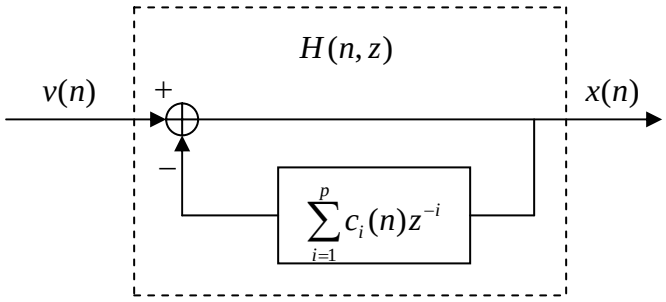

Figure 2.2: Time-varying AR model in direct form.

2.2.2 Time-varying Model Parameterization

If arbitrary variations in the TVAR model parameters are allowed, then the system identification will become an ill-posed problem, so appropriate assumptions on the nature of time variations are essential. Using basis function methods, the model parameters are constrained to a subspace spanned by a set of time functions.

The parameters of the TVAR model in direct form are formed as

$$c_i(n) = \sum_{j=0}^{q} c_{ij} f_j(n),\ 1 \le i \le p,\ n = 1,...,N\ , \tag{2.7}$$

where $\{f_j(n), 0 \le j \le q\}$ is a set of linearly independent basis functions (BFs) defined on the *analysis interval* $[1,...,N]$, q is the basis dimension and $\{c_{ij}\}$ is a set of $p(q+1)$ basis coefficients. Without a loss of generality, it is assumed that $f_0(n) = 1$, which accounts for the stationary portion of model parameters. The projection of the nonstationary signals onto the BFs allows a transformation of the TV parameters into a subspace, where they can be represented by the time-invariant basis coefficients. In this way, the estimation of TV parameters converts to the estimation of time-invariant basis coefficients. A wide variety of parameter variations can be approximated by using suitable BFs with proper basis dimensions.

2.3 Time-varying AR Parameter Estimation in Direct Form

2.3.1 Prediction Error Identification in Direct Form

The time-varying (TV) AR process can also be considered as the TV linear prediction in direct form, as shown in Figure 2.3. The TV linear predictor is given as

$$\hat{x}(n) = -\sum_{i=1}^{p} c_i(n) x(n-i), \tag{2.8}$$

and the prediction error is defined as

$$\varepsilon(n) = x(n) - \hat{x}(n). \tag{2.9}$$

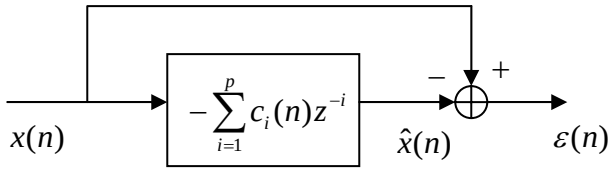

Figure 2.3: Time-varying linear prediction in direct form.

The parameter estimation can be obtained through the minimization of the squared prediction error using two basis function (BF) methods. One is the blockwise least-squares (LS) BF method [MAA1983], in which the parameter estimation is performed over a block of data at one time. The other is the recursive weighted-least-squares (WLS) BF method [MN1987], in which the parameter estimation is updated through the processing upon each datum sequentially.

2.3.2 Blockwise Least-Squares Basis Function Method

For the blockwise least-squares processing, the criterion of optimality is the minimization of the squared prediction error in the whole block

$$\begin{aligned} \xi &= \sum_n \varepsilon^2(n) \\ &= \sum_n \left(x(n) + \sum_{i=1}^{p} c_i(n) x(n-i) \right)^2 \\ &= \sum_n \left(x(n) + \sum_{i=1}^{p} \sum_{j=0}^{q} c_{ij} f_j(n) x(n-i) \right)^2 \end{aligned} \quad , \tag{2.10}$$

where different limits of summation over n yields two estimation methods [MAA1983], namely the *covariance* method with the squared error summed only over those signal samples that can be predicted from the past p samples and the *autocorrelation* method with the error summed over the entire time interval. Only the *covariance* method is used here, since it yields better performance than the *autocorrelation* method [MAA1983].

The total squared error is minimized with respect to each basis coefficient

$$\frac{\partial \xi}{\partial c_{kl}} = 2\sum_{n=p+1}^{N} \varepsilon(n)\frac{\partial \varepsilon(n)}{\partial c_{kl}} = 2\sum_{n=p+1}^{N}\left(x(n) + \sum_{i=1}^{p}\sum_{j=0}^{q} c_{ij} f_j(n)x(n-i)\right) f_l(n)x(n-k) = 0 \quad \begin{matrix} 1 \le k \le p \\ 0 \le l \le q \end{matrix}, \tag{2.11}$$

where i and k are the indices of time delay, and j and l are the indices of basis functions. Since the squared error ξ is a quadratic form of basis coefficients $\{c_{ij}\}$, the minimization will lead to a set of linear system equations for solving basis coefficients.

Rearranging (2.11) and changing the order of summation, the system equations become

$$\sum_{i=1}^{p}\sum_{j=0}^{q} c_{ij}\sum_{n=p+1}^{N} f_j(n) f_l(n)x(n-i)x(n-k) = -\sum_{n=p+1}^{N} f_l(n)x(n)x(n-k), \tag{2.12}$$

where the cross-correlation function is defined as

$$\phi_{lj}(k,i) = \sum_{n=p+1}^{N} f_j(n) f_l(n)x(n-i)x(n-k), \tag{2.13}$$

which has the symmetric property with $\phi_{lj}(k,i) = \phi_{jl}(k,i) = \phi_{lj}(i,k) = \phi_{jl}(i,k)$.

Using the definition in (2.13), the system equations (2.12) can be written as

$$\sum_{i=1}^{p}\sum_{j=0}^{q} c_{ij}\phi_{lj}(k,i) = -\phi_{l0}(k,0), \quad \begin{matrix} 1 \le k \le p \\ 0 \le l \le q \end{matrix}, \tag{2.14}$$

and the basis coefficients $\{c_{ij}\}$ are calculated by solving the $p(q+1)$ linear equations.

To solve the equations in (2.14) in a systematic manner, a certain ordering for the basis coefficients need to be established. The basis coefficient vectors are defined as

$$C_i = \lfloor c_{i0} . \quad . \quad . c_{iq} \rfloor, \quad 1 \le i \le p, \tag{2.15a}$$

$$C = \left[C_1, . \quad . \quad ., C_p\right]^T = \left[c_{10} . \quad . c_{1q}, . \quad . \quad ., c_{p0,} . \quad ., c_{pq}\right]^T. \tag{2.15b}$$

The cross-correlation vectors are defined as

$$r_k = \lfloor \phi_{00}(k,0), . \quad . \quad ., \phi_{q0}(k,0) \rfloor, \quad 1 \le k \le p, \tag{2.16a}$$

$$r = \left[r_1, \ldots, r_p\right]^T = \left[\phi_{00}(1,0), \ldots, \phi_{q0}(1,0), \ldots, \phi_{00}(p,0), \ldots, \phi_{q0}(p,0)\right]. \tag{2.16b}$$

Following the above ordering, the covariance matrix Φ_{ki} is defined as

$$\Phi_{ki} = \begin{bmatrix} \phi_{00}(k,i) & \cdots & \phi_{0q}(k,i) \\ \vdots & & \vdots \\ \phi_{q0}(k,i) & \cdots & \phi_{qq}(k,i) \end{bmatrix}, \; 1 \le i,k \le p, \tag{2.17a}$$

where $\Phi_{ki} = \Phi_{ik} = \Phi_{ki}^T$. The block covariance matrix R is defined as

$$R = \begin{bmatrix} \Phi_{11} & \cdots & \Phi_{1p} \\ \vdots & & \vdots \\ \Phi_{p1} & \cdots & \Phi_{pp} \end{bmatrix}, \tag{2.17b}$$

where R is a $p \times p$ block symmetric matrix with $(q+1) \times (q+1)$ symmetric blocks.

Using the equations (2.15) to (2.17), the system equations (2.14) can be finally written in the matrix form as

$$RC = -r. \tag{2.18}$$

The computational complexity of the blockwise least-squares basis function method depends on the model order and basis dimension. Most of the computational effort is involved with calculating the elements of the covariance matrix R and cross-correlation vector r. The symmetric property of R can be utilized to reduce the number of elements to be calculated, and many elements can be calculated recursively from previously computed elements [MAA1983].

The direct or iterative method can be used to solve the system matrix equation (2.18) for the basis coefficients. The direct method, such as Gaussian elimination, orthogonal-triangular decomposition (QR) and singular value decomposition (SVD) [SH1996],

involves a finite number of calculation steps before the solutions are obtained. The iterative method, as in [LAL1975], [MBTA1977] and [LM1985], calculates a sequence of approximations to the solution without inverting the covariance matrix, and the iteration can be stopped whenever a desired accuracy is achieved or a number of iteration steps are completed.

2.3.3 Recursive Weighted-Least-Squares Basis Function Method

To achieve on-line tracking, the recursive weighted-least-squares (WLS) basis function (BF) method can be used, which is regarded as a combination of the common WLS with the BF method [MN1987]. It has the parameter *matching* ability due to additional degrees of freedom offered by the BFs and the parameter *tracking* ability due to the adaptive nature offered by the recursive WLS. When the BF set consists of just one constant function $f_0(n) = 1$, the WLS BF method reduces to the common WLS. The greater versatility of the WLS BF estimator is achieved at the cost of the moderately increased computational complexity.

Following the derivations in [MN2000], the observation vector $X_n = \left[x(n) f_0(n),..., x(n) f_q(n)\right]^T$ is defined by projecting the $x(n)$ into the subspace spanned by the basis functions, and the generalized regression vector is denoted as $Y_{n-1}^T = \left[X_{n-1}^T,..., X_{n-p}^T\right]$. The time-varying (TV) AR model of order p can be represented by a time-invariant AR model of order $p(q+1)$ as

$$x(n) = -Y_{n-1}^T C_{n-1} + v(n), \tag{2.19}$$

where $C_{n-1} = \left[c_{10}. \quad .c_{1q},. \quad . \quad .,c_{p0,}. \quad .,c_{pq}\right]_{n-1}^T$ is the basis coefficients estimate at the time instant $n-1$.

The corresponding TV linear predictor equation is given as [MN2000]

$$\hat{x}(n) = -Y_{n-1}^T C_{n-1}, \tag{2.20}$$

and the prediction error for the time instant n is denoted as ε_n.

The weighted squared prediction error given the observations up to the time instant n is defined as

$$\xi_n = \sum_{i=0}^{n} \lambda^{n-i} \varepsilon_i^2 = \sum_{i=0}^{n} \lambda^{n-i} \left[x(i) + Y_{i-1}^T C_n \right]^2 , \tag{2.21}$$

where $0 << \lambda < 1$ is called the *forgetting factor*, which is used to localize the estimation, namely to make the estimation less sensitive to the observations of the distant past.

The weighted error is minimized with respect to the basis coefficients

$$\frac{\partial \xi_n}{\partial C_n} = 2 \sum_{i=0}^{n} \lambda^{n-i} \varepsilon_i \frac{\partial \varepsilon_i}{\partial C_n} = 2 \sum_{i=0}^{n} \lambda^{n-i} Y_{i-1} \left[x(i) + Y_{i-1}^T C_n \right] = 0 , \tag{2.22}$$

and the system equations can be obtained as

$$\left(\sum_{i=0}^{n} \lambda^{n-i} Y_{i-1} Y_{i-1}^T \right) C_n = - \sum_{i=0}^{n} \lambda^{n-i} Y_{i-1} x(i) . \tag{2.23}$$

The covariance matrix is denoted as

$$R_n = \sum_{i=0}^{n} \lambda^{n-i} Y_{i-1} Y_{i-1}^T , \tag{2.24}$$

and the cross-correlation vector is denoted as

$$r_n = \sum_{i=0}^{n} \lambda^{n-i} Y_{i-1} x(i) . \tag{2.25}$$

Both of them can be calculated recursively as

$$R_n = \lambda R_{n-1} + Y_{n-1} Y_{n-1}^T , \tag{2.26a}$$

$$r_n = \lambda r_{n-1} + Y_{n-1} x(n) . \tag{2.26b}$$

Using the above notations, the basis coefficients estimate at the time instant n can be calculated as

$$
\begin{aligned}
C_n &= -R_n^{-1} r_n \\
&= -R_n^{-1}\left[\lambda r_{n-1} + Y_{n-1} x(n)\right] \\
&= -R_n^{-1}\left[-\lambda R_{n-1} C_{n-1} + Y_{n-1} x(n)\right] \\
&= -R_n^{-1}\left[-(R_n - Y_{n-1} Y_{n-1}^T) C_{n-1} + Y_{n-1} x(n)\right] \\
&= -R_n^{-1}\left[-R_n C_{n-1} + Y_{n-1}(x(n) + Y_{n-1}^T C_{n-1})\right] \\
&= C_{n-1} - R_n^{-1} Y_{n-1} \varepsilon_n
\end{aligned}
\qquad (2.27)
$$

To avoid direct matrix inversion, the *matrix inversion lemma* [MN2000] will be used

$$\left[Z + UVW\right]^{-1} = Z^{-1} - Z^{-1}U\left[WZ^{-1}U + V^{-1}\right]^{-1} WZ^{-1}, \qquad (2.28)$$

where Z, U, V and W are matrices of appropriate dimensions, Z and V are nonsingular. Let us denote P_n as the inverse of R_n

$$P_n = R_n^{-1} = \left(\lambda P_{n-1}^{-1} + Y_{n-1} Y_{n-1}^T\right)^{-1}, \qquad (2.29a)$$

then we can obtain

$$P_n = R_n^{-1} = \frac{1}{\lambda}\left(P_{n-1} - \frac{P_{n-1} Y_{n-1} Y_{n-1}^T P_{n-1}}{\lambda + Y_{n-1}^T P_{n-1} Y_{n-1}}\right), \qquad (2.29b)$$

by choosing $Z = \lambda P_{n-1}^{-1}, U = W^T = Y_{n-1}$ and $V = 1$ for the *matrix inverse lemma*.

Using the recursive weighted-least-squares basis function method, the basis coefficients estimate is updated upon each data sample, which is summarized as follows:

$P_0 = \delta I$ (δ : positive constant, I : identity matrix)

C_0 initialized to random values

For $n = 1 \ldots N$

$\varepsilon_n = x(n) + Y_{n-1}^T C_{n-1}$

$P_n = \frac{1}{\lambda}\left(P_{n-1} - \frac{P_{n-1} Y_{n-1} Y_{n-1}^T P_{n-1}}{\lambda + Y_{n-1}^T P_{n-1} Y_{n-1}}\right)$

$C_n = C_{n-1} - P_n Y_{n-1} \varepsilon_n$

2.4 Time-varying Spectrum and Instantaneous Frequency Estimation

A common type of nonstationary process is a pseudo-sinusoidal or narrowband signal with time-varying (TV) frequencies [KB1984]. Once the model parameters are obtained, the TV spectrum can be estimated and the instantaneous frequencies of the signal can be extracted by the *peak-picking* or *root-finding* method.

The *power spectral density* $S_x(n, f)$ of a TVAR process is defined as [KB1984]

$$S_x(n, f) = \frac{\sigma_v^2}{\left|1 + \sum_{i=1}^{p} c_i(n) e^{-j2\pi fi}\right|^2}, \tag{2.30}$$

where $0 \le f \le 0.5 f_s$ with the sampling frequency f_s. In practice, the input noise variance is unknown and approximated by

$$\sigma_v^2 \approx \frac{1}{N-p} \sum_{n=p}^{N} \left(x(n) + \sum_{i=1}^{p} c_i(n) x(n-i) \right)^2. \tag{2.31}$$

The *peak-picking* method is to locate the spectral peak from the TV spectrum, where the instantaneous frequency (IF) is the corresponding peak frequency. When there are m frequency components in the signal, the IFs can be obtained from the m largest spectral peaks. However, the closely spaced frequencies may not be differentiated by the *peak-picking* method. The *root-finding* method is to factorize the denominator polynomial $P(n, z)$ and calculate the poles at each time instant [KB1984], where the IF is obtained from the angle of the pole as $\frac{\angle z_i(n)}{2\pi} f_s$. When there are m frequency components in the signal, the IFs can be obtained from the m closest poles to the unit circle. However, the correct IFs may not be obtained when the unreasonable pole locations are obtained from the polynomial factorization.

2.5 Model Order and Basis Function Selection

Appropriate model order and basis functions are important for the time-varying (TV) AR model. According to the *principle of parsimony* [MN2000], one should not use extra parameters if not necessary when describing a dynamic process. The rule of thumb is to build a model with the number of estimated parameters less than $0.2\times$number of observations.

2.5.1 Model Order

The accuracy of the TVAR model is sensitive to the choice of model order. If the model order is not appropriate, the model parameters will not characterize the underlying nature of the process and the representation of the signal will be inaccurate. For the model based spectral analysis, a model order that is too low will result in a smoothed spectral estimate and a model order that is too high will cause spurious spectral peaks. The common criteria for determining model order are the *Akaike's information criterion* (AIC) and the *minimum description length* (MDL) [SH1996], which are based on asymptotic results and originally created for the time-invariant systems. Some approaches were proposed for the TV case, such as the AIC for a class of TVAR models in [FF1980], the Bayesian approach in [JP1996], and the maximum likelihood estimation in [KBE1999].

2.5.2 Basis Function

The goodness of fitting achieved using the basis function (BF) method partly depends on the subspace spanned by the chosen time functions, because it influences the smoothness and variations of parameter estimate. If some prior information about the TV process is available, the BF should be chosen to capture the dominant trends of parameter variations. When applied to a general TV system, the BFs which give general approximation (i.e. the power time functions and Fourier series), should be chosen [MN2000]. In practice, the BF is adopted because of its greater *matching* flexibility rather than the detailed prior knowledge of time variations. In addition, proper basis dimension is important to avoid the over-fitting or the insufficient representation.

2.6 Performances of Time-varying AR Model in Direct Form

The general performance characteristics of the time-varying (TV) AR modeling in direct form are obtained through simulations on synthetic data, in terms of parameter estimation error, prediction gain, frequency estimation error and estimated pole trajectory.

2.6.1 Simulations on Synthetic Data

The synthetic data set of length $N = 256$ is generated as the output of a second-order all-pole TV filter

$$H(n,z) = \frac{1}{1 + c_1(n)z^{-1} + c_2(n)z^{-2}}, \tag{2.32}$$

driven by a white Gaussian noise with zero mean and unit variance. The model parameter $c_1(n) = -2\cos[2\pi f(n)]$, where the normalized frequency is

$$f(n) = \begin{cases} 0.1 + 0.2\dfrac{n}{N}, & 1 \le n \le 128 \\ 0.3 + 0.3\left(\dfrac{n-128}{N}\right)^2, & 129 \le n \le 256 \end{cases}. \tag{2.33}$$

And $c_2(n) = 1$, which can be considered as the radius of the pole in this case.

The model order $p = 2$ is assumed to be known for the analysis process. The simple and commonly used power time functions $f_j(n) = \left(\dfrac{n}{N}\right)^j$ ($j = 0$ to 8) [LAL1975] are chosen as basis functions (BFs), as shown in Figure 2.4. Both the blockwise and recursive ($\lambda = 0.96$) BF methods are used for parameter estimation. The simulations are performed over 200 independent realizations to obtain the average performance.

2.6.2 Performance Measures

2.6.2.1 Parameter Estimation Error

Let $\{\hat{c}_i(n)\}$ $(1 \le i \le p)$ denote the model parameter estimates based on a set of data in one realization, then the *expected path* of parameter estimates is denoted as [MN1988]

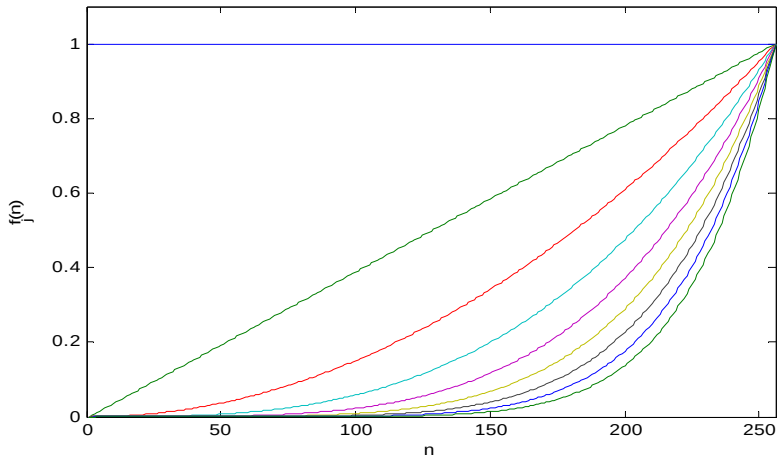

Figure 2.4: Power time functions $f_j(n)$ ($j = 0$ to 8).

$$\bar{c}_i(n) = \mathrm{E}[\hat{c}_i(n)], \tag{2.34}$$

which gives the average trend of parameter evolutions. If the true parameter trajectory can be exactly represented as a linear combination of BFs, we will have *unbiased* estimate $\bar{c}_i(n) = c_i(n)$. However, the actual parameters do not vary in a totally predictable way, so there is *bias*

$$b_{c_i}(n) = c_i(n) - \bar{c}_i(n), \tag{2.35a}$$

in the estimate, which indicates the *difference* between the *expected path* of the parameter estimates and the true parameter trajectory. In addition, the *variance* of the parameter estimate is

$$\sigma^2_{c_i}(n) = \mathrm{E}[(\hat{c}_i(n) - \bar{c}_i(n))^2], \tag{2.35b}$$

which represents the *spread* of the estimates about the *expected path*.

The *mean squared error* (MSE) of parameter estimates is expressed as

$$MSE_{c_i}(n) = \mathrm{E}\left[\left|c_i(n) - \hat{c}_i(n)\right|^2\right], \tag{2.36a}$$

which shows the overall model parameter estimation accuracy and can be decomposed into the *bias* and *variance* components as

$$MSE_{c_i}(n) = b^2_{c_i}(n) + \sigma^2_{c_i}(n). \tag{2.36b}$$

2.6.2.2 Prediction Gain

Effective model-based linear prediction is one goal of modeling. Thus, a direct quality indicator of the TVAR modeling is the *average prediction gain* $\overline{PG}$, given by the ratio (in dB) between the average signal energy and prediction error energy as [RMGJ1987]

$$\overline{PG} = 10\log_{10}\left(\frac{\bar{\sigma}_x^2}{\bar{\sigma}_\varepsilon^2}\right), \tag{2.37}$$

where $\bar{\sigma}_x^2 = \mathrm{E}\left[\sum_{n=1}^{N}|x(n)|^2\right]$ and $\bar{\sigma}_\varepsilon^2 = \mathrm{E}\left[\sum_{n=1}^{N}|\varepsilon(n)|^2\right]$. This criterion shows the goodness of fit between the predicted and true signal, which can be used to evaluate the model's adequacy for choosing the appropriate basis dimension.

2.6.2.3 Frequency Estimation Error

Model-based spectral analysis and frequency estimation is another goal of modeling. The *expected path* of the TV frequency estimates is denoted as

$$\bar{f}(n) = \mathrm{E}[\hat{f}(n)], \tag{2.38}$$

which gives a general trend of frequency variation. The *average frequency estimation error* $\overline{FE}$ is defined as

$$\overline{FE} = \frac{1}{N}\sum_{n=1}^{N}\left|f(n) - \bar{f}(n)\right|, \tag{2.39}$$

which indicates the average frequency estimation accuracy at each time instant.

2.6.2.4 Pole Trajectory

In addition to the *quantitative* measures, the average estimated TV pole trajectory, which plots the real part of each pole on the ordinate and the imaginary part on the abscissa, gives a *qualitative* view of dynamic system behavior [MAA1983]. The unconstrained TV poles of the estimated model might be outside the unit circle in the z-plane, and the unstable output could lead to failure of the system. The average number of

TV poles that are outside the unit circle is counted as $\overline{N}_{unstable}$, which is used to indicate the degree of the possible instability for the estimated TVAR model.

2.6.3 Results and Discussions

The performances of the time-varying (TV) AR modeling in direct form using the blockwise and recursive basis function parameter estimation methods are evaluated in terms of the aforementioned measures.

Figure 2.5 compares the *expected path* of parameter estimates (a) $\bar{c}_1(n)$ and (b) $\bar{c}_2(n)$ of the TVAR model in direct form using blockwise and recursive basis function methods with a medium basis dimension ($q = 4$), where the true parameter trajectory is also shown for comparison. The blockwise method works as parameter *matching*, with the global optimization over the whole block of data. Actually, there is an implicit average embedded in estimation using the blockwise method. The recursive method works as parameter *tracking*, with the local approximation adjusted upon each data sequentially. For an abrupt parameter change, the blockwise method gives a smooth approximation while the recursive method catches up with the new trend with an overshoot. The value of $\bar{c}_2(n)$ (squared radius of pole) exceeds one at some time instants, where the estimated model becomes temporarily unstable.

Figure 2.6 shows $\sum_i MSE_{c_i}(n)$ ($i = 1,2$) of the TVAR model in direct form using blockwise and recursive basis function (BF) methods with various basis dimensions ($q = 0,2,4,8$). In Figure 2.6 (a), the blockwise BF method with $q = 0$, which corresponds to the time-invariant approach, totally fails for the nonstationary case with very large MSE. In Figure 2.6 (b), the recursive BF method with $q = 0$, namely the common weighted-least-squares (WLS), has acceptable MSE before the abrupt change. However, the MSE becomes larger than those of the WLS BF method ($q \geq 1$) after the abrupt change, which shows that the common WLS is only suitable for slow time variations. The error is larger at both ends of the interval than the inner part for the blockwise

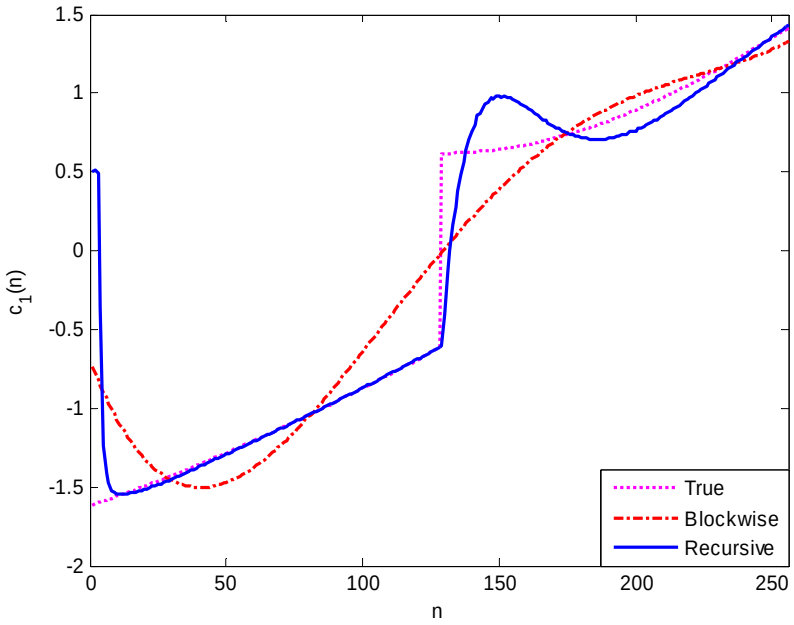

(a) Expected path of parameter estimate $\bar{c}_1(n)$

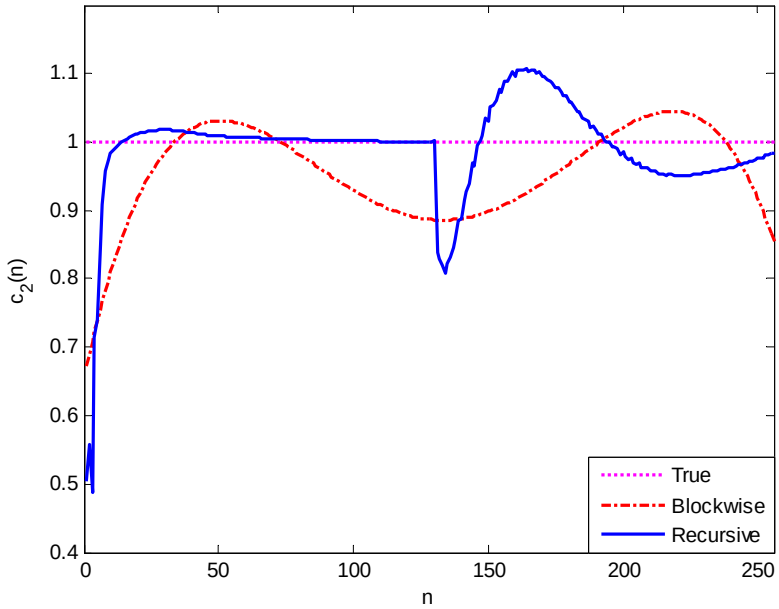

(b) Expected path of parameter estimate $\bar{c}_2(n)$

Figure 2.5: The *expected path* of parameter estimates of the TVAR model in direct form using blockwise and recursive basis function methods with basis dimension $q = 4$.

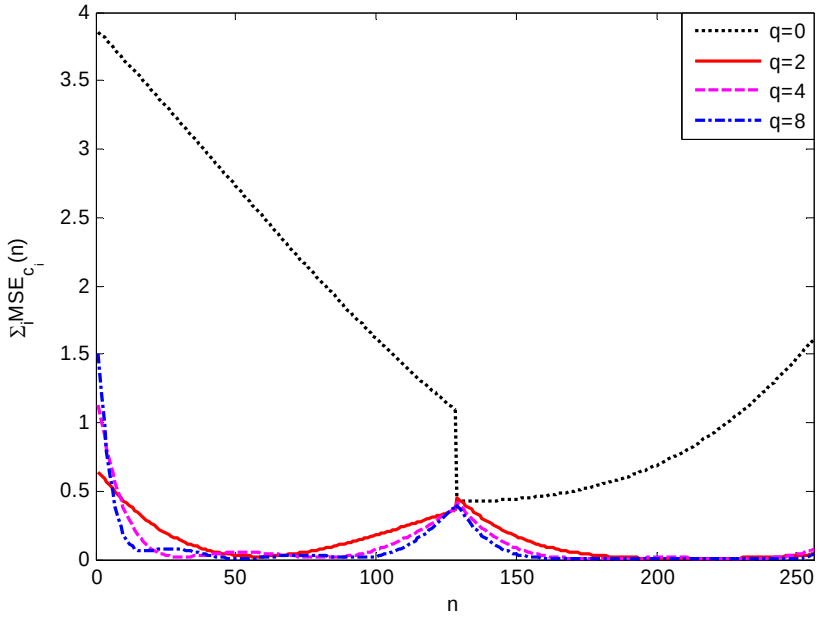

(a) Blockwise basis function method

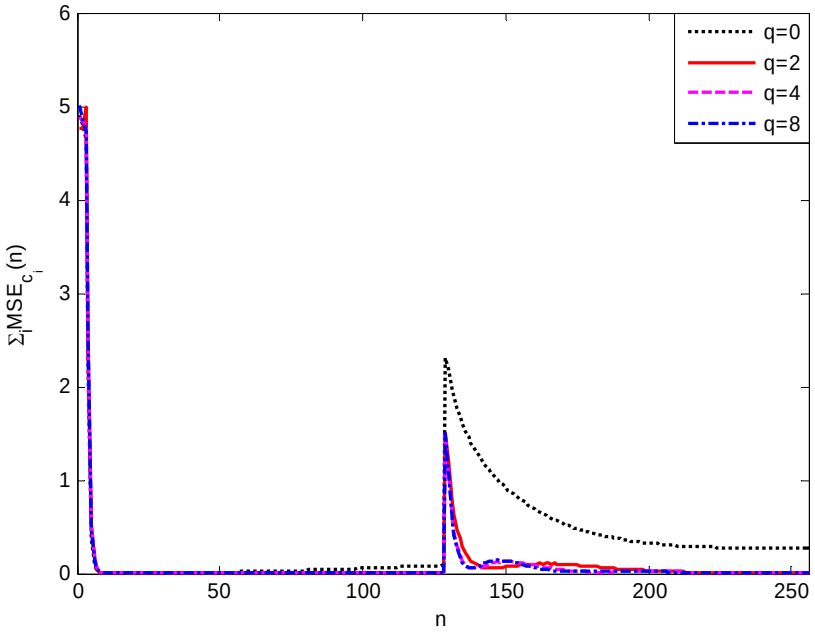

(b) Recursive basis function method

Figure 2.6: $\sum_i MSE_{c_i}(n)$ ($i = 1,2$) of the TVAR model in direct form using blockwise and recursive basis function methods with various basis dimensions ($q = 0,2,4,8$).

method due to the discontinuity of the data. The error is large at the beginning for the recursive method due to the transient stage. At the abrupt change point, the MSE of both methods increases immediately, where the error is relatively small for larger q because higher basis dimensions give more freedom to approximate the jump.

Figure 2.7 shows *the average prediction gain* $\overline{PG}$ via the TVAR modeling in direct form using blockwise and recursive basis function methods with various basis dimensions ($q = 0$ to 8). For $q = 0$, the $\overline{PG}$ is about 2dB and 9dB for the blockwise and recursive methods respectively, showing again that the time-invariant modeling, especially when using the blockwise estimation, does not work for the time-varying condition. For smaller q, the $\overline{PG}$ improves quickly with the increasing q, and the recursive method has higher $\overline{PG}$ than the blockwise method for $q \le 5$. For larger q, the

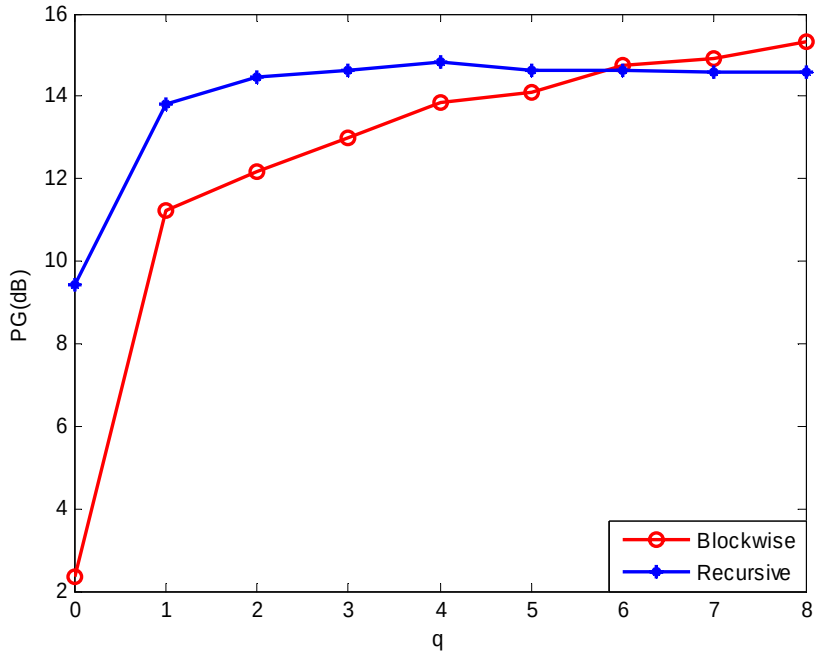

Figure 2.7: $\overline{PG}$ via the TVAR modeling in direct form using blockwise and recursive basis function methods with various basis dimensions ($q = 0$ to 8).

improvement in $\overline{PG}$ is negligible for the recursive method, while the $\overline{PG}$ for the blockwise method still increases and becomes larger than that of the recursive method for $q > 6$. Hence, the medium basis dimension ($q = 4$) is enough for the recursive method to achieve suitable tracking performance, while the blockwise method needs a relatively large basis dimension to obtain good matching performance.

Figure 2.8 shows the *expected path* of the frequency estimate $\bar{f}(n)$ via the TVAR modeling in direct form using blockwise and recursive basis function methods by *root-finding*, where the true frequency trajectory is also shown for comparison. The frequency estimates obtained from the *peak-picking* are almost the same and thus not shown here. Similar to the parameter estimate in Figure 2.5 (a), the blockwise method behaves as frequency *matching* and the recursive method behaves as frequency *tracking*.

Figure 2.9 compares the *average frequency estimation error* $\overline{FE}$ of the TVAR modeling in direct form using blockwise and recursive basis function methods with various basis dimensions ($q = 0$ to 8). The $\overline{FE}$ for the blockwise method is much larger than that for the recursive method for small q. With increasing q, $\overline{FE}$ for the blockwise approaches to that for the recursive method but still remains slightly larger. This shows that the recursive method performs better than the blockwise method when there are abrupt changes in the frequency variations.

Figures 2.10 (a) and (b) show the average estimated pole trajectories of the TVAR model in direct form using blockwise and recursive basis function methods ($q = 4$). The true pole trajectory and the unit circle are also shown for comparison. In Figure 2.10 (a), the estimated pole trajectory using the blockwise method matches the general trend of the true trajectory, with smooth movement through the jump point. Some estimated poles leave the unit circle at both ends due to the poor estimation accuracy. In Figure 2.10 (b), the pole trajectory using the recursive method follows the true trajectory and catches up with the abrupt change. Some estimated poles leave the unit circle at the transient stage

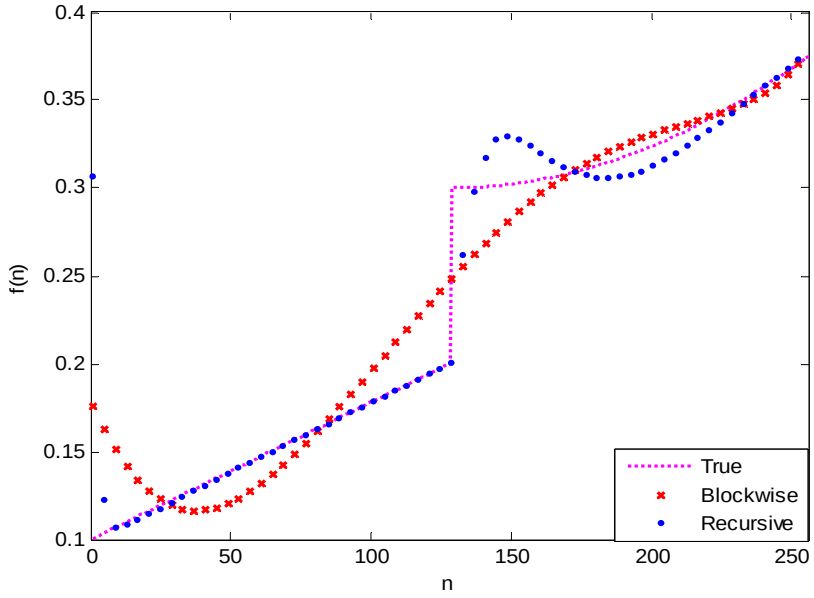

Figure 2.8: The *expected path* of frequency estimates $\bar{f}(n)$ via the TVAR modeling in direct form using blockwise and recursive basis function methods with basis dimension $q = 4$.

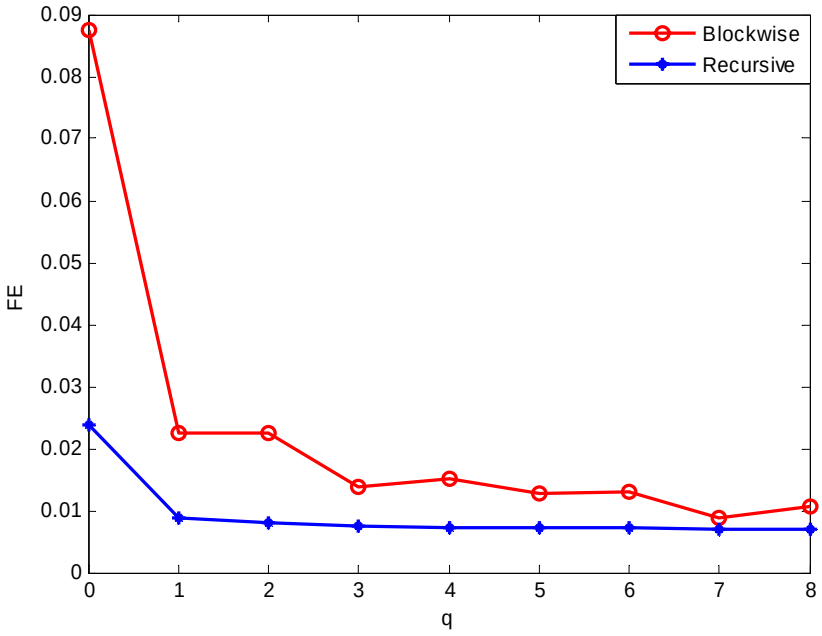

Figure 2.9: $\overline{FE}$ via the TVAR modeling in direct form using blockwise and recursive basis function methods with various basis dimensions ($q = 0$ to 8).

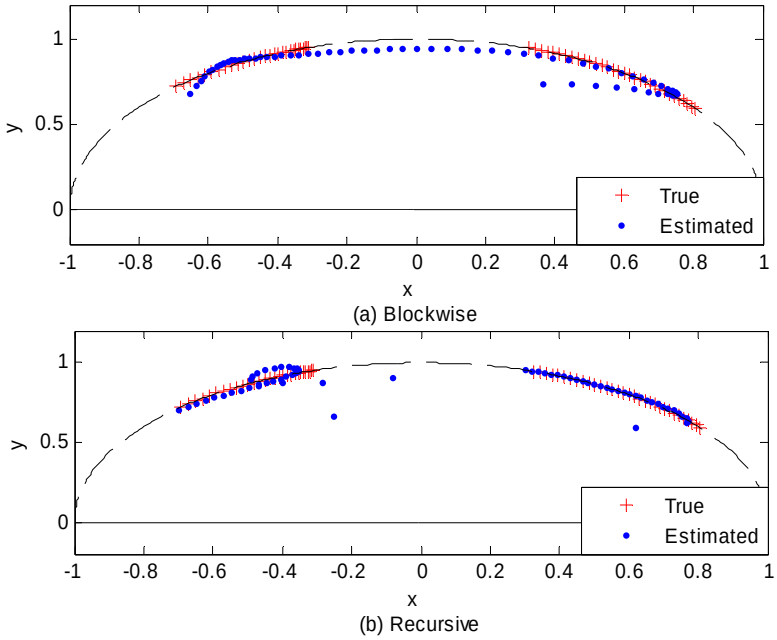

Figure 2.10: The average estimated pole trajectories of the TVAR model in direct form using blockwise and recursive basis function methods with basis dimension $q = 4$.

especially after the abrupt change due to the overshooting in the estimates. In general, the TV synthesis filter, which is obtained from the estimated TVAR model, with poles outside the unit circle would be of no practical value. Thus, the possible temporary instability of the TVAR model is a limitation for its application.

Figure 2.11 shows the $\overline{N}_{unstable}$ for the TVAR model in direct form using blockwise and recursive basis function (BF) methods with various basis dimensions ($q = 0$ to 8). The $\overline{N}_{unstable}$ becomes larger with increasing q and stabilizes for larger q, which shows that the instability is brought by the use of BFs. The estimated TVAR model using the recursive BF method is much more easily to become unstable than that using the blockwise BF method. The oscillation in unconstrained local estimations makes the recursive method become unstable more easily, while the implicit average embedded in the blockwise method helps reduce the unreasonable estimates thus possible instability.

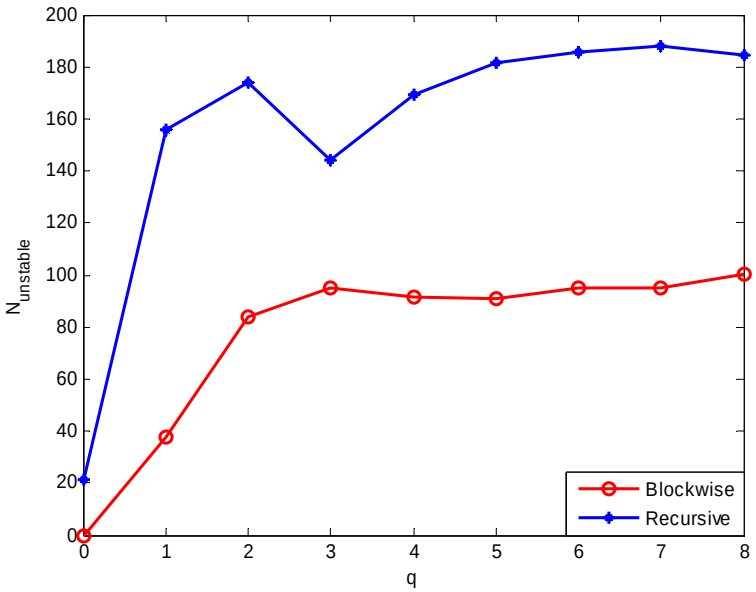

Figure 2.11: $\overline{N}_{unstable}$ of the TVAR model in direct form using blockwise and recursive basis function methods with various basis dimensions ($q = 0$ to 8).

2.7 Chapter Summary

The time-varying (TV) AR model in direct form was reviewed, where the blockwise least-squares and recursive weighted-least-squares basis function (BF) parameter estimation methods were described. Simulations on synthetic data demonstrate that the TVAR model in direct form performs well in identifying the nonstationary process and estimating the TV frequencies, with equivalent overall performance achieved by the two BF methods. The blockwise BF method works as parameter *matching*, and a relatively large basis dimension is needed to obtain good global optimization. The recursive BF method works as parameter *tracking*, and a relatively small basis dimension is enough to follow the local changes.

The estimated TVAR model may become temporarily unstable, which is mainly caused by the large estimation error at both ends of the *analysis interval* and the abrupt change points. Due to the oscillation in unconstrained local estimations, the recursive BF

method is more easily to become unstable than the blockwise BF method. Thus, reliable and convenient stability monitoring is needed for the current TVAR model in direct form.

CHAPTER III

Time-varying Autoregressive Modeling in Cascade Form

In this chapter, the motivations for cascade formulation for the time-varying (TV) AR model are given firstly. The proposed TVAR model in cascade form (CF) is then formulated through the parameterization in terms of TV poles, with four possible forms of pole representation, using the basis function method. Next, the error-gradient generating and basis coefficients calculation processes are described for the TVAR parameter estimation in CF. Finally, the performance characteristics of the TVAR model in CF with different pole representations are explored and compared with those of the TVAR model in direct form via simulations on synthetic data.

3.1 Motivations for Cascade Formulation

The limitations of the time-varying (TV) AR model in direct form motivate formulating the TVAR model in cascade form through the parameterization in terms of TV poles.

First, the possible temporary instability of the estimated TVAR model in direct form (DF) is a major limitation for its application, thus reliable and convenient stability monitoring is needed. The clipping technique in [MNI1987] tries to reduce the possible instability at both ends of the *analysis interval* by estimating the model parameters with the data on the whole interval and using the estimates for modeling on a smaller subinterval. However, this method can not completely eliminate the possible instability. Another method in [MJJ1998] adds constraints on the parameters of the TVAR model in DF through moving the estimated poles to the stable region. Due to highly nonlinear mapping of the polynomial coefficients to the poles, it is solved iteratively to sequentially linearize the nonlinear constraints, which is computationally expensive.

Second, the parameters of the TVAR model in direct form (DF) may not provide the most convenient information for some applications, while the poles of the system transfer function usually contain the physical information of the underlying process. For example, the positions of poles determine the formant frequencies and bandwidths in speech processing [LS1978] and the frequency information of sinusoid signals is also contained in the poles [KB1984]. The TV poles can be obtained by identifying the spectral peaks or factorizing the transfer function polynomial in DF, but these methods are computationally intensive and not suitable for TV pole tracking.

Third, the parameterization of the TVAR model in terms of transfer function coefficients may not yield a natural representation for frequency variations of the nonstationary process. A monotonic evolution of TVAR parameters may not convey a smooth transition in the signal frequency. The parameterization of the TVAR model in terms of TV poles may provide a more appropriate representation of the nonstationary process.

3.2 Time-varying AR Model in Cascade Form

3.2.1 Modeling in Cascade Form

To allow the pole locations to be readily estimated and constrained, the time-varying (TV) AR model is formulated in cascade form (CF), as shown Figure 3.1. The TV transfer function $H(n,z)$ is represented as the product of cascade sections [LS1978]

$$H(n,z) = \frac{1}{\prod_{k=1}^{p/2} P_k(n,z)} = \frac{1}{P(n,z)}, \tag{3.1}$$

where $P_k(n,z) = 1 + p1_k(n)z^{-1} + p2_k(n)z^{-2}$ is the transfer function denominator in each cascade second-order section, $P(n,z) = 1 + \sum_{i=1}^{p} c_i(n)z^{-i}$ is the transfer function denominator of direct form, and the model order p is assumed to be a even number.

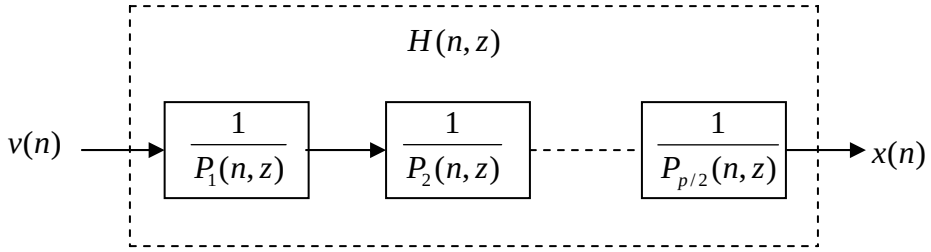

Figure 3.1: Time-varying AR model in cascade form.

Let us denote the direct form (DF) model parameters as $\{P(n)\} = \{1, c_1(n), ..., c_p(n)\}$ and the parameters of each cascade section as $\{P_k(n)\} = \{1, p1_k(n), p2_k(n)\}$. The DF parameters can be calculated through a multiple convolution of CF parameters

$$\{P(n)\} = \underset{k=1}{\overset{p/2}{Conv}} \{P_k(n)\}, \tag{3.2}$$

which shows the *nonlinear* mapping between the model parameters of DF and CF.

Compared with the model in DF, the model in CF has certain advantages:

- It is convenient to control stability by checking the pole locations in each cascade section and projecting the unstable poles into the admissible regions.
- The poles can be directly estimated and more finely adjusted from the data rather than from the estimated model parameters.
- It is a more natural representation of the nonstationary process, with the variations in the frequency domain easily related to the pole movements.

3.2.2 Time-varying Parameterization in Cascade Form

3.2.2.1 Parameterization in terms of Time-varying Pole

Assume that each cascade section consists of a TV conjugate complex pole pair $\{z_k(n), z_k^*(n)\}$, so the transfer function denominator in each section can be expressed as

$$\begin{aligned} P_k(n,z) &= (1 - z_k(n)z^{-1})(1 - z_k^*(n)z^{-1}) \\ &= 1 - 2\,\mathrm{Re}[z_k(n)]z^{-1} + |z_k(n)|^2 z^{-2} \end{aligned}, \; 1 \le k \le p/2, n = 1, ..., N, \tag{3.3}$$

which is appropriate when the signals and model parameters are real-valued. Each pole pair may be represented in form of second-order section coefficients, Cartesian coordinates or polar coordinates.

Let $\omega_k(n)$ denote a general representation of each parameter related to the TV pole in the k th cascade section, and the time variation of $\omega_k(n)$ is assumed to be the linear combination of time functions as

$$\omega_k(n) = \sum_{j=0}^{q} \omega_{kj} f_j(n), \tag{3.4}$$

where $\{f_j(n), 0 \le j \le q\}$ is a set of basis functions and $\{\omega_{kj}\}$ is a set of basis coefficients. In this way, it can be viewed as transforming the TV poles into a sub-space where they can be represented by the time-invariant basis coefficients. Four possible types of TV pole representation are described respectively in the following sections.

3.2.2.2 Parameterization using Second-order Section Representation

The second-order section coefficients are related to each TV complex pole pair as

$$\begin{aligned} \tilde{c}1_k(n) &= -2\,\mathrm{Re}(z_k(n)) \\ \tilde{c}2_k(n) &= |\, z_k(n)\,|^2 \end{aligned}, 1 \le k \le p/2, n = 1,...,N, \tag{3.5}$$

so the denominator of the TV transfer function for each second-order section can be expressed as

$$\begin{aligned} P_k(n,z) &= 1 + \tilde{c}1_k(n) z^{-1} + \tilde{c}2_k(n) z^{-2} \\ \{P_k(n)\} &= \{1, \tilde{c}1_k(n), \tilde{c}2_k(n)\} \end{aligned}, \tag{3.6}$$

where the TV parameters are formed as a linear combination of basis functions

$$\begin{aligned} \tilde{c}1_k(n) &= \sum_{j=0}^{q} \tilde{c}1_{kj} f_j(n) \\ \tilde{c}2_k(n) &= \sum_{j=0}^{q} \tilde{c}2_{kj} f_j(n) \end{aligned}, \tag{3.7}$$

and the corresponding basis coefficient vectors are denoted as

$$\begin{aligned}\tilde{C}1_k &= \left[\tilde{c}1_{k0},...,\tilde{c}1_{kq}\right] \\ \tilde{C}2_k &= \left[\tilde{c}2_{k0},...,\tilde{c}2_{kq}\right]\end{aligned}, \tag{3.8a}$$

$$\tilde{C} = \left[\tilde{C}1_1,...,\tilde{C}1_{p/2},\tilde{C}2_1,...\tilde{C}2_{p/2}\right]^T. \tag{3.8b}$$

3.2.2.3 Parameterization using Cartesian Coordinate Representation

In Cartesian coordinates, each TV complex pole pair is represented as

$$\{z_k(n), z_k^*(n)\} = dx_k(n) \pm jdy_k(n), 1 \le k \le p/2, n = 1,...,N. \tag{3.9}$$

so the denominator of the TV transfer function for each cascade section with Cartesian coordinate representation can be expressed as

$$\begin{aligned}P_k(n,z) &= 1 - 2dx_k(n)z^{-1} + (dx_k^2(n) + dy_k^2(n))z^{-2} \\ \{P_k(n)\} &= \{1, -2dx_k(n), dx_k^2(n) + dy_k^2(n)\}\end{aligned}, \tag{3.10}$$

where the real and imaginary parts are formed as a linear combination of basis functions

$$\begin{aligned}dx_k(n) &= \sum_{j=0}^{q} dx_{kj} f_j(n) \\ dy_k(n) &= \sum_{j=0}^{q} dy_{kj} f_j(n)\end{aligned}, \tag{3.11}$$

and the corresponding basis coefficient vectors are denoted as

$$\begin{aligned}Dx_k &= \left\lfloor dx_{k0},...,dx_{kq}\right\rfloor \\ Dy_k &= \left[dy_{k0},...,dy_{kq}\right]\end{aligned}, \tag{3.12a}$$

$$D = \left[Dx_1,...,Dx_{p/2},Dy_1,...,Dy_{p/2}\right]^T. \tag{3.12b}$$

3.2.2.4 Parameterization using Polar Coordinate Representation (r,θ)

In polar coordinates (r,θ), each TV complex pole pair is represented as

$$\{z_k(n), z_k^*(n)\} = r_k(n)(\cos\theta_k(n) \pm j\sin\theta_k(n)), 1 \le k \le p/2, n = 1,...,N. \tag{3.13}$$

so the denominator of the TV transfer function for each section with (r,θ) representation can be expressed as

$$\begin{aligned}P_k(n,z) &= 1 - 2r_k(n)\cos\theta_k(n)z^{-1} + r_k^2(n)z^{-2} \\ \{P_k(n)\} &= \{1, -2r_k(n)\cos\theta_k(n), r_k^2(n)\}\end{aligned}, \tag{3.14}$$

where the pole radius and angle are formed as a linear combination of basis functions

$$\begin{aligned} r_k(n) &= \sum_{j=0}^{q} r_{kj} f_j(n) \\ \theta_k(n) &= \sum_{j=0}^{q} \theta_{kj} f_j(n) \end{aligned}, \tag{3.15}$$

and the corresponding basis coefficient vectors are denoted as

$$\begin{aligned} R_k &= \lfloor r_{k0},...,r_{kq} \rfloor \\ \Theta_k &= \lfloor \theta_{k0},...,\theta_{kq} \rfloor \end{aligned}, \tag{3.16a}$$

$$\eta = \lfloor R_1,...,R_{p/2},\Theta_1,...,\Theta_{p/2} \rfloor^T . \tag{3.16b}$$

3.2.2.5 Parameterization using Polar Coordinate Representation (α, β)

In polar coordinates (α, β), each TV complex pole pair can also be represented as

$$\{z_k(n), z_k^*(n)\} = \alpha_k(n)\left(\beta_k(n) \pm j\sqrt{1-\beta_k^2(n)}\right), 1 \le k \le p/2, n = 1,...,N , \tag{3.17}$$

where $\alpha_k(n) = r_k(n)$ and $\beta_k(n) = \cos\theta_k(n)$. The denominator of the TV transfer function for each section with (α, β) representation can be expressed as

$$\begin{aligned} P_k(n,z) &= 1 - 2\alpha_k(n)\beta_k(n)z^{-1} + \alpha_k^2(n)z^{-2} \\ \{P_k(n)\} &= \{1, -2\alpha_k(n)\beta_k(n), \alpha_k^2(n)\} \end{aligned}, \tag{3.18}$$

where the radius and cosine-angle are formed as a linear combination of basis functions

$$\begin{aligned} \alpha_k(n) &= \sum_{j=0}^{q} \alpha_{kj} f_j(n) \\ \beta_k(n) &= \sum_{j=0}^{q} \beta_{kj} f_j(n) \end{aligned}, \tag{3.19}$$

and the corresponding basis coefficient vectors are denoted as

$$\begin{aligned} A_k &= \lfloor \alpha_{k0},...,\alpha_{kq} \rfloor \\ B_k &= \lfloor \beta_{k0},...,\beta_{kq} \rfloor \end{aligned}, \tag{3.20a}$$

$$\zeta = \lfloor A_1,...,A_{p/2},B_1,...,B_{p/2} \rfloor^T . \tag{3.20b}$$

3.3 Time-varying AR Parameter Estimation in Cascade Form

3.3.1 Prediction Error Identification in Cascade Form

Using the model in cascade form, the time-varying (TV) AR process can be considered as the TV linear prediction in cascade form, as shown in Figure 3.2. The prediction error $\varepsilon(n)$ is generated by passing $x(n)$ through all the cascade sections [LS1978], which can be expressed in z-domain as

$$E(n,z) = X(z)\prod_{k=1}^{p/2} P_k(n,z), \tag{3.21}$$

where the z-domain representation can be considered as a short-hand form for the time-domain operation.

The system equations for parameter estimation are obtained by minimizing the squared prediction error $\xi = \sum_n \varepsilon^2(n)$ with respect to each basis coefficient ω_{kj}

$$\frac{\partial \xi}{\partial \omega_{kj}} = 2\sum_n \varepsilon(n)\frac{\partial \varepsilon(n)}{\partial \omega_{kj}} = 0, 1 \le k \le p/2, 0 \le j \le q, \tag{3.22}$$

where the error gradient component is denoted as

$$g_{\omega_{kj}}(n) = \frac{\partial \varepsilon(n)}{\partial \omega_{kj}}, \tag{3.23a}$$

and its corresponding z-domain representation is

$$G_{\omega_{kj}}(n,z) = \frac{\partial E(n,z)}{\partial \omega_{kj}}. \tag{3.23b}$$

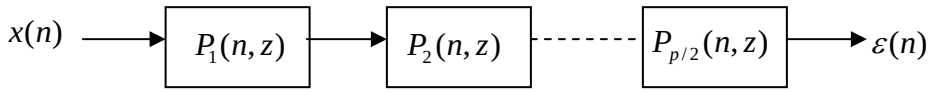

Figure 3.2: Time-varying linear prediction in cascade form.

3.3.2 Error Gradient Generation in Cascade Form

The general error-gradient generating process for each basis coefficient is first described. The gradient components for four possible forms of pole representation are then given in the following sections respectively.

3.3.2.1 General Error Gradient Generating Process

The gradient component can be directly calculated by taking the partial derivatives of the prediction error with respect to ω_{kj}

$$\begin{aligned} G_{\omega_{kj}}(n,z) &= X(z)\frac{\partial P(n,z)}{\partial \omega_{kj}} \\ &= X(z)\prod_{\substack{m=1 \\ m\neq k}}^{p/2} P_m(n,z)\cdot\frac{\partial P_k(n,z)}{\partial \omega_{kj}}, \end{aligned} \tag{3.24a}$$

which can be represented by a linear combination of the input samples $[x(n-1),...,x(n-p)]$ as

$$g_{\omega_{kj}}(n) = \sum_{i=1}^{p} w_{i,\omega_{kj}}(n)x(n-i), \tag{3.24b}$$

where

$$\begin{aligned} \{w_{i,\omega_{kj}}(n)\} &= \frac{\partial\{P(n)\}}{\partial \omega_{kj}} \\ &= \frac{\partial\{P_k(n)\}}{\partial \omega_{kj}} * \underset{\substack{m=1 \\ m\neq k}}{Conv}^{p/2}\{P_m(n)\}. \end{aligned} \tag{3.24c}$$

When the number of cascade sections is large, the computational complexity for this gradient generating process will be much higher than that for the model in direct form.

Similar to that in [LS1978], another computationally more efficient gradient generating process can be obtained as

$$\begin{aligned} G_{\omega_{kj}}(n,z) &= X(z)P(n,z)P_k^{-1}(n,z)\cdot\frac{\partial P_k(n,z)}{\partial \omega_{kj}} \\ &= E(n,z)P_k^{-1}(n,z)\cdot\frac{\partial P_k(n,z)}{\partial \omega_{kj}}, \end{aligned} \tag{3.25}$$

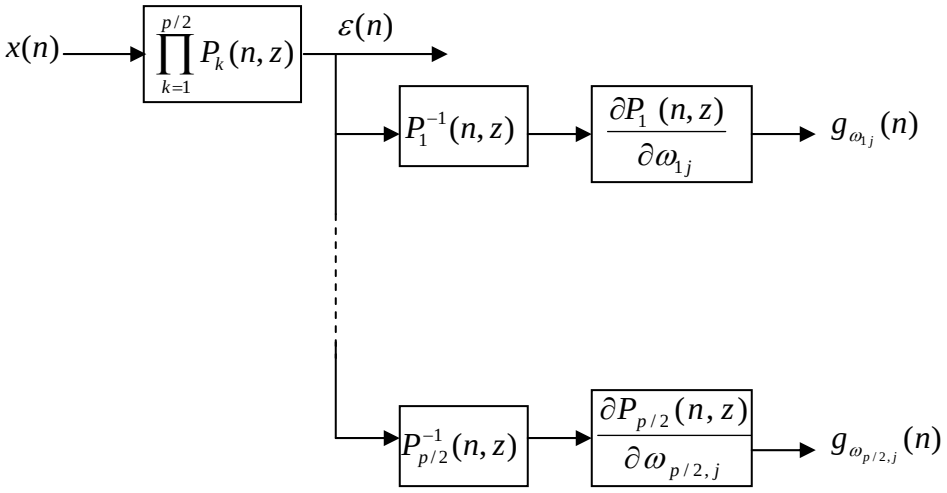

Figure 3.3: Error gradient generating process for the time-varying AR model in cascade form.

where $P_k^{-1}(n,z)$ is the inverse transfer function of the k th cascade section. In this way, the gradient component can be generated by passing $\varepsilon(n)$ through the inverse filter of the k-th section and linearly combining the outputs according to the partial derivative of $P_k(n,z)$ with respect to ω_{kj}, as shown in Figure 3.3.

3.3.2.2 Error Gradient for Second-order Section Representation

The error-gradient components for the second-order section representation are denoted as

$$\begin{aligned} g_{\tilde{c}1_{kj}}(n) &= \frac{\partial \varepsilon(n)}{\partial \tilde{c}1_{kj}} \\ g_{\tilde{c}2_{kj}}(n) &= \frac{\partial \varepsilon(n)}{\partial \tilde{c}2_{kj}} \end{aligned}, \; 1 \le k \le p/2, 0 \le j \le q, n = 1,...,N, \tag{3.26}$$

and the corresponding gradient vectors are

$$\begin{aligned} \psi_{\tilde{C}1_k}(n) &= \left[g_{\tilde{c}1_{k0}}(n),..., g_{\tilde{c}1_{kq}}(n) \right] \\ \psi_{\tilde{C}2_k}(n) &= \left[g_{\tilde{c}2_{k0}}(n),..., g_{\tilde{c}2_{kq}}(n) \right], \end{aligned} \tag{3.27a}$$

$$\Psi_{\tilde{C}}(n) = \left[\psi_{\tilde{C}1_1}(n),..., \psi_{\tilde{C}1_{p/2}}(n), \psi_{\tilde{C}2_1}(n),..., \psi_{\tilde{C}2_{p/2}}(n) \right]^T. \tag{3.27b}$$

The direct gradient calculation is

$$\begin{aligned} g_{\tilde{c}1_{kj}}(n) &= \sum_{i=1}^{p} w_{i,\tilde{c}1_{kj}}(n)x(n-i) \\ g_{\tilde{c}2_{kj}}(n) &= \sum_{i=1}^{p} w_{i,\tilde{c}2_{kj}}(n)x(n-i) \end{aligned}, \tag{3.28a}$$

where

$$\begin{aligned} \{w_{i,\tilde{c}1_{kj}}(n)\} &= \{0,1,0\} * \underset{\substack{m=1 \\ m\neq k}}{\overset{p/2}{Conv}} \{P_m(n)\} \cdot f_j(n) \\ \{w_{i,\tilde{c}2_{kj}}(n)\} &= \{0,0,1\} * \underset{\substack{m=1 \\ m\neq k}}{\overset{p/2}{Conv}} \{P_m(n)\} \cdot f_j(n) \end{aligned}, \tag{3.28b}$$

and the efficient gradient calculation is

$$\begin{aligned} G_{\tilde{c}1_{kj}}(n,z) &= E(n,z)P_k^{-1}(n,z) \cdot z^{-1} \cdot f_j(n) \\ G_{\tilde{c}2_{kj}}(n,z) &= E(n,z)P_k^{-1}(n,z) \cdot z^{-2} \cdot f_j(n) \end{aligned}. \tag{3.29}$$

3.3.2.3 Error Gradient for Cartesian Coordinate Representation

The error-gradient components for the Cartesian coordinate representation are denoted as

$$\begin{aligned} g_{dx_{kj}}(n) &= \frac{\partial \varepsilon(n)}{\partial dx_{kj}} \\ g_{dy_{kj}}(n) &= \frac{\partial \varepsilon(n)}{\partial dy_{kj}} \end{aligned}, \; 1 \le k \le p/2, 0 \le j \le q, n = 1,...,N, \tag{3.30}$$

and the corresponding gradient vectors are

$$\begin{aligned} \psi_{Dx_k}(n) &= \left\lfloor g_{dx_{k0}}(n),...,g_{dx_{kq}}(n) \right\rfloor \\ \psi_{Dy_k}(n) &= \left\lfloor g_{dy_{k0}}(n),...,g_{dy_{kq}}(n) \right\rfloor \end{aligned}, \tag{3.31a}$$

$$\Psi_D(n) = \left\lfloor \psi_{Dx_1}(n),...,\psi_{Dx_{p/2}}(n),\psi_{Dy_1}(n),...,\psi_{Dy_{p/2}}(n) \right\rfloor^T. \tag{3.31b}$$

The direct gradient calculation is

$$\begin{aligned} g_{dx_{kj}}(n) &= \sum_{i=1}^{p} w_{i,dx_{kj}}(n)x(n-i) \\ g_{dy_{kj}}(n) &= \sum_{i=1}^{p} w_{i,dy_{kj}}(n)x(n-i) \end{aligned}, \tag{3.32a}$$

where

$$\begin{aligned} \{w_{i,dx_{kj}}(n)\} &= \{0,-2,2dx_k(n)\} * \underset{\substack{m=1 \\ m\neq k}}{\overset{p/2}{Conv}} \{P_m(n)\} \cdot f_j(n) \\ \{w_{i,dy_{kj}}(n)\} &= \{0,0,2dy_k(n)\} * \underset{\substack{m=1 \\ m\neq k}}{\overset{p/2}{Conv}} \{P_m(n)\} \cdot f_j(n) \end{aligned}, \tag{3.32b}$$

and the efficient gradient calculation is

$$\begin{aligned} G_{dx_{kj}}(n,z) &= E(n,z)P_k^{-1}(n,z)\cdot(-2z^{-1}+2dx_k(n)z^{-2})\cdot f_j(n) \\ G_{dy_{kj}}(n,z) &= E(n,z)P_k^{-1}(n,z)\cdot(2dy_k(n)z^{-2})\cdot f_j(n) \end{aligned}. \tag{3.33}$$

3.3.2.4 Error Gradient for Polar Coordinate Representation (r,θ)

The error-gradient components for the (r,θ) representation are denoted as

$$\begin{aligned} g_{r_{kj}}(n) &= \frac{\partial \varepsilon(n)}{\partial r_{kj}} \\ g_{\theta_{kj}}(n) &= \frac{\partial \varepsilon(n)}{\partial \theta_{kj}} \end{aligned}, 1 \le k \le p/2, 0 \le j \le q, n = 1,...,N, \tag{3.34}$$

and the corresponding gradient vector is

$$\begin{aligned} \psi_{R_k}(n) &= \left\lfloor g_{r_{k0}}(n),...,g_{r_{kq}}(n) \right\rfloor \\ \psi_{\Theta_k}(n) &= \left[g_{\theta_{k0}}(n),...,g_{\theta_{kq}}(n) \right], \end{aligned} \tag{3.35a}$$

$$\Psi_\eta(n) = \left[\psi_{R_1}(n),...,\psi_{R_{p/2}}(n),\psi_{\Theta_1}(n),...,\psi_{\Theta_{p/2}}(n) \right]^T. \tag{3.35b}$$

The direct gradient calculation is

$$\begin{aligned} g_{r_{kj}}(n) &= \sum_{i=1}^{p} w_{i,r_{kj}}(n)x(n-i) \\ g_{\theta_{kj}}(n) &= \sum_{i=1}^{p} w_{i,\theta_{kj}}(n)x(n-i) \end{aligned}, \tag{3.36a}$$

where

$$\{w_{i,r_{kj}}(n)\} = \{0,-2\cos\theta_k(n),2r_k(n)\} * \underset{\substack{m=1\\m\neq k}}{\overset{p/2}{Conv}}\{P_m(n)\}\cdot f_j(n)$$
$$\{w_{i,\theta_{kj}}(n)\} = \{0,2r_k(n)\sin\theta_k(n),0\} * \underset{\substack{m=1\\m\neq k}}{\overset{p/2}{Conv}}\{P_m(n)\}\cdot f_j(n) \quad , \tag{3.36b}$$

and the efficient gradient calculation is

$$G_{r_{kj}}(n,z) = E(n,z)P_k^{-1}(n,z)\cdot(-2\cos\theta_k(n)z^{-1} + 2r_k(n)z^{-2})\cdot f_j(n)$$
$$G_{\theta_{kj}}(n,z) = E(n,z)P_k^{-1}(n,z)\cdot(2r_k(n)\sin\theta_k(n)z^{-1})\cdot f_j(n) \quad . \tag{3.37}$$

3.3.2.5 Error Gradient for Polar Coordinate Representation (α,β)

The error-gradient components for the (α,β) representation are denoted as

$$g_{\alpha_{kj}}(n) = \frac{\partial\varepsilon(n)}{\partial\alpha_{kj}}$$
$$g_{\beta_{kj}}(n) = \frac{\partial\varepsilon(n)}{\partial\beta_{kj}} \quad , 1\le k\le p/2, 0\le j\le q, n = 1,...,N \, , \tag{3.38}$$

and the corresponding gradient vectors are

$$\psi_{A_k}(n) = \left[g_{\alpha_{k0}}(n),...,g_{\alpha_{kq}}(n)\right]$$
$$\psi_{B_k}(n) = \left[g_{\beta_{k0}}(n),...,g_{\beta_{kq}}(n)\right], \tag{3.39a}$$

$$\Psi_\zeta(n) = \left[\psi_{A_1}(n),...,\psi_{A_{p/2}}(n),\psi_{B_1}(n),...,\psi_{B_{p/2}}(n)\right]^T . \tag{3.39b}$$

The direct gradient calculation is

$$g_{\alpha_{kj}}(n) = \sum_{i=1}^{p} w_{i,\alpha_{kj}}(n)x(n-i)$$
$$g_{\beta_{kj}}(n) = \sum_{i=1}^{p} w_{i,\beta_{kj}}(n)x(n-i) \quad , \tag{3.40a}$$

where

$$\{w_{i,\alpha_{kj}}(n)\} = \{0,-2\beta_k(n),2\alpha_k(n)\} * \underset{\substack{m=1\\m\neq k}}{\overset{p/2}{Conv}}\{P_m(n)\}\cdot f_j(n)$$
$$\{w_{i,\beta_{kj}}(n)\} = \{0,-2\alpha_k(n),0\} * \underset{\substack{m=1\\m\neq k}}{\overset{p/2}{Conv}}\{P_m(n)\}\cdot f_j(n) \quad , \tag{3.40b}$$

and the efficient gradient calculation is

$$G_{\alpha_{kj}}(n,z) = E(n,z)P_k^{-1}(n,z)\cdot(-2\beta_k(n)z^{-1} + 2\alpha_k(n)z^{-2})\cdot f_j(n)$$
$$G_{\beta_{kj}}(n,z) = E(n,z)P_k^{-1}(n,z)\cdot(-2\alpha_k(n)z^{-1})\cdot f_j(n) \quad . \tag{3.41}$$

3.3.3 Basis Coefficients Calculation in Cascade Form

Let Ω denote a general basis coefficient vector, the corresponding error gradient vector can be expressed as

$$\Psi_\Omega = \frac{\partial\varepsilon(n)}{\partial\Omega}, \tag{3.42}$$

and the system equations (3.22) can be written in vector form as

$$\sum_n \varepsilon(n)\Psi_\Omega = 0\,. \tag{3.43}$$

Due to the gradient generating process in cascade form (CF), the gradient components are necessarily coupled, so the gradient vector Ψ_Ω depends on Ω. Thus, the system equations for the TVAR model in CF are nonlinear with respect to basis coefficients.

The error surface for the direct form (DF) model in the least squares identification is quadratic and possesses a unique global minimum, while the error surface for the cascade form (CF) model is non-quadratic and possesses multiple minima [JJS1987]. In fact, this is a consequence of cascading individual sections without affecting the overall transfer function, keeping the value of corresponding error signal unaltered. By reordering the $\frac{p}{2}$ second-order sections, there can be as many as $\frac{p}{2}!$ equivalent configurations [MW1989]. The solution to the nonlinear equations for the CF corresponds to the same point on the error surface of DF (with respect to the new coordinated system). Thus, the nonlinear system equations for the model in CF also possess a unique solution.

To solve the set of nonlinear system equations, the Gauss-Newton algorithm [LT1983] is used, where the minimization of the prediction error is obtained by performing searches in the Newton direction using the error gradient and the inverse of the estimated Hessian matrix. The basis coefficients estimate is updated as

$$\Omega_n = \Omega_{n-1} - \gamma \tilde{P}_n \Psi_{\Omega_n} \varepsilon(n), \tag{3.44}$$

where γ is the step size to control the convergence rate and $\tilde{P}_n$ is the inverse of the estimated Hessian matrix, updated according to

$$\tilde{P}_n = \frac{1}{1-\gamma}\left[\tilde{P}_{n-1} - \frac{\tilde{P}_{n-1}\Psi_{\Omega_n}\Psi_{\Omega_n}^T\tilde{P}_{n-1}}{\frac{1-\gamma}{\gamma} + \Psi_{\Omega_n}^T\tilde{P}_{n-1}\Psi_{\Omega_n}^T}\right]. \tag{3.45}$$

The form of the Gauss-Newton algorithm is the same for different forms of pole representation, and the essential difference lies on the corresponding basis coefficients and gradient vectors. The model stability is checked after each basis coefficient update. The pole with radius greater than one will be projected back into the unit circle, by multiplying each unstable pole $z_k(n)$ by $|z_k(n)|^{-2}$. The poles too close to the origin will also be avoided, because the pole angle may be arbitrary when the radius is too small.

The basis coefficients calculation process in cascade form is summarized as follows

$\tilde{P}_0 = \delta I$ (δ : positive constant, I : identity matrix)

Ω_0 initialized to random values

For $n = 1...N$

Calculate $\hat{x}(n)$ from Ω_{n-1}

$\varepsilon(n) = x(n) - \hat{x}(n)$

$$\Psi_{\Omega n} = \frac{\partial \varepsilon(n)}{\partial \Omega_n}$$

$$\tilde{P}_n = \frac{1}{1-\gamma}\left[\tilde{P}_{n-1} - \frac{\tilde{P}_{n-1}\Psi_{\Omega_n}\Psi_{\Omega_n}^T\tilde{P}_{n-1}}{\frac{1-\gamma}{\gamma} + \Psi_{\Omega_n}^T\tilde{P}_{n-1}\Psi_{\Omega_n}^T}\right]$$

$$\Omega_n = \Omega_{n-1} - \gamma \tilde{P}_n \Psi_{\Omega_n} \varepsilon(n)$$

Check the stability and adjust Ω_n to project unstable poles into admissible regions.

3.4 Performances of Time-varying AR Model in Cascade Form

Simulations are performed on synthetic data for the single and double pole pairs cases, to illustrate the performance characteristics of the time-varying (TV) AR model in cascade form and compare with those of the TVAR model in direct form. The model order is assumed to be known for the analysis process, the power time functions are used for basis functions, and the simulations are performed over 200 independent realizations.

3.4.1 Test1: Single Pole Pair Case

The single-pole-pair case is mainly used to explore the performance characteristics of the TVAR model with parameterization in TV poles and benefits of constrained estimation. The synthetic data of length $N = 256$ are generated by the second-order all-pole TV filter described by the equations (2.32)-(2.33) in Chapter II. $\gamma = 0.04$ is used in the Gauss-Newton algorithm.

Figure 3.4 shows the average estimated pole trajectory of the TVAR model in cascade form with the Cartesian coordinate pole representation with a medium basis dimension ($q = 4$). The estimated pole moves along the true trajectory and follows the abrupt change. All the estimated TV poles remain inside the unit circle, due to the stability monitoring after each basis coefficients update.

Figure 3.5 compares the $\overline{PG}$ via the TVAR modeling in direct form (DF, blockwise and recursive) and cascade form (CF, four forms of pole representation) with various basis dimensions ($q = 0$ to 8). The $\overline{PG}$ of the CF show similar trends to that of the recursive DF, because the basis coefficients of the CF are also updated sequentially as the recursive DF. The TV pole representation in Cartesian coordinate shows its superior performance with the $\overline{PG}$ about 1dB higher than those of other pole representations, which are all close to that of the recursive DF. The orthogonality between the real and imaginary parts of the Cartesian pole representation makes it more robust to estimation errors. When there is a

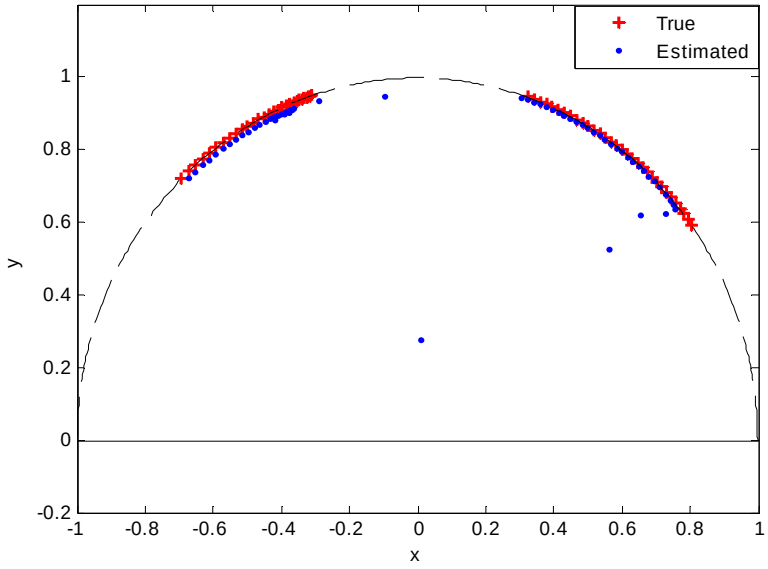

Figure 3.4: The average estimated pole trajectory of the TVAR model in cascade form using the pole representation in Cartesian coordinate with basis dimension $q = 4$ in test1.

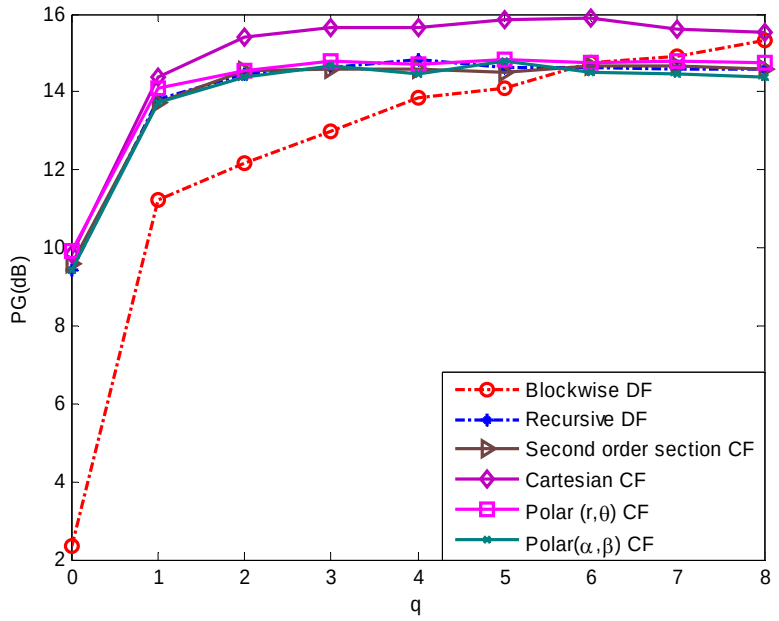

Figure 3.5: $\overline{PG}$ via the TVAR modeling in direct form (blockwise and recursive) and cascade form (four forms of pole representation) with various basis dimensions ($q = 0$ to 8) in test1.

small error in one direction, it will have negligible effect on the other direction, and thus good pole estimate can still be obtained. Although the radius and angle of the (r,θ) pole representation are orthogonal, it is sensitive to deviations of angle when the radius is large, because a small error in the angle estimate may bring the estimated pole far from its true position. The parameters for the (α,β) pole representation are not orthogonal, so it doesn't gain any advantage over the DF. The second-order section representation is similar to the DF, because it is actually the DF with stability control for the single pole pair case.

Figure 3.6 shows the *expected path* of parameter estimates $\bar{c}_i(n)$ $(i=1,2)$ of the TVAR model in cascade form (CF, Cartesian), where the estimates of the TVAR model in direct form (DF, blockwise and recursive) and the true parameter trajectory are also shown for comparison. In Figure 3.6 (a), the estimate of the Cartesian CF is similar to that of the recursive DF, but it has smaller overshooting and hence closer approximation after the abrupt change. In Figure 3.6 (b), the estimates of the Cartesian CF do not oscillate around the true parameter trajectory and remain less than one, which again show the benefit of constrained estimation.

Figure 3.7 compares the $\overline{FE}$ via the TVAR modeling in direct form (DF, blockwise and recursive) and cascade form (CF, four forms of pole representation) with various basis dimensions ($q=0$ to 8). The $\overline{FE}$ of the CF with different forms of pole representation is similar to that of the recursive DF. The $\overline{FE}$ of the Cartesian and (r,θ) representations are slightly lower than that of the recursive DF due to better pole representation and adjustment. The $\overline{FE}$ of the second order section and (α,β) representations are slightly higher than that of the DF, so using these pole representations gain no benefit in frequency estimation.

Figure 3.8 shows the *expected path* of the frequency estimate $\bar{f}(n)$ via the TVAR modeling in cascade form (CF, Cartesian), where the estimates via the TVAR modeling

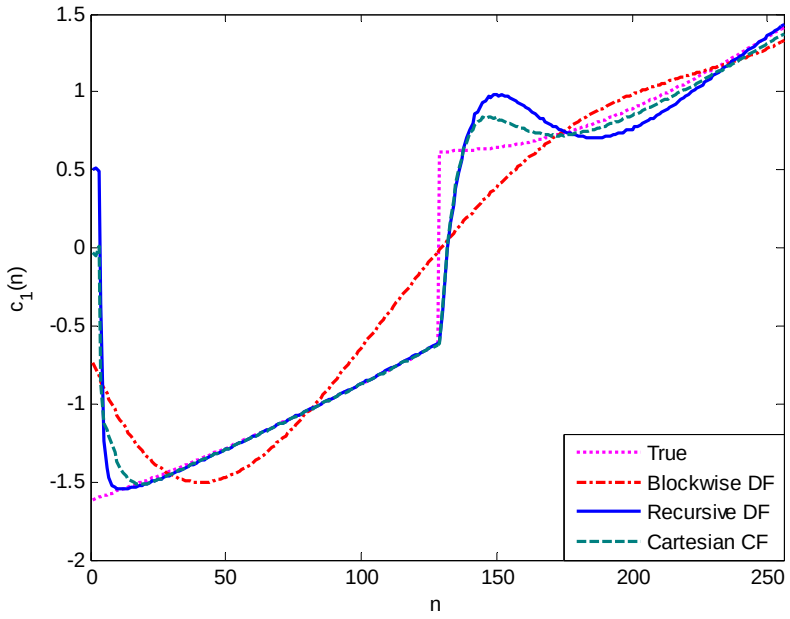

(a) Expected path of parameter estimate $\bar{c}_1(n)$

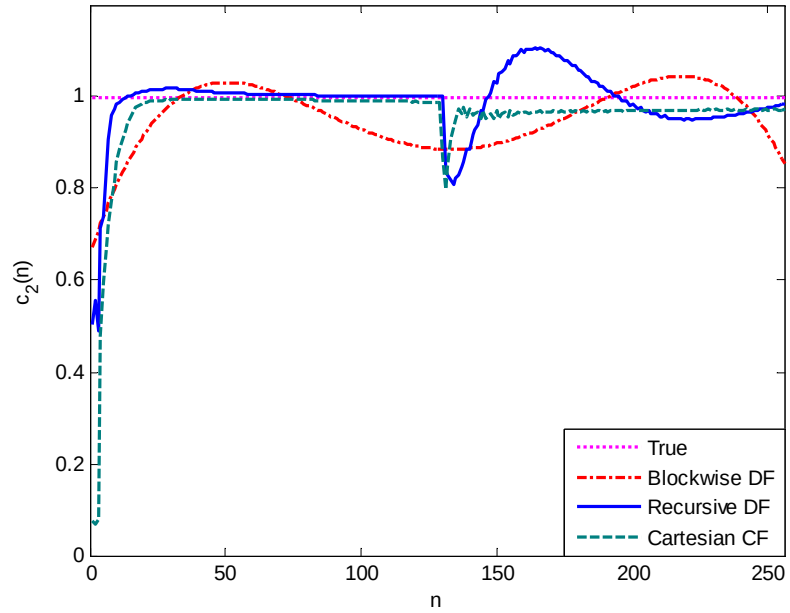

(b) Expected path of parameter estimate $\bar{c}_2(n)$

Figure 3.6: The *expected path* of parameter estimates of the TVAR model in direct form (blockwise and recursive) and cascade form (Cartesian) with basis dimension $q = 4$ in test1.

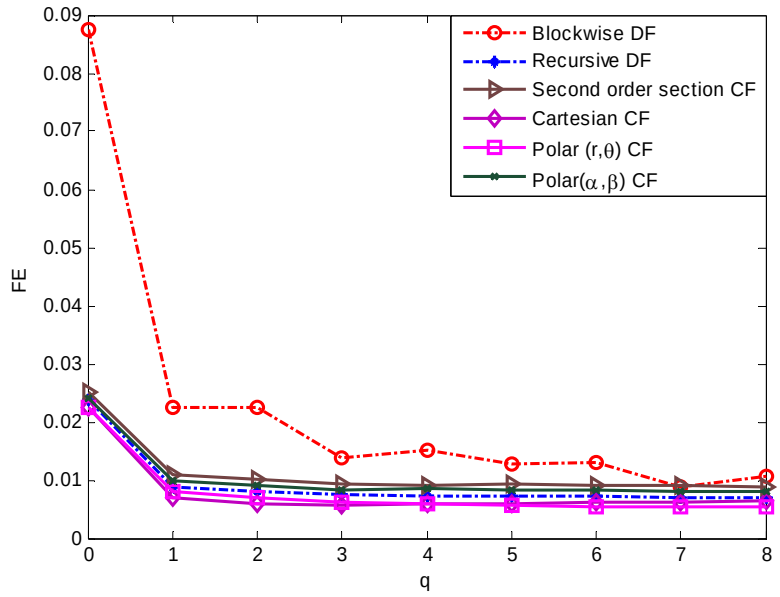

Figure 3.7: $\overline{FE}$ via the TVAR modeling in direct form (blockwise and recursive) and cascade form (four forms of pole representation) with various basis dimensions ($q = 0$ to 8) in test1.

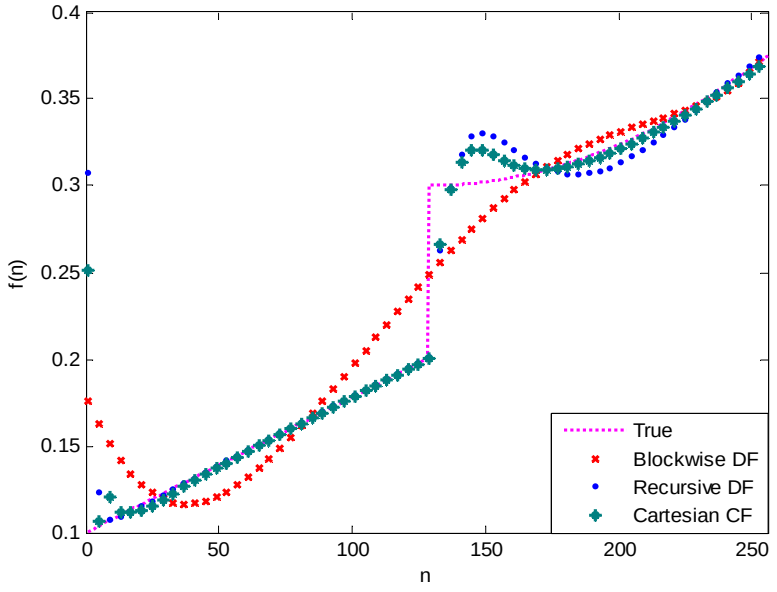

Figure 3.8: The *expected path* of frequency estimates $\bar{f}(n)$ via the TVAR modeling in direct form (blockwise and recursive) and cascade form (Cartesian) with basis dimension $q = 4$ in test1.

in direct form (DF, blockwise and recursive) and the true frequency trajectory are also shown for comparison. Again, the estimate for the CF is similar to that for the recursive DF, but it has closer approximation to the true frequency trajectory.

3.4.2 Test2: Double Pole Pairs Case

The double-pole-pair case is used to explore benefits gained by individual TV pole estimation for the signal with multiple frequency components. The synthetic data set of length $N = 512$ is generated as the output of a fourth-order all-pole TV filter

$$H(n,z) = \frac{1}{(1+c_{11}(n)z^{-1}+c_{12}(n)z^{-2})(1+c_{21}(n)z^{-1}+c_{22}(n)z^{-2})}\ , \tag{3.46}$$

driven by the white Gaussian noise with zero mean and unit variance. The TV parameters of each cascade section are $c_{11}(n) = -2\cos[2\pi f_1(n)]$, $c_{12}(n) = 1$, and $c_{21}(n) = -2\cos[2\pi f_2(n)]$ and $c_{22}(n) = 1$, where the normalized TV frequencies are

$$f_1(n) = \begin{cases} 0.1 + 0.2\dfrac{n}{N} & 1 \le n \le 256 \\ 0.3 + 0.2\left(\dfrac{n-256}{N}\right) & 257 \le n \le 512 \end{cases} \tag{3.47}$$

and

$$f_2(n) = 0.4 - 0.3\left(\frac{n}{N}\right)^2 \qquad 1 \le n \le 512\,. \tag{3.48}$$

In the double-pole-pair case, model order $p = 4$ is assumed known. The two estimated frequencies cannot be categorized to their corresponding true trajectories, so the $\overline{FE}$ cannot be calculated for the individual frequency. The performances of the TVAR modeling in direct form ($\lambda = 0.98$) and cascade form ($\gamma = 0.02$) are evaluated by the average estimated pole trajectories and the *expected paths* of frequency estimates ($q = 4$) in Figure 3.9 and the $\overline{PG}$ in Figure 3.10.

In Figure 3.9 (a), the frequency estimates via the TVAR modeling in direct form (DF, blockwise) match the true frequency points, but the estimates give two separate and

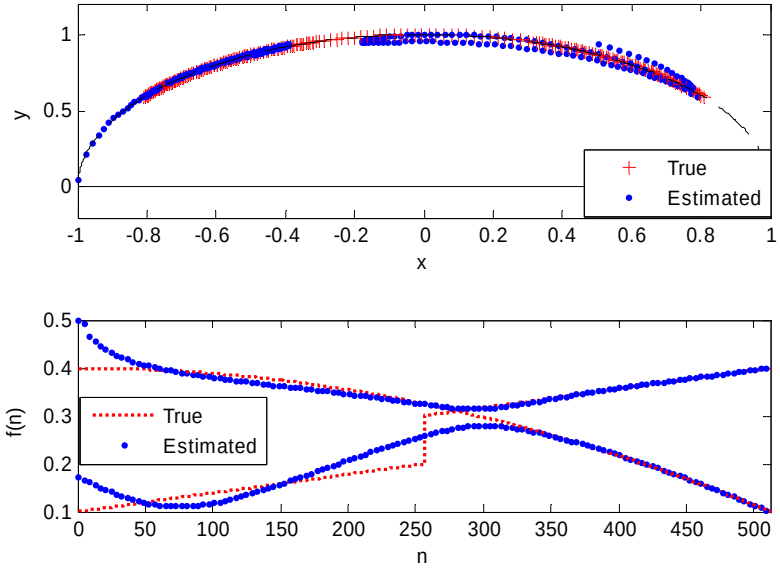

(a) Direct form (blockwise)

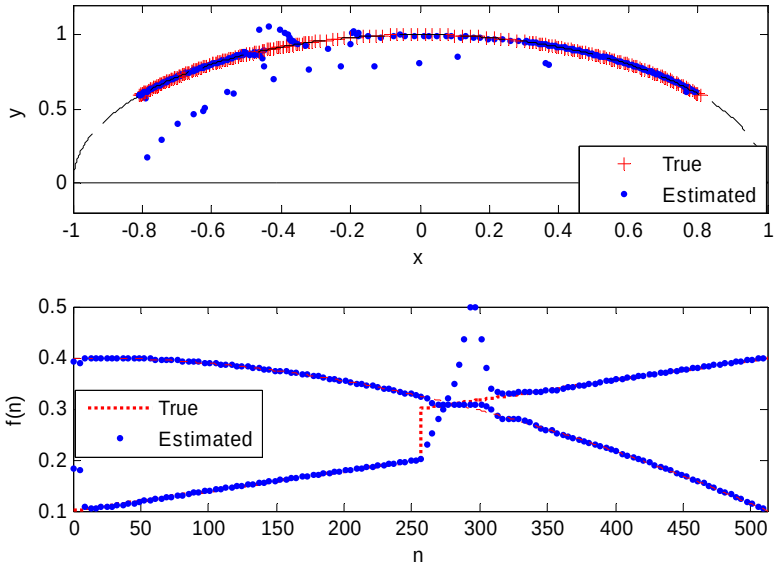

(b) Direct form (recursive)

Figure 3.9: The average estimated pole trajectories and expected paths of frequency estimates via the TVAR modeling in direct form (blockwise and recursive) and cascade form (Cartesian) with basis dimension $q = 4$ in test2.

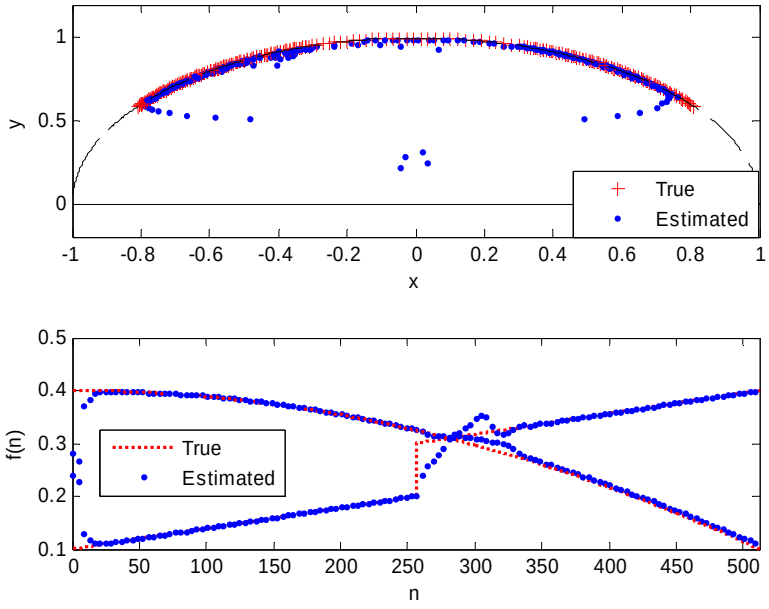

(c) Cascade form (Cartesian)

Figure 3.9: Continued.

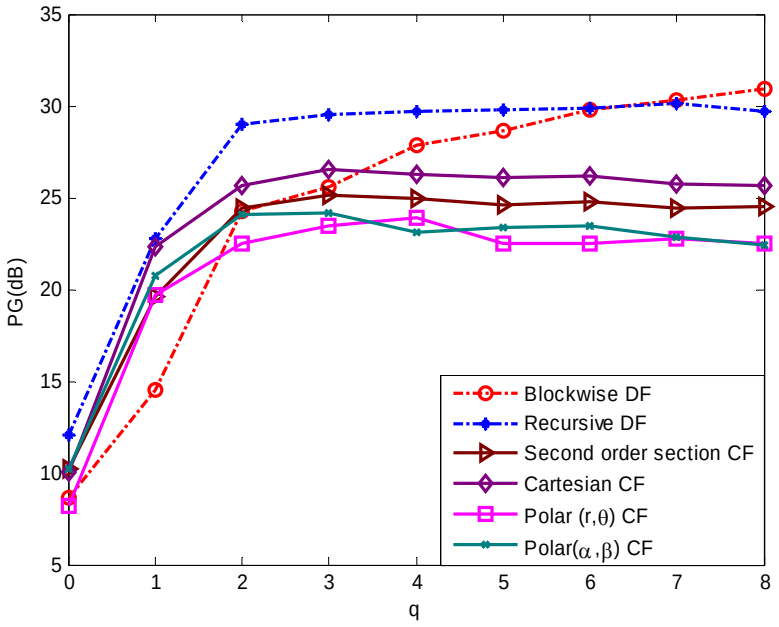

Figure 3.10: $\overline{PG}$ via the TVAR modeling in direct form (blockwise and recursive) and cascade form (four forms of pole representation) with various basis dimensions ($q = 0$ to 8) in test2.

smooth frequency trajectories without showing the actual abrupt change and crossing. The average estimated pole trajectories also show two distinct roundtrip pole movements, instead of the actual two one-way movements with crossing. Similar phenomena were found in [KBE1999]. Thus, the frequency-varying trend may not be correctly revealed via the global optimization of the blockwise DF.

In Figure 3.9 (b), the frequency estimates via the recursive direct form (DF) closely track the true trajectories and show the frequency jump and crossing. However, there is a large overshooting due to the unconstrained estimation after the frequency jump and crossing point, with the normalized frequency reaching the value of 0.5. The overshooting causes obvious model instabilities, with the TV poles migrating outside the unit circle.

In Figure 3.9 (c), the frequency estimates via the cascade form (CF, Cartesian) is shown for comparison with the direct form, since it yields the best performance among four pole representations. The frequency estimates obtained by the Cartesian representation closely follow the true frequency trajectories, with the jump and crossing. Since the constraints are placed on the poles during the estimation, the overshooting in estimates after the abrupt change is relatively small and within a reasonable range. Moreover, all the estimated TV poles remain inside the unit circle.

In Figure 3.10, the $\overline{PG}$ via the TVAR modeling in direct form (DF, blockwise and recursive) are higher than those via the TVAR modeling in cascade form (CF, four forms of pole representation) in the double-pole-pair case. This may be caused by the error propagation via the convolution between the cascade sections in gradient computations. In addition, constrained estimation in individual cascade section may reduce the overall signal prediction accuracy. The CF with the Cartesian pole representation has higher $\overline{PG}$ than the other forms of pole representation.

3.5 Chapter Summary

The proposed time-varying (TV) AR model in cascade form (CF) was formulated through the parameterization in terms of TV poles, where four possible forms of TV poles are represented and estimated using the basis function (BF) method. Simulations were performed on synthetic data with single and double pole pairs to explore the performance characteristics of TVAR model in CF.

Using the TVAR model in cascade form (CF), the estimated TV poles can be easily constrained within the unit circle during the identification process, thus the model stability is guaranteed. Due to the sequential basis coefficients estimate update, the CF model show similar performance trends to the direct form (DF) model using the recursive basis function method. The TV pole representation in Cartesian coordinate gives a natural and robust approximation of time variations in frequencies, and outperforms other forms of pole representation, which all yield similar performances to the recursive DF. Since the poles are adjusted separately in each cascade section, the actual varying trend of individual frequency component can be clearly revealed by the TVAR modeling in CF, when several frequency components are present in the nonstationary signal. In addition to stability control, the constraints placed on the estimated TV poles also help avoid the possible large overshooting in frequency estimates caused by the random oscillation in local estimations, as that occurs for the recursive DF.

CHAPTER IV

Instantaneous Frequency Estimation via Time-varying Autoregressive Modeling

In this chapter, the basics of instantaneous frequency (IF) are first reviewed. The performance characteristics of IF estimation via the time-varying AR modeling in direct form (blockwise and recursive) and cascade form (Cartesian) are then explored through simulations on synthetic sinusoidal signals with different frequency variations, where the influences of various basis dimensions, different basis functions and additive white noise are investigated. Finally, experiments are carried on real electromyography (EMG) data for frequency estimation in the analysis of muscle fatigue.

4.1 Instantaneous Frequency

In some situations, such as seismic, radar, sonar, communications and biomedical applications, the instantaneous frequency is a parameter of practical importance, which defines the location of the nonstationary signal's spectral peak as it varies with time [BB11992].

The instantaneous frequency (IF) of a continuous-time signal $x(t)$ can be uniquely defined as the first derivative of the phase of the *analytic signal* [BB11992]

$$f_i(t) = \frac{1}{2\pi}\frac{d\varphi(t)}{dt}, \tag{4.1}$$

where $\varphi(t)$ is the phase function of the *analytic* signal $z(t) = a(t)e^{j\varphi(t)}$. $z(t)$ is generated from the real signal $x(t)$ as

$$z(t) = x(t) + jH[x(t)], \tag{4.2}$$

where $H[\cdot]$ denotes the *Hilbert* transform. Physically, IF has meaning only for monocomponent signals, where there is only one frequency or a narrow range of frequencies varying as a function of time. For multicomponent signals, the notion of a single-valued IF becomes meaningless, and a break-down into its component is needed.

Several methods may be used to estimate the instantaneous frequencies [BB21992], such as calculating the first-order central finite difference of the *analytic* signal, counting the number of zero-crossings, calculating the *spectrogram* from the short-time Fourier transform, computing the moments of the time-frequency distribution, and finding the TV poles via the TVAR modeling.

4.2 Simulations on Sinusoidal Signals with Time-varying Frequencies

To explore the performance characteristics of instantaneous frequency estimation via the time-varying (TV) AR modeling, simulations are performed on the synthetic sinusoidal signals with different TV frequencies.

4.2.1 Time-varying AR Model for Sinusoidal Signals

The sinusoidal signal $x(nT_s) = \cos[2\pi f_i(nT_s)]$ $(1 \le n \le N)$ with a single frequency component has its TV pole on the unit circle at the angle corresponding to its instantaneous frequency (IF) [KB1984]. In simulations, the sampling frequency and interval are both normalized to unit ($F_s = 1, T_s = 1$). Using the trigonometric identities, it can be shown that $x(n)$ satisfies a second order recursion as [KB1984]

$$x(n) = -c_1(n)x(n-1) - c_2(n)x(n-2), \tag{4.3}$$

where the TV parameters $c_1(n) \approx -2\cos 2\pi[f_i(n-1)]$ and $c_2(n) \approx 1$. This recursion is valid for the sinusoidal signal with different TV frequencies, such as linear, quadratic and periodic variations, which is shown in Appendix A. Thus, the IF of a sinusoidal signal can be estimated via the TVAR modeling.

The following four sinusoidal signals with linear, quadratic, periodic and abrupt frequency changes are used in simulations.

- ***Signal 1:*** a sinusoid with a normalized frequency piecewise *linearly* varying over $N = 256$ samples, increasing from $f_0 = 0.1$ to $f_{\max} = 0.4$ over the first $N_c = 128$ samples, then decreasing back to $f_0 = 0.1$ over the next 128 samples.

$$x_1(n) = \begin{cases} \cos\left[2\pi(f_0 + \frac{\mu_1}{2} n)n \right], & 1 \le n \le 128 \\ \cos\left[2\pi(f_{\max} - \mu_1(\frac{n}{2} - N_c))n \right], & 129 \le n \le 256 \end{cases}, \tag{4.4}$$

where $\mu_1 = \left| \frac{f_{\max} - f_0}{N_c} \right|$ and $f_{i'}(n) = \begin{cases} f_0 + \mu_1 n, & 1 \le n \le 128 \\ f_{\max} - \mu_1(n - N_c), & 129 \le n \le 256 \end{cases}$.

- ***Signal 2:*** a sinusoid with a normalized frequency nonlinearly varying over $N = 256$ samples in a *quadratic* manner, decreasing from $f_0 = 0.4$ to $f_{\min} = 0.1$ over the first $N_c = 128$ samples then increasing back to $f_0 = 0.4$ over the next 128 samples.

$$x_2(n) = \begin{cases} \cos\left\{ 2\pi\left[f_{\min} + \mu_2(\frac{n^2}{3} - nN_c + N_c^2) \right] n \right\} \\ \cos\left\{ 2\pi\left[f_0 - \mu_2(\frac{n^2}{3} - nN + N^2) \right] n \right\} \end{cases}, \tag{4.5}$$

where $\mu_2 = \left| \frac{f_0 - f_{\min}}{N_c^2} \right|$, and $f_i(n) = \begin{cases} f_{\min} + \mu_2(n - N_c)^2, & 1 \le n \le 128 \\ f_0 - \mu_2(n - N)^2, & 129 \le n \le 256 \end{cases}$.

- ***Signal 3*:** a sinusoid with a normalized frequency nonlinearly varying in a *periodic* manner over $N = 256$ samples, starting from $f_0 = 0.25$ and oscillating between $f_{\max} = 0.4$ and $f_{\min} = 0.1$, with a sweeping rate of $\mu_f = \frac{4}{N}$.

$$x_3(n) = \cos\left\{ 2\pi\left[f_0 n - \frac{\mu_3}{2\pi\mu_f}\cos(2\pi\mu_f n) \right] \right\}, 1 \le n \le 256, \tag{4.6}$$

where $\mu_3 = \left| \frac{f_{\max} - f_{\min}}{2} \right|$ and $f_i(n) = f_0 + \mu_3 \sin(2\pi\mu_f n), 1 \le n \le 256$.

- ***Signal 4:*** a sinusoid with a frequency *jump*. The frequency remains constant

at $f_0 = 0.1$ for the first 127 samples and then it jumps to $f_N = 0.4$ at the 128th sample and remains constant over the next 128 samples.

$$x_4(n) = \begin{cases} \cos(2\pi f_0 n) & 1 \le n \le 127 \\ \cos[2\pi(f_0 + \Delta f)n] & 128 \le n \le N \end{cases}, \tag{4.7}$$

where $\Delta f = f_N - f_0$ and $f_i(n) = \begin{cases} f_0, & 1 \le n \le 127 \\ f_0 + \Delta f, & 128 \le n \le 256 \end{cases}$.

To have a general view of the frequency variations in the four sinusoidal signals, the short-time Fourier transform (STFT) is performed on the synthetic data, using 32 samples in each short interval with a overlapping of 27 samples between adjacent intervals. The *spectrograms* of four signals, the squared magnitude of the STFT, are shown in Figure 4.1. The trends of frequency variations and rough frequency ranges can be seen from the *spectrograms*, but the time and frequency resolutions are relatively low due to the small number of analysis intervals and the short length of each analysis interval.

4.2.2 Instantaneous Frequency Estimates

The instantaneous frequency (IF) estimates for the four synthetic sinusoidal signals are obtained via the TVAR modeling in direct form (DF, blockwise and recursive) and cascade form (CF, Cartesian), where the IF estimates from the DF model are extracted by *root-finding*. Since the sinusoidal signals are real and have one frequency component, the model order $p = 2$ is used in the analysis process. The power time functions are used as basis functions, and various basis dimensions ($q = 1,4,7,10$) are used. $\lambda = 0.94$ is used for the recursive DF and $\gamma = 0.08$ is used for the Cartesian CF.

The instantaneous frequency estimates for the four synthetic sinusoidal signals are shown in Fig. 4.2-4.5 respectively. Compared with the rough frequency range on each short time interval shown in the spectrograms, a single frequency estimate is obtained at each time instant via the TVAR modeling, which gives both higher time and frequency resolutions.

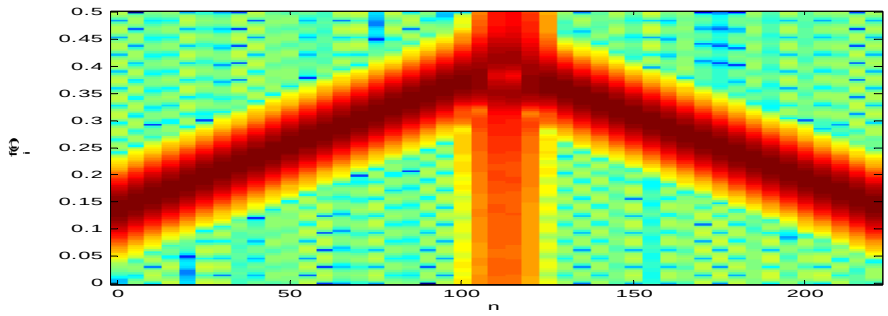

(a) Signal 1

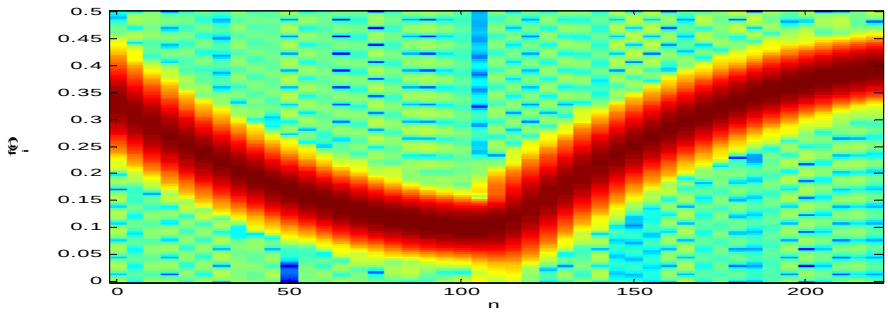

(b) Signal 2

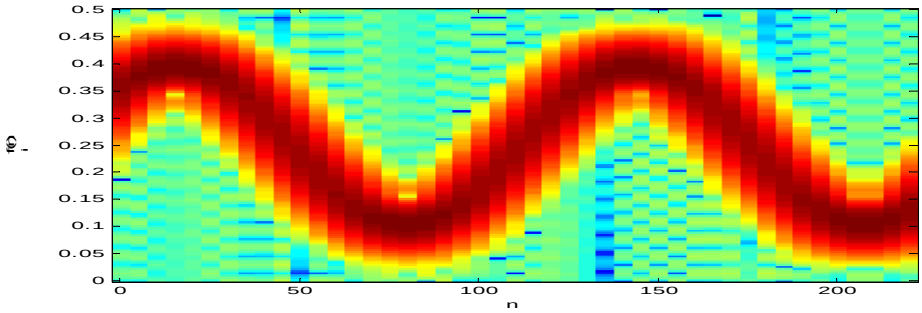

(c) Signal 3

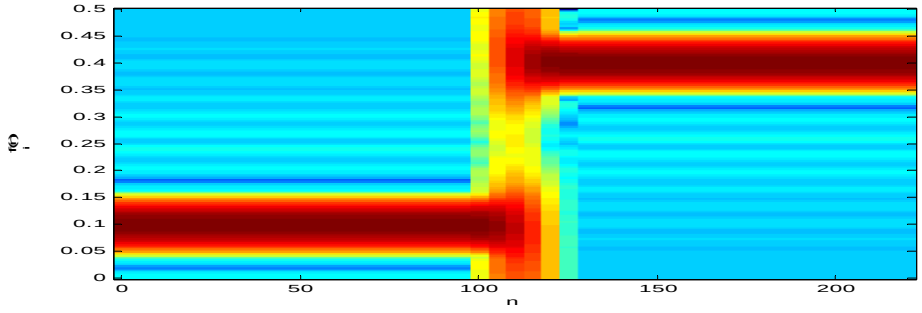

(d) Signal 4

Figure 4.1: Spectrograms of four sinusoidal signals with time-varying frequencies.

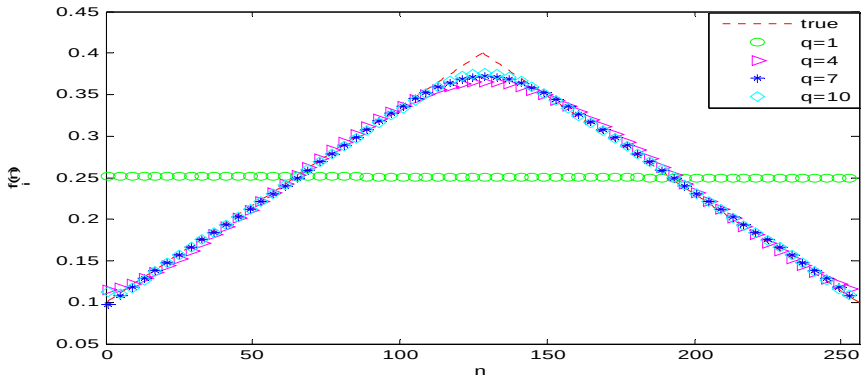

(a) Direct form (blockwise)

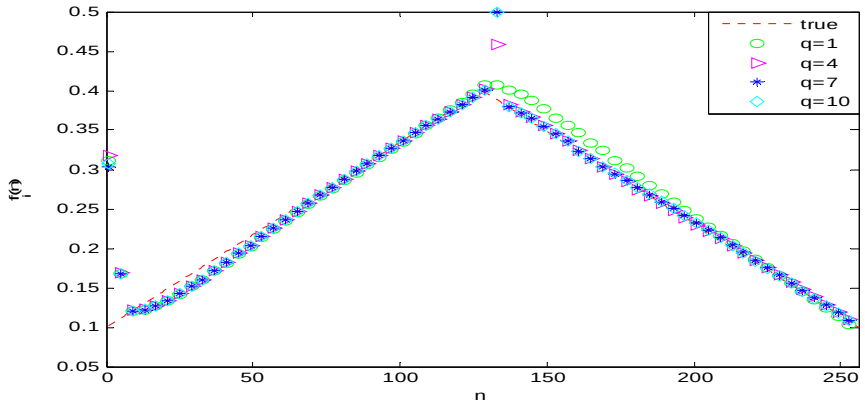

(b) Direct form (recursive)

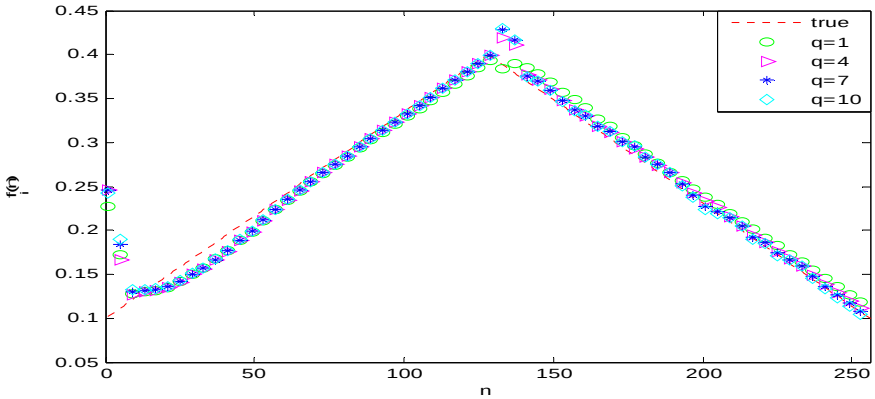

(c) Cascade form (Cartesian)

Figure 4.2: Instantaneous frequency estimates of the *signal 1* via the TVAR modeling in direct form (blockwise and recursive) and cascade form (Cartesian) with various basis dimensions ($q = 1,4,7,10$).

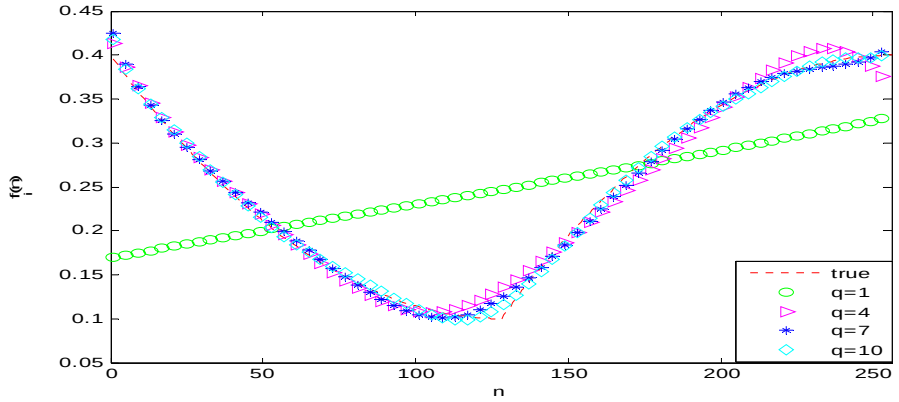

(a) Direct form (blockwise)

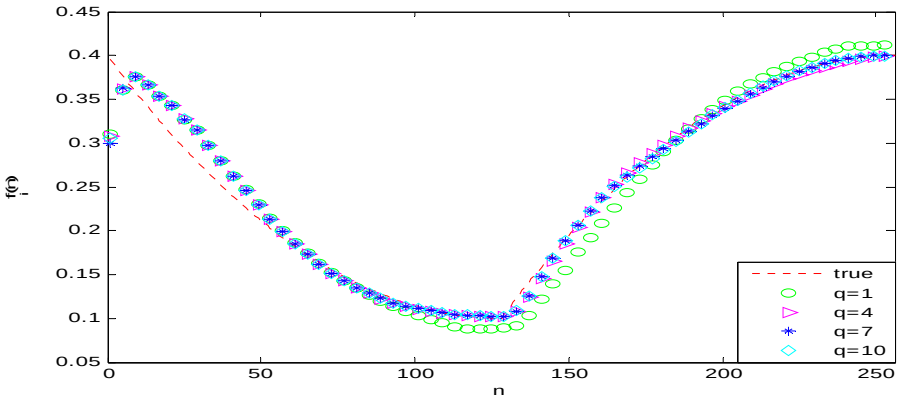

(b) Direct form (recursive)

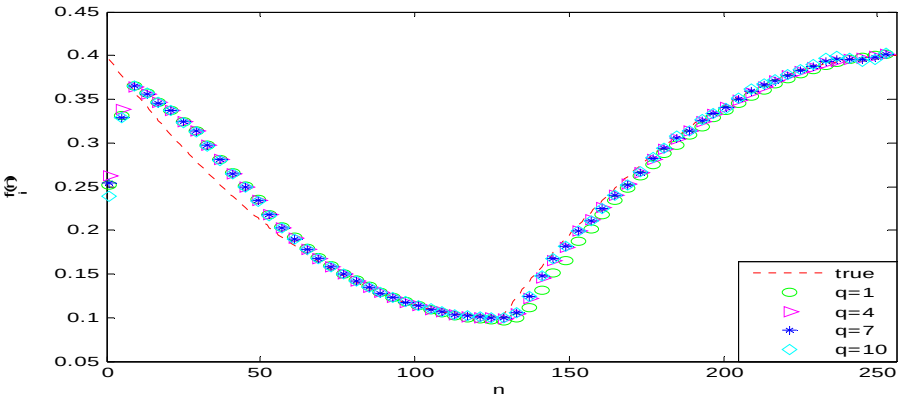

(c) Cascade form (Cartesian)

Figure 4.3: Instantaneous frequency estimates of the *signal 2* via the TVAR modeling in direct form (blockwise and recursive) and cascade form (Cartesian) with various basis dimensions ($q = 1,4,7,10$).

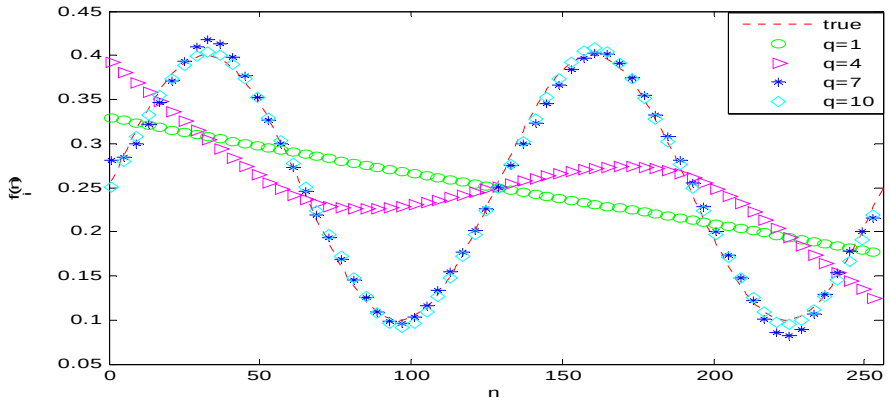

(a) Direct form (blockwise)

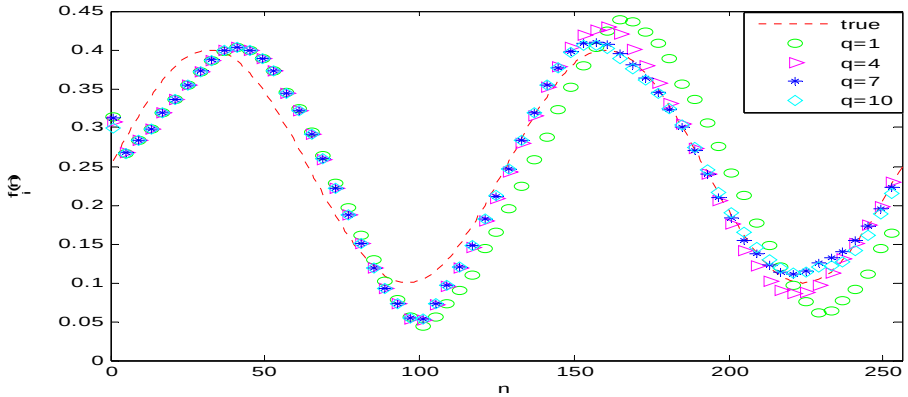

(b) Direct form (recursive)

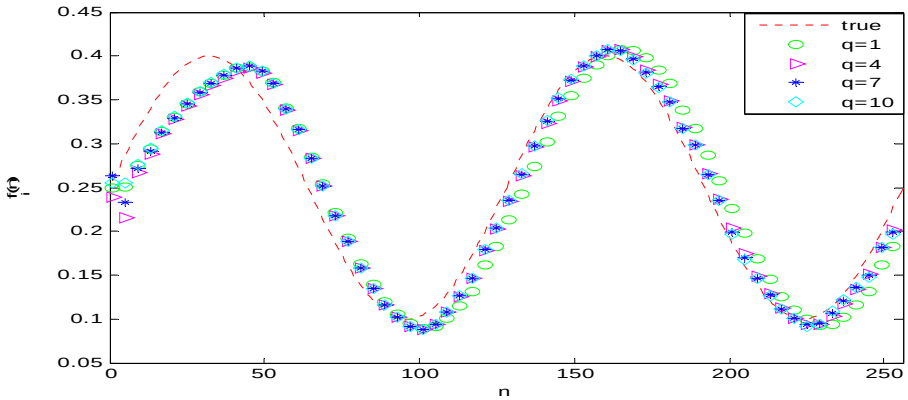

(c) Cascade form (Cartesian)

Figure 4.4: Instantaneous frequency estimates of the *signal 3* via the TVAR modeling in direct form (blockwise and recursive) and cascade form (Cartesian) with various basis dimensions ($q = 1,4,7,10$).

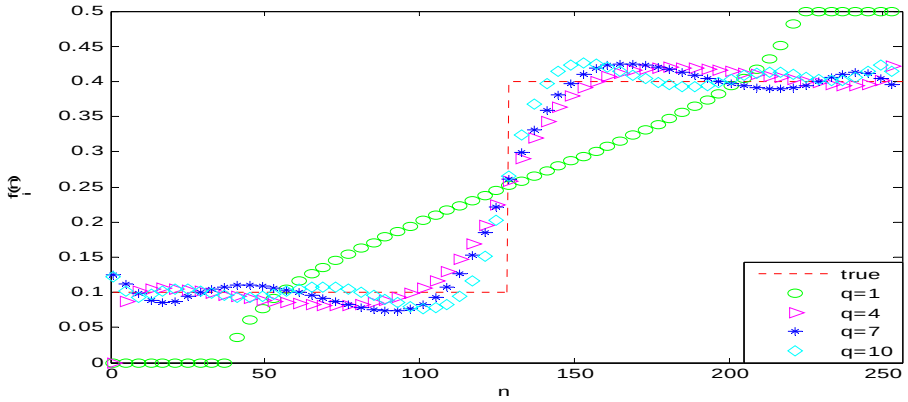

(a) Direct form (blockwise)

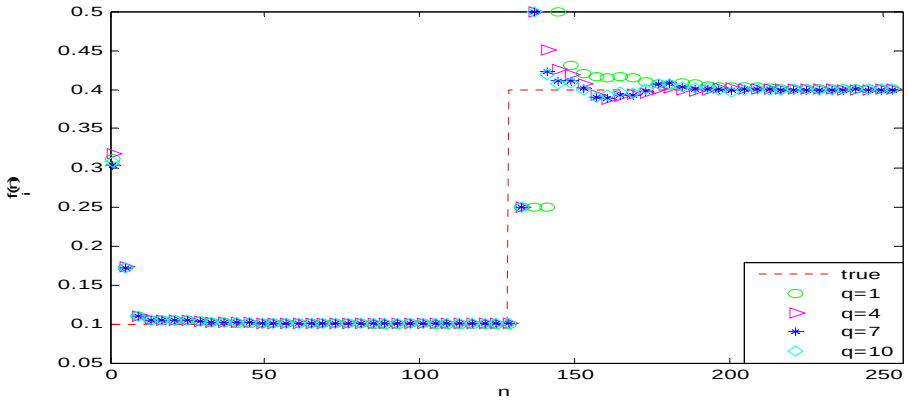

(d) Direct form (recursive)

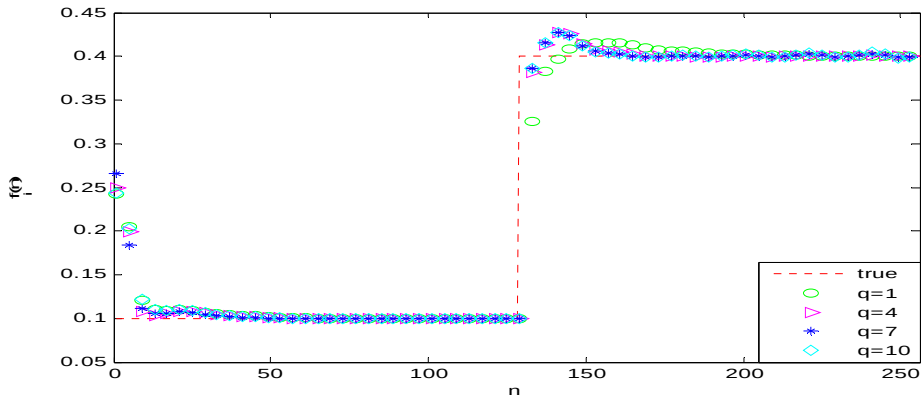

(c) Cascade form (Cartesian)

Figure 4.5: Instantaneous frequency estimates of the *signal 4* via the TVAR modeling in direct form (blockwise and recursive) and cascade form (Cartesian) with various basis dimensions ($q = 1,4,7,10$).

As shown in (a) of Figure 4.2-4.5, the instantaneous frequency (IF) estimates via the TVAR modeling in direct form (DF, blockwise) are based on the global *matching*, which heavily depends on the subspace spanned by the basis functions (BFs), so the basis dimension (BD) is an important factor on the estimation accuracy. When the BD is small, the blockwise DF can not even give the approximate trend of frequency variations, while the IF estimates approach to the true frequency trajectories with increasing BD. However, the IF estimates do not have a good match for the abrupt frequency change points, even when the BD is large enough.

As shown in (b) of Figure 4.2-4.5, the instantaneous frequency (IF) estimates via the TVAR modeling in direct form (DF, recursive) are based on the local *tracking*, which does not completely rely on the whole subspace spanned by the basis functions, so the basis dimension (BD) is not a critical factor. However, there are obvious delays between the IF estimates and true frequency trajectories when the BD is too small. The BD $q = 4$ is usually large enough, and further increase of BD will not improve but may degrade the performance due to over-parameterization. The recursive DF can track the abrupt change, but some large overshooting may occur in the IF estimates due to the unconstrained parameter estimation, which may also cause possible temporary model instabilities.

As shown in (c) of Figure 4.2-4.5, the instantaneous frequency (IF) estimates via the TVAR modeling in cascade form (CF) (Cartesian) show similar trends to those of the recursive direct form, but the Cartesian CF gives a closer approximation and smaller estimation delay with small basis dimension (BD). The parameterization in terms of TV poles enables a more direct approximation to the frequency variations than the parameterization in terms of transfer function coefficients, thus smaller BDs are needed by the Cartesian CF. Moreover, there is smaller overshooting in the IF estimates at the abrupt frequency change, since the constraints have been placed on the estimated poles.

Figure 4.6 (a)-(d) compares the *frequency estimation error* $\overline{FE}$ via the TVAR

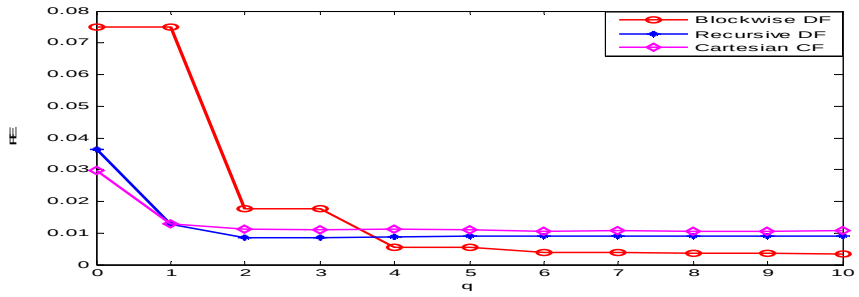

(a) Signal 1

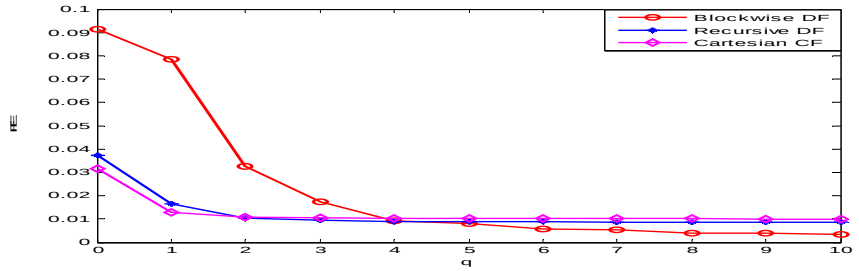

(b) Signal 2

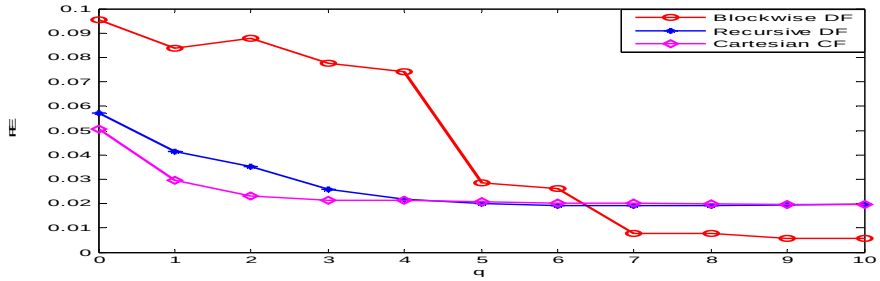

(c) Signal 3

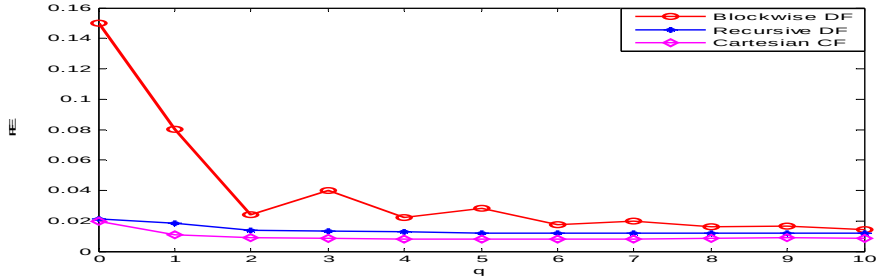

(d) Signal 4

Figure 4.6: $\overline{FE}$ of four sinusoidal signals via the TVAR modeling in direct form (blockwise and recursive) and cascade form (Cartesian) with various basis dimensions ($q = 0$ to 10).

modeling in direct form (DF, blockwise and recursive) and cascade form (CF, Cartesian) with various basis dimensions (BDs) ($q = 0$ to 10) for four sinusoidal signals respectively. With small BDs, the $\overline{FE}$ of the blockwise DF is much higher than those of the recursive DF and the Cartesian CF, and the $\overline{FE}$ of the Cartesian CF is slightly lower than that of the recursive DF. With large BDs, the $\overline{FE}$ of the recursive DF and the Cartesian CF are almost the same. The $\overline{FE}$ of the blockwise DF decreases lower than those of the recursive DF and Cartesian CF in the smooth frequency varying conditions but still keeps slightly higher in the frequency jump condition. In addition, larger BD is needed for the blockwise DF to match the complex frequency variation than the simple change, while the effect of different BDs is not obvious for the recursive DF and the Cartesian CF.

4.2.3 Effects of Different Basis Functions

To explore the influences of different basis functions (BFs) on the instantaneous frequency estimates, the following three types of common BFs ($0 \le j \le 10$), as shown in Figure 4.7, are also used in simulations on the four sinusoidal signals.

- ***Fourier series*** [MAA1983]

$$f_j(n) = \begin{cases} \cos\left(\frac{j\pi n}{2N}\right), & j \text{ even} \\ \sin\left(\frac{(j+1)\pi n}{2N}\right), & j \text{ odd} \end{cases} . \tag{4.8}$$

- ***Legendre polynomials*** [CD1974]

$$\begin{aligned} f_0(n) &= 1 \\ f_1(n) &= \frac{n}{N} \\ (j+1) f_{j+1}(n) &= (2j+1)\frac{n}{N} f_j(n) - j f_{j-1}(n) \end{aligned} \quad . \tag{4.9}$$

- ***Discrete prolate spheroidal sequence (DPSS)*** [DS1978]

  $f_j(n)$ is the j th sequence most concentrated in the frequency band $|w| \le 2\pi W$ with half bandwidth W.

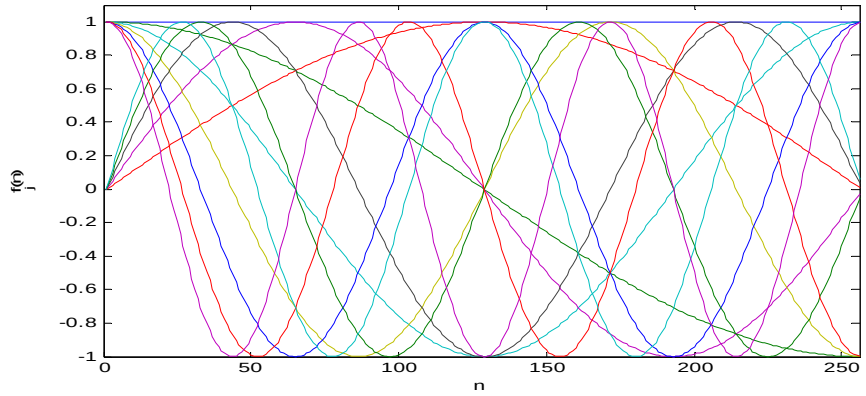

(a) Fourier Series

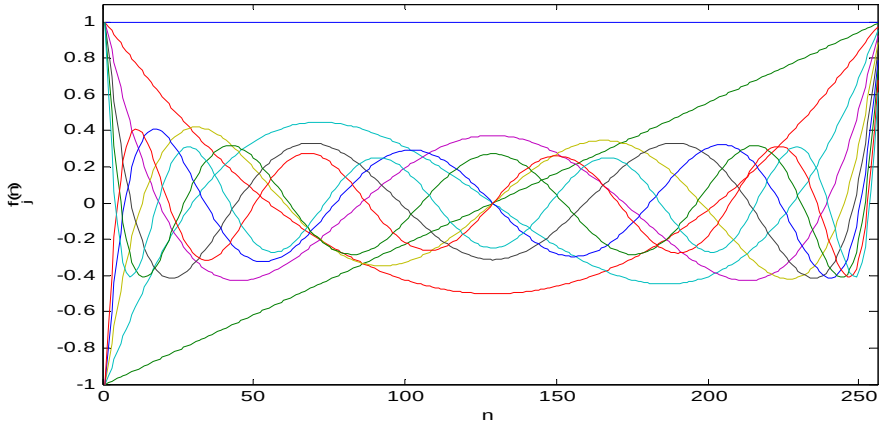

(b) Legendre Polynomials

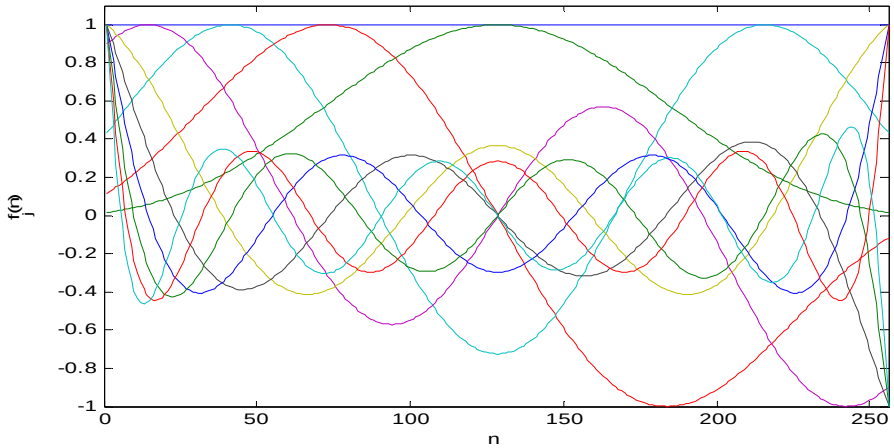

(c) Discrete prolate spheroidal sequence

Figure 4.7: Three types of basis functions ($j = 0$ to 10).

In addition to those commonly used BFs, some special BFs were used for certain conditions, such as the wavelet basis for obtaining multi-resolution [MG1993], the discrete Karhuen-Loeve transform (DKLT) for energy compaction [JP1996], and the walsh functions for burst-like dynamics [RHK2003]. However, these BFs may not be suitable for general approximation and the computational load for them is relatively high.

Figure 4.8 and Figure 4.9 show the *frequency estimation error* $\overline{FE}$ of the four sinusoidal signals via the TVAR modeling in direct form (DF, blockwise) and cascade form (CF, Cartesian) using different BFs with various basis dimensions ($q =$ 0 to 10) respectively.

For the blockwise direct form, as shown in Figure 4.8, only three lines can be seen on the plots for four basis functions (BFs), because the power time functions and the legendre polynomials have the same $\overline{FE}$. They are linearly related to each other and thus span the same subspace. When the basis dimension (BD) is relatively small, various BFs yield different estimation accuracy, because the subspace is not equally spanned. For linear and quadratic frequency changes, the discrete prolate spheroidal sequence (DPSS) is better than the other BFs. For periodic frequency changes, the Fourier series is slightly better than the others. For frequency jumps, the DPSS is the worst and the other BFs are similar. Therefore, there is no best BF suitable for all kinds of frequency variations, and the proper selection of BF partially depends on the dynamic characteristics of the nonstationary process being modeled. When the BD is large enough, the difference in the estimation accuracy among various BFs becomes insignificant, because the BFs with large BD approximately span the subspace equally.

For the cascade form (CF, Cartesian), as shown in Figure 4.9, the difference of estimation accuracy among various basis functions (BFs) is not obvious when the basis dimension is small, because the difference in the entire subspace has little influence on the local approximation performance. Moreover, the $\overline{FE}$ of the power time functions and the legendre polynomials are not the same, which shows again that the subspace is no

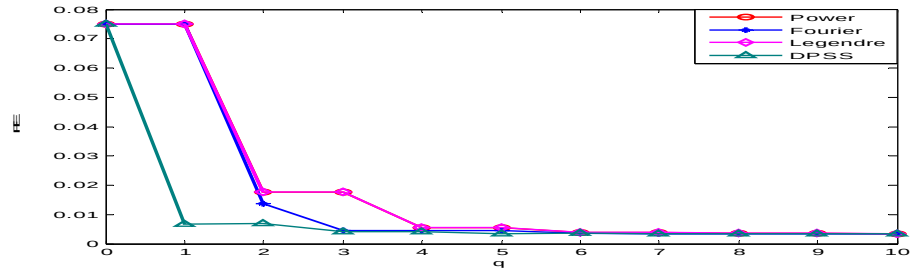

(a) Signal 1

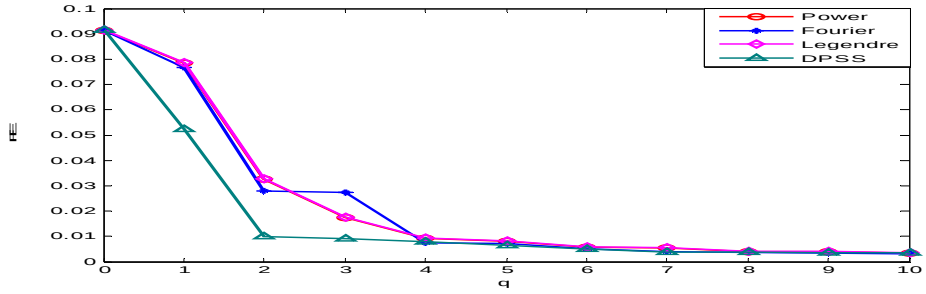

(b) Signal 2

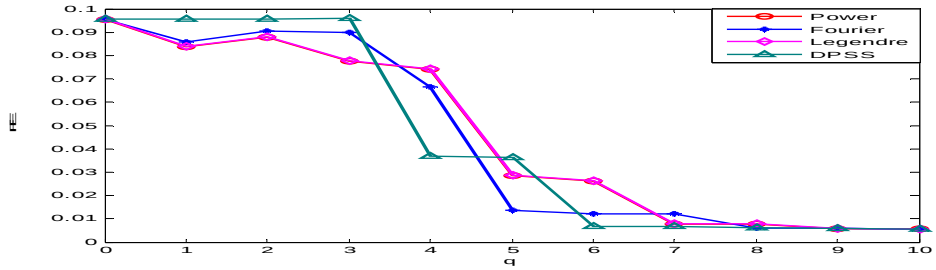

(c) Signal 3

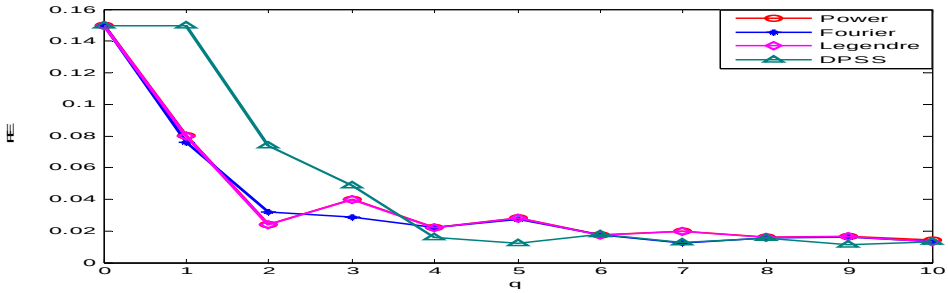

(d) Signal 4

Figure 4.8: $\overline{FE}$ of four sinusoidal signals via the TVAR modeling in direct form (blockwise) using different basis functions with various basis dimensions ($q = 0$ to 10).

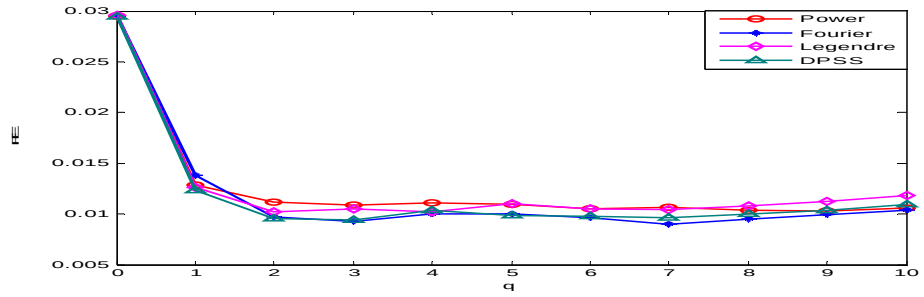

(a) Signal 1

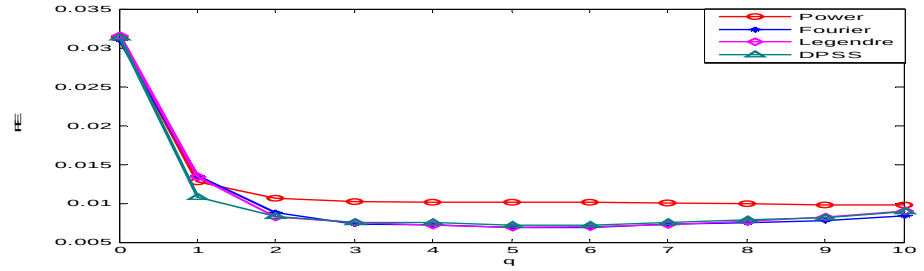

(b) Signal 2

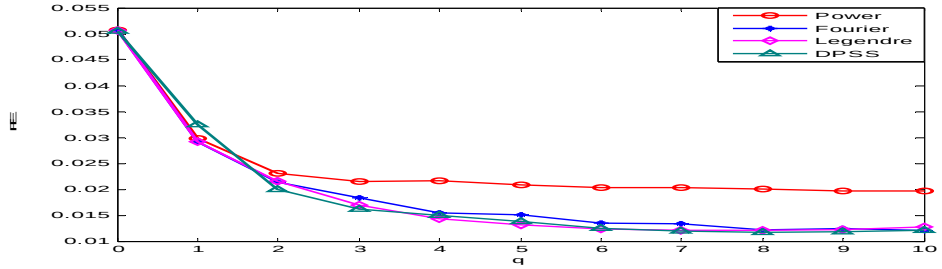

(c) Signal 3

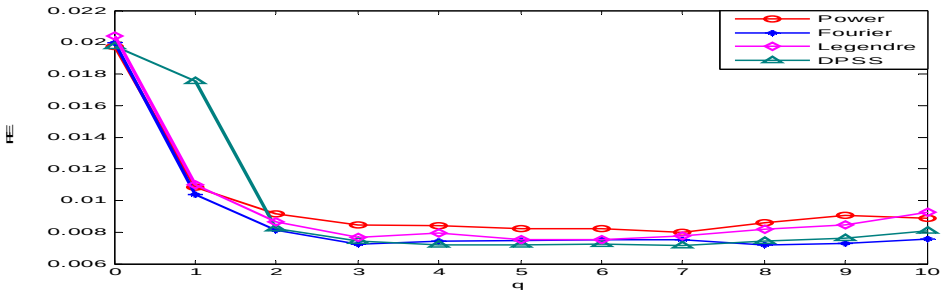

(d) Signal 4

Figure 4.9: $\overline{FE}$ of four sinusoidal signals via the TVAR modeling in cascade form (Cartesian) using different basis functions with various basis dimensions ($q = 0$ to 10).

longer a determinant factor as that for the direct form (blockwise). Different BFs give similar frequency estimation accuracy for linear frequency change and frequency jump, while the performance of power time functions is worse than the other BFs for quadratic and periodic frequency changes.

4.2.4 Influences of Additive White Noise

All the previous simulations are performed in the *noise-free* condition, in practice, there is additive white noise (AWN) in the observed signals. Thus, the influences of AWN on the instantaneous frequency estimation are studied at different *signal-to-noise ratios* (SNRs) and the model order is increased to account for the noise factor. Here, the synthetic sinusoidal signal with periodic frequency change, as described in equation (4.6), is used as an example.

Figure 4.10 shows the instantaneous frequency (IF) estimates of the *signal 3* via the TVAR modeling (model order $p = 2$) in direct form (DF, blockwise and recursive) and in cascade form (CF, Cartesian) at different SNRs, where the basis dimensions $q = 7,4,4$ are used for the three methods respectively. The corresponding $\overline{FE}$ is given in Table 4.1. For the three methods, there is negligible degradation on the IF estimates at high SNR (20dB) and the performance is acceptable at moderate SNR (10dB), while the performances deteriorate at low SNRs (5dB and 0dB). With decreasing SNR, the dynamic ranges of IF estimates are largely reduced from that of the true trajectory, especially for the Cartesian CF. The AR spectral estimate in the presence of additive white noise becomes a smoothed and flattened version of the AR spectral estimate under noise-free condition [SMK1988], so the ranges of peak frequencies (or the corresponding root frequencies) shrink. Moreover, for the recursive DF, some extreme overshooting (i.e. the normalized frequency of 0 and 0.5), occurs in IF estimates due to the unconstrained parameter estimation. Thus, the TVAR(2) model, which can sufficiently represent the sinusoidal signal with a single TV frequency under the noise-free condition, may no longer be valid for the signal with high noise.

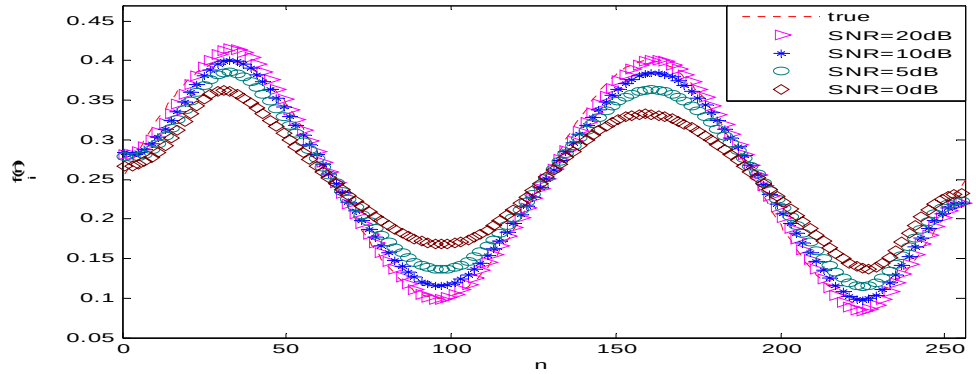

(a) Direct form (blockwise) with basis dimension $q = 7$

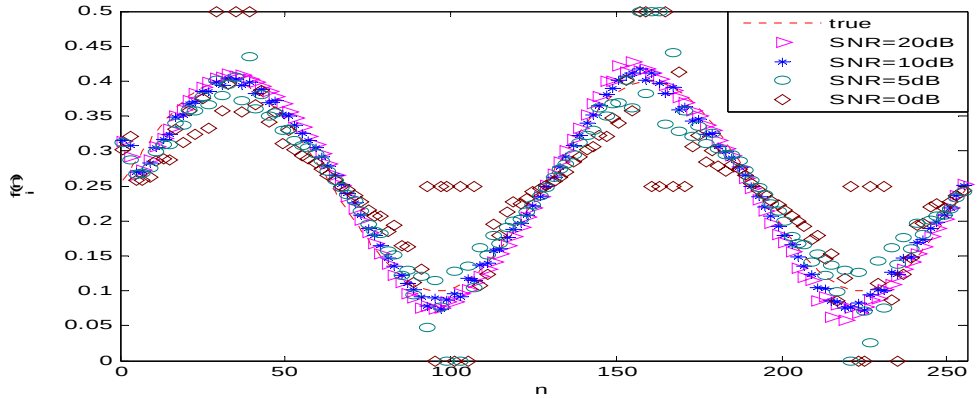

(b) Direct form (recursive) with basis dimension $q = 4$

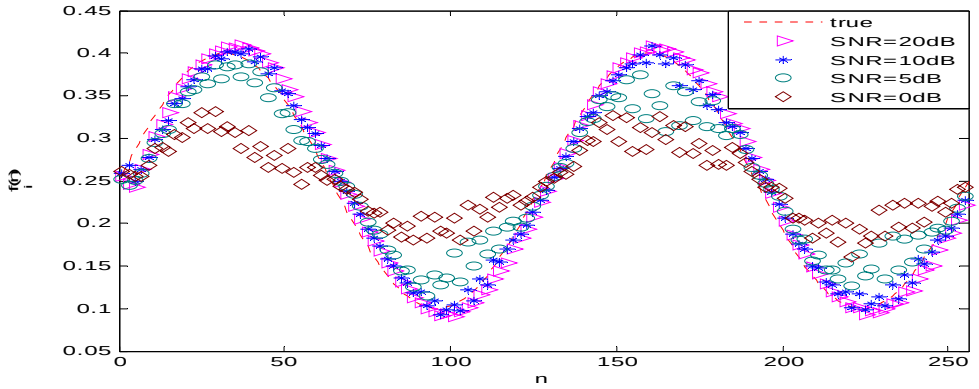

(c) Cascade form (Cartesian) with basis dimension $q = 4$

Figure 4.10: Instantaneous frequency estimates of the *signal 3* via the TVAR modeling (model order $p = 2$) in direct form (blockwise and recursive) and cascade form (Cartesian) at different signal-to-noise ratios (0,5,10,20 dB).

Table 4.1: $\overline{FE}$ of the *signal 3* via the TVAR modeling (model order $p = 2$) in direct form (blockwise and recursive) and cascade form (Cartesian) at different signal-to-noise ratios (0,5,10,20 dB).

SNR\ $\overline{FE}$	Direct form (blockwise, $q = 7$)	Direct form (recursive, $q = 4$)	Cascade form (Cartesian, $q = 4$)
20dB	0.0077	0.0113	0.0125
10dB	0.0119	0.0126	0.0131
5dB	0.0206	0.0221	0.0233
0dB	0.0390	0.0483	0.0535

Similar to the stationary case [SMK1988], a TVAR(p) process in additive white noise (AWN) algebraically becomes a TVARMA(p, p) process, which is shown in Appendix B. Also, a TVAR(∞) model can be used to represent a TVARMA(p, p) process, which is shown in Appendix C. To take into account the noise factor and reduce the bias in the IF estimates due to the model mismatch caused by the AWN, the TVAR model with higher order can be used to approximate the actual TVARMA(2,2) process. With the increasing model order, the desired IF estimate need to be chosen by picking the highest peak of the TVAR spectrum or finding the pole of the largest radius.

Figure 4.11 shows the instantaneous frequency (IF) estimates of the *signal 3* via the TVAR modeling (model order $p = 4$) in direct form (DF, blockwise and recursive) and in cascade form (CF, Cartesian) at different SNRs. The corresponding $\overline{FE}$ is given in Table 4.2. Using the TVAR(4) model, the frequency estimation accuracy is significantly improved at low SNRs (5dB and 0dB), particularly for the Cartesian CF. Increasing the model order at moderate or high SNR slightly improves the performance of the blockwise DF, however, it deteriorates the performances of the recursive DF and Cartesian CF. Particularly, the extreme overshooting appears again for the recursive DF at high SNR. The signal with low noise still approximates a TVAR(2) process, so the model of

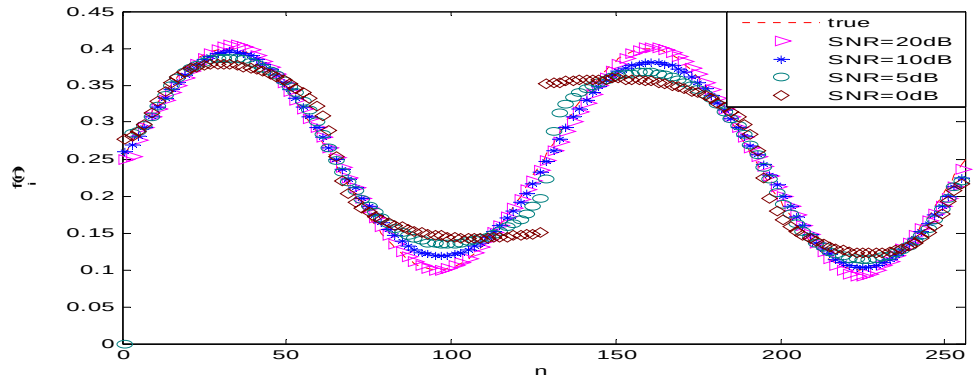

(a) Direct form (blockwise) with basis dimension $q = 7$

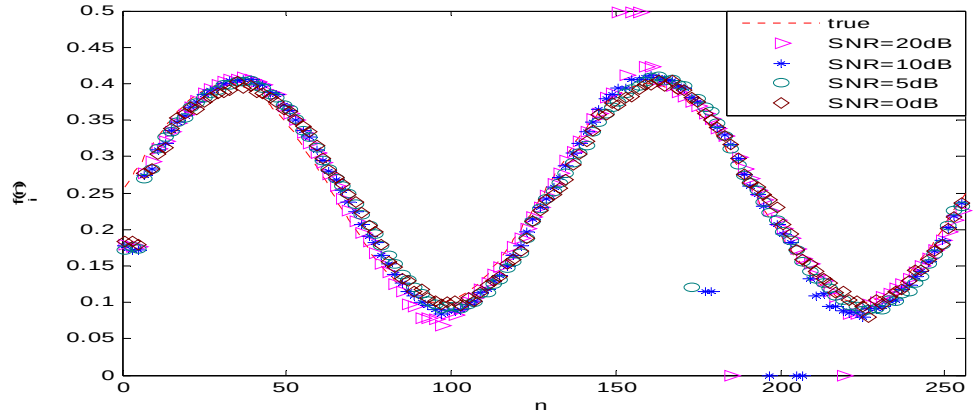

(b) Direct form (recursive) with basis dimension $q = 4$

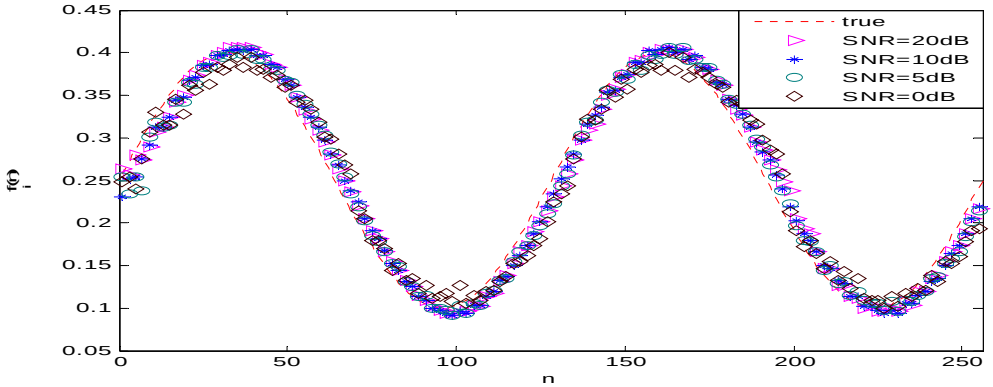

(c) Cascade form (Cartesian) with basis dimension $q = 4$

Figure 4.11: Instantaneous frequency estimates of the *signal 3* via the TVAR modeling (model order $p = 4$) in direct form (blockwise and recursive) and cascade form (Cartesian) at different signal-to-noise ratios (0,5,10,20 dB).

Table 4.2: $\overline{FE}$ of the *signal 3* via the TVAR modeling (model order $p = 4$) in direct form (blockwise and recursive) and cascade form (Cartesian) at different signal-to-noise ratios (0,5,10,20 dB).

SNR\ $\overline{FE}$	Direct form (blockwise, $q = 7$)	Direct form (recursive, $q = 4$)	Cascade form (Cartesian, $q = 4$)
20dB	0.0064	0.0221	0.0164
10dB	0.0093	0.0245	0.0162
5dB	0.0160	0.0191	0.0159
0dB	0.0232	0.0219	0.0197

over-determined order gives rise to spurious spectral peaks. The spurious peak is easier to be the highest peak for the recursive DF and Cartesian CF due to the random error in the local approximation. Moreover, using higher model order $p = 6$ will not further improve the performance even if at low SNR.

4.3 Experiments on Electromyography Data

In addition to simulations, experiments are also carried on real electromyography (EMG) data for frequency estimation in the study of muscle fatigue.

Surface EMG signals represent a random summation of action potentials propagating from many motor units which are activated during a particular movement. The surface EMG offers valuable information concerning the timing of muscular activity and its relative intensity [MJ1998]. It is commonly used in the study of muscle fatigue during sustained, isometric muscle contractions, as it can provide the electrophysiological properties of the muscle over time [ALG2003]. The myoelectric manifestations of muscle fatigue can be quantified by the time course of spectral variables of the EMG signal, and the most commonly used are the mean frequency (MNF) and median frequency. The MNF is used in our study, since it has less oscillation than the median frequency.

4.3.1 Experiment Procedures

4.3.1.1 Data Preprocessing

EMG data sampled at a rate of 50kHz were recorded from a healthy human object during voluntary isometric contractions at 60% MVC (maximum voluntary contraction) for 20 seconds. Before performing the frequency estimation, the EMG data are preprocessed as follows

- The original EMG data are down sampled with the new sampling rate of 2.5kHz, to reduce the data samples to be processed and thus the computational load.
- The down-sampled EMG data are then band-pass filtered with cutoff frequencies of 10Hz and 500Hz, in which the EMG signal contains most of its power, to eliminate the low and high frequency noise as well as other possible artifacts. The butterworth filter of order 2 is used because of its smooth pass band.
- The EMG data are finally segmented into consecutive and non-overlapping intervals of 0.5s (1250 samples). The mean of the data on each interval is subtracted, since the TVAR method is suitable for processing the signals with zero mean.

The EMG signal after down sampling and bandpass filtering is shown in Figure 4.12.

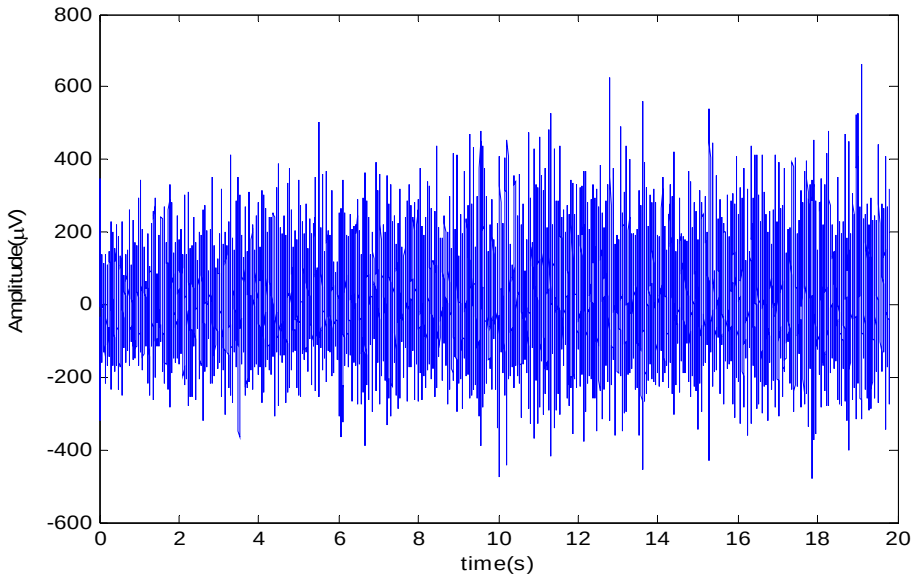

Figure 4.12: The EMG signal after down sampling and bandpass filtering (20s).

4.3.1.2 Mean Frequency Estimation

Using the short-time Fourier transform, the frequency spectrum of EMG signal in each interval is obtained through the Fourier transform, and the mean frequency (MNF) of each interval is computed as the average frequency of the power spectrum [ALG2003]

$$\overline{f} = \frac{\int_0^{f_s/2} f\left|H_x(f)\right|^2 df}{\int_0^{f_s/2} \left|H_x(f)\right|^2 df}, \tag{4.10}$$

where $H_x(f)$ is the frequency spectrum of EMG signal. The time course of $\overline{f}$ provides the basic information about the changes of the power spectrum over time.

Using the time-varying (TV) AR modeling, the instantaneous frequency (IF) estimates of the EMG signal are obtained in each interval, and the MNF is calculated as the time average of IFs [BB11992]

$$\overline{f_i} = \frac{\sum_{n=1}^{N} f_i(n) \mid x(n) \mid^2}{\sum_{n=1}^{N} \mid x(n) \mid^2}, \tag{4.11}$$

where $x(n)$ is the data sample of EMG signal. In [BB11992], it is stated that the average frequency in a signal's spectrum is equal to the time average of the IFs, that is $\overline{f} = \overline{f_i}$. In experiments, the TVAR model in direct form (DF, blockwise) and cascade form (CF, Cartesian, $\gamma = 0.02$) is used for IF estimates. Since there is some undesired overshooting in the IF estimates of the recursive DF, it is not used here. In experiments, the model order $p = 4$ and the Legendre polynomials are used as basis functions. Basis dimension $q = 10$ are found suitable for the blockwise DF, and $p = 2$ and $q = 4$ is suitable for the Cartesian CF. To eliminate the effect of random error in the IF estimates, only the IF estimates within the passband (10-500Hz) are used to calculate the MNF.

The initial value and the fall rate of the MNF are calculated by fitting a least-square regression line to the estimated MNF points, where the intercept and slope of the linear

regression curve serve as fatigue indices, since the MNF decreases with the onset of muscle fatigue.

4.3.2 Results and Discussions

Figure 4.13 shows the frequency spectrum via Fourier transform and the instantaneous frequency (IF) estimates via the TVAR modeling in direct form (DF, blockwise) and cascade form (CF, Cartesian) in one interval (0.5s). In Figure 4.13 (a), the frequency spectrum shows that the EMG signal contains most of its power in frequencies less than 200Hz, mainly within the range of 50-100Hz. However, the spectrum does not provide any information about the changes in the signal's frequency content over the time. In Figure 4.13 (b), the IF estimates via the TVAR modeling give a view of the frequency variations over the time. The blockwise DF shows the average trend of frequency changes through its global *matching* and implicit *averaging*, while the Cartesian CF shows the frequency variations at each time instant through its local *tracking*. Actually, the IF estimates obtained by the Cartesian CF gives the approximate frequency trajectories around the average trend obtained by the blockwise DF.

Figure 4.14 shows the frequency spectrum via Fourier transform and the probability distributions of instantaneous frequency (IF) estimates (within the passband) via the TVAR modeling in direct form (DF, blockwise) and cascade form (CF, Cartesian) over the entire EMG data interval (20s). In Figure 4.14(a), the power distribution of the EMG signal shows that most of signal power is contained in the range of 0-200Hz and the power peak is about 60-80Hz. In Figure 4.14(b), the probability distribution of the *average* frequency variations obtained by the blockwise DF is in the range of 50-100Hz. In Figure 4.14(c), the probability distribution of *instant* frequency variations obtained by the Cartesian CF is within a larger frequency range of 10-200Hz, which is fit with the power distribution in frequency spectrum.

Figure 4.15 shows the time course of the mean frequency (MNF) estimates via the short-time Fourier transform (STFT) and TVAR modeling in direct form (DF, blockwise)

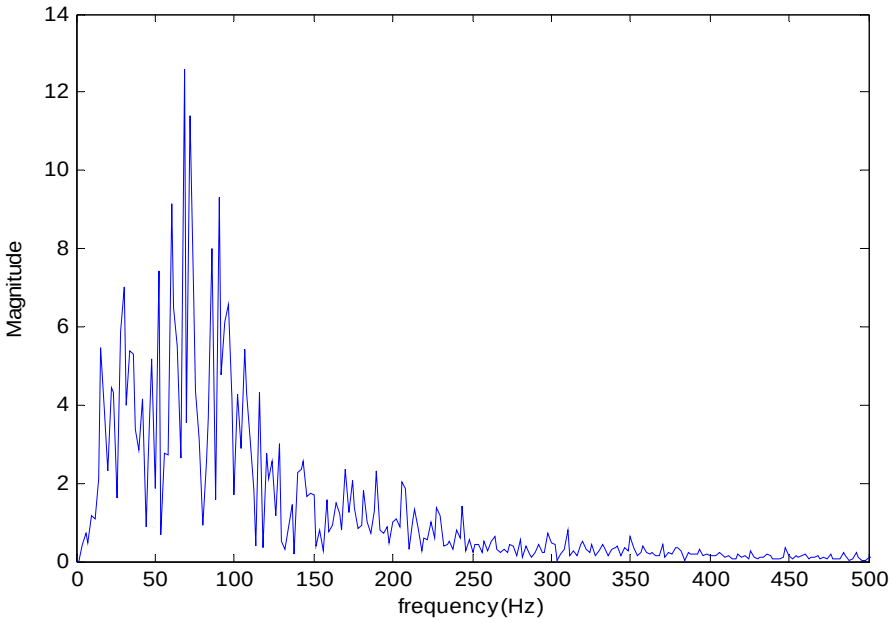

(a) Frequency spectrum via Fourier transform

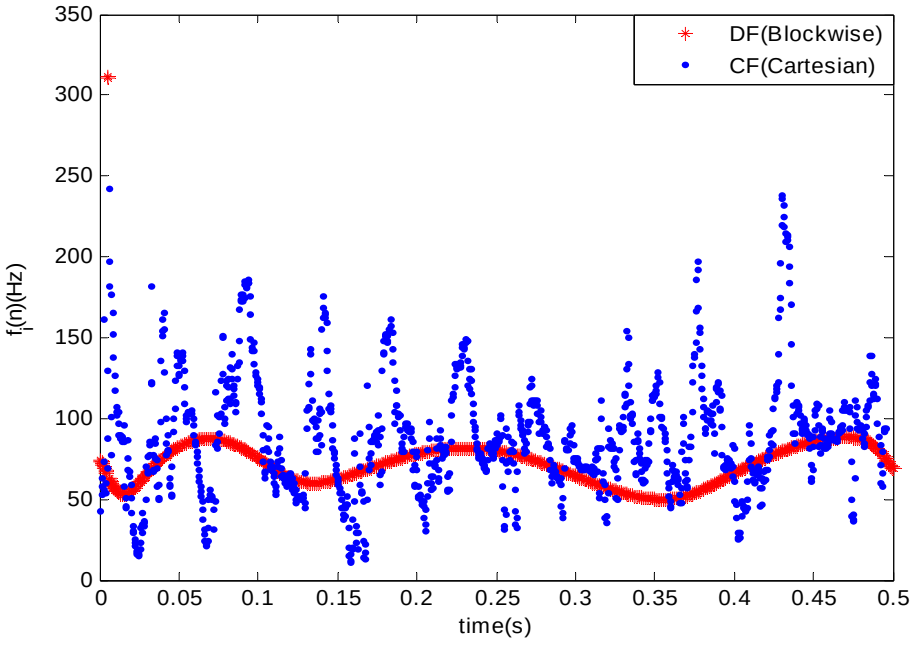

(b) Instantaneous frequency estimates via TVAR modeling in direct form (blockwise) and cascade form (Cartesian)

Figure 4.13: Frequency spectrum and instantaneous frequency estimates of the EMG signal in one interval (0.5s).

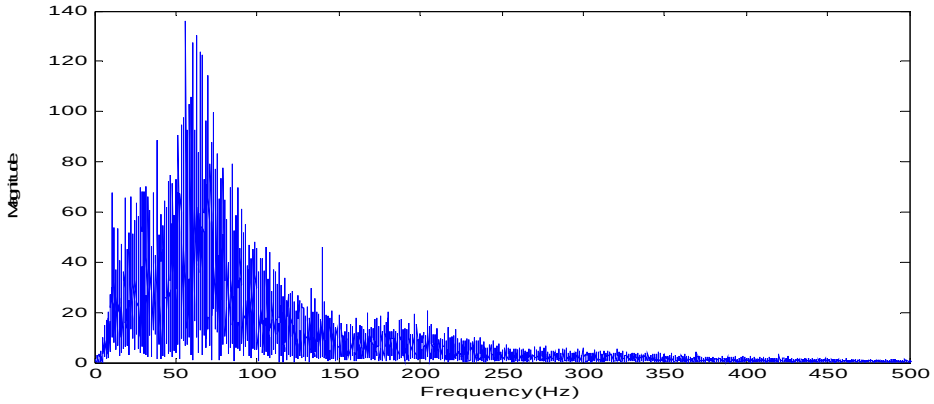

(a) Frequency spectrum

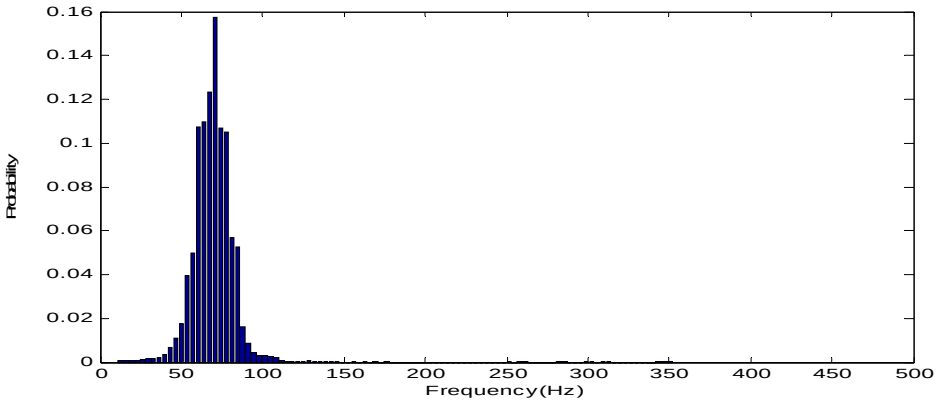

(b) Probability distribution of instantaneous frequency estimates (direct form, blockwise)

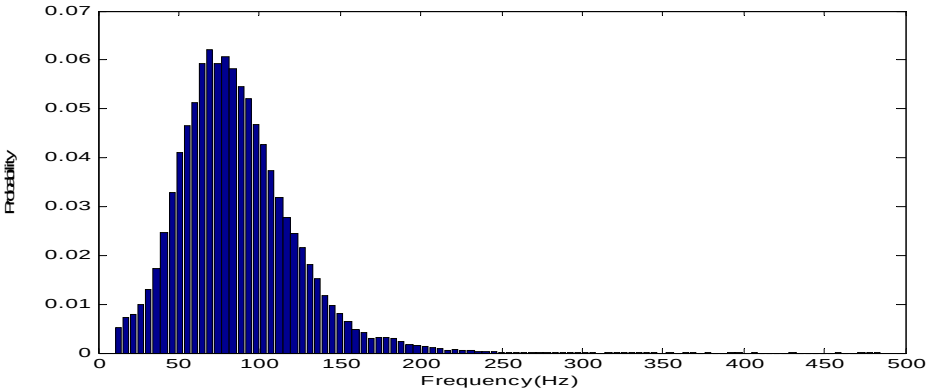

(c) Probability distribution of instantaneous frequency estimates (cascade form,Cartesian)

Figure 4.14: Frequency spectrum via Fourier transform and probability distributions of instantaneous frequency estimates via the TVAR modeling in direct form and cascade form over the entire EMG data interval (20s).

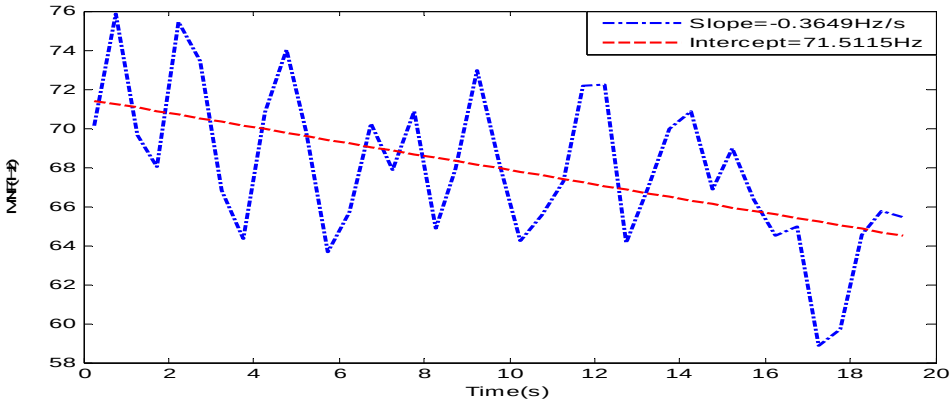

(a) Short-time Fourier transform

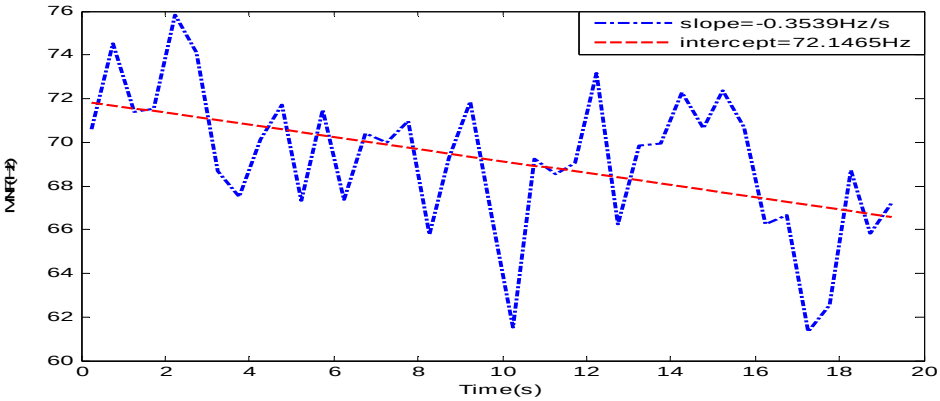

(b) TVAR modeling in direct form (blockwise)

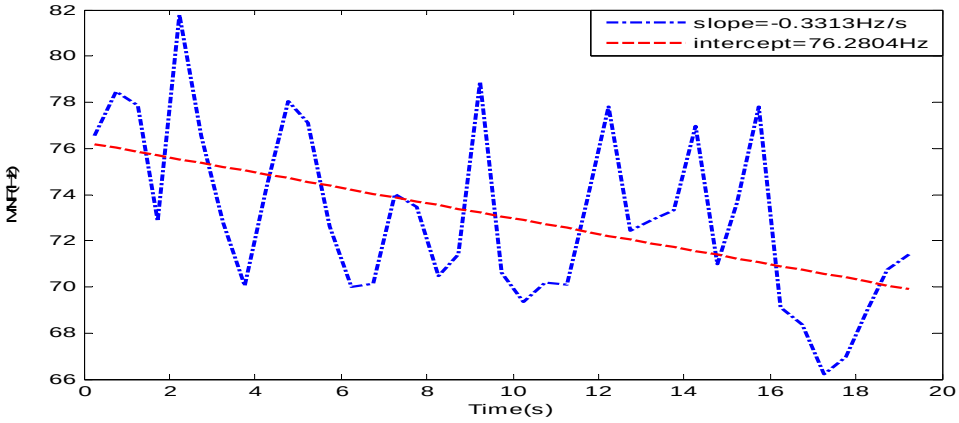

(c) TVAR modeling in cascade form (Cartesian)

Figure 4.15: Time course of the mean frequency estimates via short-time Fourier transform and the TVAR modeling in direct form and cascade form.

and cascade form (CF, Cartesian). The MNF estimates via the TVAR modeling in Figure 4.15 (b) and (c) decrease with the time and have similar variations to that of the conventional STFT in Figure 4.15 (a). Thus, the MNF can be correctly obtained via the TVAR modeling, which also verifies that the average frequency in a signal's spectrum is equal to the time average of the instantaneous frequencies (Ifs). The MNF estimates of the Cartesian CF are larger than those of the STFT and the blockwise DF, because there are some large IF values in the estimates. The slope and intercept of the linear regression line obtained by the blockwise DF is closer to those of the STFT than those of the Cartesian CF.

4.4 Chapter Summary

Simulations were performed on synthetic sinusoidal signals with different frequency variations for instantaneous frequency estimation via the time-varying (TV) AR modeling in direct form and cascade form. Experiments were also carried on real EMG data for mean frequency estimation in the analysis of muscle fatigue.

Compared with the short-time Fourier transform (STFT), both higher time and frequency resolutions are achieved in IF estimates via the TVAR modeling. For the TVAR model in direct form (DF, blockwise), the basis dimension (BD) is an important factor on frequency estimation accuracy and the relatively large BD is needed. Various basis functions (BFs) yield different frequency estimation accuracy for small BD, and the difference becomes insignificant with increasing BD. For the TVAR model in DF (recursive) and cascade form (CF, Cartesian), the influences of BD are negligible when the BD is not too small, and different BFs yield similar frequency estimation accuracy (except for the power time functions). Large additive white noise (AWN) present in the signal reduces the accuracy and dynamic range of IF estimates. The degradation caused by the AWN can be reduced by using the TVAR model of higher order, since it approximates the actual TVARMA process for the noisy signal.

The average trend of frequency variations and instant frequency trajectories of the EMG signal were obtained via the TVAR modeling in direct form (DF, blockwise) and cascade form (CF, Cartesian) respectively. The mean frequency (MNF) from the time average of IF estimates via the TVAR modeling in DF and CF are similar to that from the average of power spectrum via the conventional STFT.

CHAPTER V

Thesis Summary and Further Research

5.1 Thesis Summary

Nonstationary signal modeling is a research topic of practical interest, and the time-varying (TV) signal can be analyzed using the *nonparametric* and *parametric* methods. The *nonparametric* approaches are based on time-dependent spectral analysis, including the short-time Fourier transform, time-frequency representation, and evolutionary spectrum, where tradeoff exists between the time and frequency resolutions. The *parametric* approaches are based on TV linear predictive models, which can achieve high time and frequency resolutions. The model parameters can be estimated using the gradient-based adaptive algorithms, Kalman filtering and basis function (BF) methods. In this study, we adopt the TVAR model using the BF parameter estimation method to identify the nonstationary process and estimate the instantaneous frequencies.

The current TVAR model in direct form (DF) with two basis function (BF) methods was reviewed. One is the blockwise least-squares (LS) BF method with parameter *matching* over a block of data at one time, where a relatively large basis dimension is needed to obtain good global optimization. The other is the recursive weighted-least-squares (WLS) BF method with parameter *tracking* upon each data sequentially, where a relatively small basis dimension is enough to obtain suitable local approximation. Simulations on synthetic data demonstrate that the TVAR model in DF with two BF methods performs well in system identification and instantaneous frequency estimation, with equivalent overall performance. However, the large estimation error at the ends of the *analysis* interval and the abrupt change points may cause temporary instabilities of the estimated TVAR model, where using the recursive BF method is more easily to become instable than using the blockwise BF method.

The limitations associated with the TVAR model in direct form (DF), i.e. possibly temporary instability, inconvenient pole tracking and unnatural representation of time variations in frequencies, motivate the proposition of the TVAR model in cascade form (CF). The TVAR model in CF was formulated through the parameterization in terms of TV poles, with possible pole representations in form of second-order section coefficients, Cartesian coordinates or polar coordinates, where the time variation of each pole parameter is assumed to be the linear combination of basis functions. Due to the cascaded error gradient generating process, the system equations for the TVAR model in CF are nonlinear with respect to basis coefficients, so the basis coefficient estimates are calculated iteratively using the Gauss-Newton algorithm.

Simulations on synthetic data generated by the TV filter of single pole pair are used to demonstrate the performances of the TVAR model in cascade form (CF) with different forms of TV pole representation. During the analysis process, the estimated TV poles can be easily constrained within the unit circle, so the model stability is guaranteed. The TVAR model in CF show similar performance trends to that in direct form (DF) using the recursive BF method, because of the sequential basis coefficients estimate update. Due to its natural and robust approximation of time variations in frequencies, the Cartesian coordinate representation shows its superior performance among four forms of TV pole representation and outperforms the recursive DF. The CF with other TV pole representations does not gain performance advantage over the DF. Simulations are also carried on synthetic data generated by the TV filter of double pole pairs to explore the benefits of individual pole estimation in each cascade section. Using the CF model, the poles are adjusted separately in each section, so the actual varying trend of each frequency can be finely tracked when there are several frequency components in the nonstationary signal. In addition to stability control, the constraints placed on the estimated TV poles also help avoid the possible extreme overshooting in frequency estimates, as that occurred for the recursive DF, caused by the random oscillation in local estimations.

The performance characteristics of instantaneous frequency (IF) estimation via the TVAR modeling in direct form (DF, blockwise and recursive) and cascade form (CF, Cartesian) were explored through simulations on synthetic sinusoidal signals with different frequency variations. Compared with the *spectrogram* obtained by the short-time Fourier transform, both higher time and frequency resolutions are achieved in IF estimates via the TVAR modeling. The influences of various basis dimensions (BDs), different basis functions (BFs) and additive white noise (AWN) on the IF estimates of the three methods were investigated. For the TVAR model in DF (blockwise), the BD is an important factor on frequency estimation accuracy and the relatively large BD is needed. Various BFs with small BDs yield different estimation accuracy, and the performance difference becomes insignificant with increasing BD. For the TVAR model in DF (recursive) and CF (Cartesian), the influences of BD are negligible and different BFs yield similar frequency estimation accuracy (except for the power time functions), when BD is not too small**.** The accuracy and dynamic range of IF estimates are reduced when there is large AWN present in the observed signal. The degradation caused by the AWN can be reduced by using the TVAR model of higher order, since it approximates the actual TVARMA process for the noisy signal.

Experiments were carried on the real electromyography (EMG) data for frequency estimation in the analysis of muscle fatigue. The average trend of frequency variations and instant frequency trajectories of the EMG signal were obtained via the TVAR modeling in DF (blockwise) and CF (Cartesian) respectively. The time course of the mean frequency (MNF) estimates obtained from the time average of IF estimates via the TVAR modeling are similar to that obtained from the average of frequency spectrum via the conventional Fourier transform method.

5.2 Further Research

In this thesis, the preliminary study has been done on the proposed time-varying (TV) AR model in cascade form, where some ideal assumptions are made to simplify the

modeling process. Further research can be carried to explore the comprehensive characteristics of the TVAR modeling in cascade form.

In this study, the model order is assumed to be known for the analysis process. In practice, the exact number of frequency components in the nonstationary process is unknown, so the model order determination is necessary, especially when the signal is noise-free or of very low noise. For the noisy signal, the determination of model order is less required, because the TVAR model with higher order is suitable to reduce noise effects at low SNR. Some current methods may be used to determine the proper model order, such as the maximum likelihood estimation in [KBE1999] and the optimal parameter search (OPS) method in [RHK2003].

Using the TVAR model of higher order is one simple method to account for the additive white noise factor in the observed signals, but the proper model order may not be easy to determine. The additive white noise in the observed signal causes the bias in the parameter estimates, and the modified least-squares estimator may be derived to subtract the bias from the estimate, similar to the bias compensation method in [GMJ1986].

In addition to the basic experiments on the real EMG data. More investigations can be performed on the instantaneous frequency estimation of the EMG signal, such as using various analysis interval lengths and at different levels of MVC (maximal voluntary contraction). Moreover, the TVAR modeling methods are not only useful to the muscle fatigue analysis, they may also be used in other applications, such as the predictive speech coding [MAA1983], ultrasound attenuation estimation [JFADF1998], and radar signature extraction [KBE1999].

REFERENCES

[AAL1994] A. S. Kayhan, A. El-Jaroudi, and L. F. Chaparro, “Evolutionary periodogram for nonstationary signals,” *IEEE Trans. on Signal Processing*, vol. 42, no. 6, pp. 1527-1536, Jun. 1994.

[AAL1995] A. S. Kayhan, A. El-Jaroudi, and L. F. Chaparro, “Data-adaptive evolutionary spectral estimation,” *IEEE Trans. on Signal Processing*, vol. 43, no. 1, pp. 204-213, Jan. 1995.

[AD1990] A. Nehorai and D. Starer, “Adaptive pole estimation,” *IEEE Trans. on Acoustics, Speech, and Signal Processing*, vol. 38, no. 5, pp. 825-838, May 1990.

[AL1994] A. Akan and L. F. Chaparro, “Adaptive time-varying parametric modeling,” in *Proc. of IEEE Int. Conf. on Acoustics, Speech and Signal Processing*, vol. 4, pp. 13-16, Adelaide, Australia, Apr. 1994.

[ALG2003] A. Georgakis, L. K. Stergioulas, and G. Giakas, “Fatigue analysis of the surface EMG signal in isometric constant force contractions using the averaged instantaneous frequency,” *IEEE Trans. on Biomedical Engineering*, vol. 50, no. 2, pp. 262-265, Feb. 2003.

[BB11992] B. Boashash, “Estimating and interpreting the instantaneous frequency of a signal—Part 1: Fundamentals,” *IEEE Proceedings*, vol. 80, no. 4, pp. 520-538, Apr. 1992.

[BB21992] B. Boashash, “Estimating and interpreting the instantaneous frequency of a signal—Part 2: Algorithms and applications,” *IEEE Proceedings*, vol. 80, no. 4, pp. 540-568, Apr. 1992.

[CD1974] C. P. Neuman and D. I. Schonbach, “Discrete (Legendre) orthogonal polynomials,” *Intl. Journal for Numerical Methods in Eng.*, vol. 8, pp. 743-770, 1974.

[DS1978] D. Slepian, “Prolate spheroidal wave functions, Fourier analysis and uncertainty, Part V: The discrete case,” *Bell Syst. Tech. J.*, vol. 57, no. 5, pp. 1371-1430, May-June, 1978

[DT1990] D. L. Jones and T. W. Parks, “A high resolution data-adaptive time-frequency representation,” *IEEE Trans. on Acoustics, Speech, and Signal Processing*, vol. 38, no. 12, pp. 2127-2135, Dec. 1990.

[FF1980] F. Kozin and F. Nakajima, “The order determination problem for linear time-varying AR models,” *IEEE Trans. on Automatic Control*, vol. AC-25, no. 2, pp. 250-257, Apr. 1980.

[FG1992] F. Hlawatsch and G. F. Boudreaux-Bartels, “Linear and quadratic time-frequency signal representations,” *IEEE Signal Processing Mag.*, pp. 21-67, Apr. 1992.

[FK1977] F. Kozin, “Estimation and modeling of nonstationary time series,” in *Proc. Symp. Appl. Comput. Meth. Eng.*, vol. 1, pp. 603-612, Los Angeles, CA, 1977.

[GMJ1986] G. Alengrin, M. Barlaud and J. Menez, “Unbiased parameter estimation of nonstationary signals in noise,” *IEEE Trans. on Acoustics, Speech, and Signal Processing*, vol. ASSP-34, no. 5, pp. 1319-1322, Oct. 1986.

[HC1961] H. Cramer, “On some classes of nonstationary stochastic processes”, in *Proc. 4th Berkeley Symp. on Math. Statist., and Probability*, vol. 2, Los Angeles, CA: University of California Press, 1961.

[HW1989] H. I. Choi and W. J. Williams, “Improved time-frequency representation of multicomponent signals using exponential kernels,” *IEEE Trans. on Acoustics, Speech, and Signal Processing*, vol. 37, no. 6, pp. 862-871, June 1989.

[JFADF1998] J. M. Girault, F. Ossant, A. Ouahabi, D. Kouame, and F. Patat, “Time-varying autoregressive spectral estimation for ultrasound attenuation in tissue characterization,” *IEEE Trans. on Ultrasonics, Ferroelectrics, and Frequency Control*, vol. 45, no. 3, pp. 650-659, May 1998.

[JJS1987] J. J. Shynk, “Performance of alternative adaptive IIR filter realizations,” *in Proc. 21st Asilomar Conf. on Signals, Systems, Computers*, Pacific Grove, California, pp. 144-150, Nov. 1987.

[JP1996] J. J. Rajan and P. J. W. Rayner, “Generalized feature extraction for time-varying autoregressive models”, *IEEE Trans. on Signal Processing*, vol. 44, no. 10, Oct. 1996.

[KB1984] K. C. Sharman and B. Friedlander, “Time-varying autoregressive modeling of a class of nonstationary signals,” in *Proc. of IEEE Int. Conf. on Acoustics, Speech and Signal Processing*, vol. 9, pp. 227-230, San Diego, CA, Mar. 1984.

[KBE1999] K. B. EOM, “Time-varying autoregressive modeling of HRR radar signatures,” *IEEE Trans. on Aerospace and Electronic Systems*, vol. 35, no. 3, pp. 974-988, July 1999.

[LAL1975] L. A. Liporace, “Linear estimation of nonstationary signals,” *J. Acoust. Soc. Am.*, vol. 58, no. 6, pp. 1288-1295, Dec. 1975.

[LC1989] L. Cohen, “Time-frequency distribution-A review,” *Proc. IEEE*, vol. 77, pp-941-981, July 1989.

[LM1985] L. F. Chaparro and M. Boudaoud, “Recursive solution of the covariance equations for linear prediction,” *J. Franklin Inst.*, vol. 320, pp. 161-167, Sept. 1985.

[LS1978] L. B. Jackson and S. L. Wood, “Linear prediction in cascade form,” *IEEE Trans. on Acoustics, Speech and Signal Processing*, vol. ASSP-26, no. 6, pp. 518-528, Dec. 1978.

[LT1983] L. Ljung and T. Soderstrom, *Theory and Practice of Recursive Identification*, Cambridge, Mass: MIT Press, 1983.

[MAA1983] M. G. Hall, A. V. Oppenheim, and A. S. Willsky, “Time-varying parametric modeling of speech,” *Elsevier Signal Processing*, vol. 5, no. 3, pp. 267-285, May 1983.

[MBP1988] M. B. Priestley, *Non-linear and Non-stationary Time Series Analysis*, Academic Press Inc., San Diego, CA, 1988.

[MBTA1977] M. Morf, B. Dickinson, T. Kailath, and A. Vieira, “Efficient solution of covariance equations for linear prediction,” *IEEE Trans. on Acoustics, Speech, and Signal Processing*, vol. ASSP-25, no. 5, pp. 429-433, Oct. 1977.

[MG1993] M. K. Tsatsanis and G. B. Giannakis, “Time-varying system identification and model validation using wavelet,” *IEEE Trans. on Signal Processing*, vol. 41, no. 12, Dec. 1993.

[MJ1998] M. Ferdjallah and J. J. Wertsch, “Anatomical and technical considerations in surface electromyography,” in *Phyical Medicine and Rehabilitation Clinics of North America*, vol. 9, no. 4, pp. 925-930, Nov. 1998.

[MJJ1998] M. Juntunen, J. Tervo, and J. P. Kaipio, “Stabilization of stationary and time-varying autoregressive models,” in *Proc. IEEE Int. Conf. on Acoustics, Speech and Signal Processing*, vol. 4, pp. 2173-2176, Seattle, WA, May 1998.

[ML1985] M. Boudaoud and L. F. Chaparro, "Composite modeling of nonstationary signals," *J. Franklin Institute,* vol. 320, pp. 113-124, Sept. 1985.

[MN1987] M. Niedzwiecki, “Recursive functional series modeling estimators for adaptive control of time-varying plants,” in *Proc. 26th Conf. on Decision and Control*, pp. 1239-1244, Los Angeles, CA, Dec. 1987.

[MNI1987] M. Niedzwiecki, “Functional series modeling identification of nonstationary stochastic systems--The clipping technique,” in *Proc. of ISSPA on Signal Processing, theories, implementations and Applications*, pp. 321-326, Brisbane, Australia, 1987.

[MN1988] M. Niedzwiecki, “Functional series modeling approach to identification of nonstationary stochastic systems,” *IEEE Trans. on Automatic Control*, vol. 33, no. 10, pp. 955-961, Oct. 1988.

[MN2000] M. Niedwiecki, *Identification of Time-varying Processes*, John Wiley & Sons, Chichester, England, 2000.

[MW1989] M. Nayeri and W. K. Jenkins, “Alternate realizations to adaptive IIR filters and properties of their performance surfaces,” *IEEE Trans. on Circuits and Systems*, vol. 36, no. 4, pp. 485-496, Apr. 1989.

[MWHRC1998] M. Arnold, W. H. R. Miltner, H. Witte, R. Bauer, and C. Braun, “Adaptive AR modeling of nonstationary time series by means of Kalman filtering,” *IEEE Trans. on Biomedical Engineering*, vol. 45, no. 5, pp. 553-562, May 1998.

[RHK2003] Rui Zou, Hengliang Wang, and Ki H. Chon, “A robust time-varying identification algorithm using basis functions,” *Annals of Biomedical Engineering*, vol. 31, pp. 840-853, 2003.

[RMGJ1987] R. Charbonnier, M. Barlaud, G. Alengrin, and J. Menez, "Results on AR modeling of nonstationary signals," *Elsevier Signal Processing*, vol. 12, no.2, pp. 143-151, Mar. 1987.

[SH1996] S. Haykin, *Adaptive Filter Theory, Third Edition*, Englewood Cliffs, NJ: Prentice Hall, 1996.

[SJO1996] S. J. Orfanidis, *Introduction to Signal Processing.* Englewood Cliffs, NJ: Prentice-Hall, 1996.

[SL1986] S. J. Orfanidis and L. M. Vail, "Zero-tracking adaptive filters," *IEEE Trans. on Acoustics, Speech and Signal Processing*, vol. ASSP-34, no. 6, pp. 1566-1572, Dec. 1986.

[SMK1988] S. M. Kay, *Modern Spectral Estimation: Theory and Application*, Englewood Cliffs, N. J.: Prentice Hall, 1988.

[TSR1970] T. S. Rao, "The fitting of non-stationary time-series models with time-dependent parameters," *J. Royal Statist. Soc. Series B*, vol. 32, no. 2, pp. 312-322, 1970.

[YLI1990] Y. Zhao, L. E. Atlas, and I. R. J. Marks, "The use of cone-shaped kernels for generalized time-frequency representation of nonstationary signals," *IEEE Trans. on Acoustics, Speech, and Signal Processing*, vol. 38, no. 7, pp. 1084-1091, July 1990.

[YG1983] Y. Grenier, "Time-dependent ARMA modeling of nonstationary signals," *IEEE trans. on Acoustics, Speech, and Signal Processing*, vol. ASSP-31, no. 4, pp.899-911, Aug. 1983.

[YPY1987] Y. H. Tam, P. C. Ching and Y. T. Chan, "Adaptive recursive filters in cascade form," *IEE Proceedings*, vol. 134, Pt. F., no. 3, pp. 245-252, Jun. 1987.

APPENDIXES

A. Represent a sinusoidal signal with a single time-varying frequency using a second order recursion

Using the trigonometric identities, it can be shown that the sinusoid signal $x(n) = \cos[2\pi f_i(n)]$ with a single time-varying (TV) frequency satisfies the second order recursion as

$$x(n) = -c_1(n)x(n-1) - c_2(n)x(n-2), \tag{A.1}$$

where $c_1(n) \approx -2\cos 2\pi\left[f_i(n-1)\right]$ and $c_2(n) \approx 1$. This recursion is valid for a sinusoidal signal with different frequency variations, such as linear, quadratic and periodic TV frequency, which is shown in the following.

A.1 Linearly TV Frequency

A sinusoidal signal with a linearly TV frequency can be expressed as

$$\begin{aligned} x(n) &= \cos 2\pi\left[(f_0 + \mu n)n\right] \\ &= \cos 2\pi\left\{[f_0 + \mu(n-1) + \mu](n-1+1)\right\} \\ &= \cos 2\pi\left\{[f_0 + \mu(n-1)](n-1) + f_0 + 2\mu n - \mu\right\} \\ &= \cos 2\pi\left\{[f_0 + \mu(n-1)](n-1)\right\}\cos 2\pi(f_0 + 2\mu n - \mu) \\ &\quad - \sin 2\pi\left\{[f_0 + \mu(n-1)](n-1)\right\}\sin 2\pi(f_0 + 2\mu n - \mu) \end{aligned} \tag{A.2}$$

and

$$\begin{aligned} x(n-2) &= \cos 2\pi\left\{[f_0 + \mu(n-2)](n-2)\right\} \\ &= \cos 2\pi\left\{[f_0 + \mu(n-1) - \mu)](n-1-1)\right\} \\ &= \cos 2\pi\left\{[f_0 + \mu(n-1)](n-1) - f_0 - 2\mu n + 3\mu\right\} \\ &= \cos 2\pi\left\{[f_0 + \mu(n-1)](n-1)\right\}\cos 2\pi(f_0 + 2\mu n - 3\mu) \\ &\quad + \sin 2\pi\left\{[f_0 + \mu(n-1)](n-1)\right\}\sin 2\pi(f_0 + 2\mu n - 3\mu) \end{aligned} \tag{A.3}$$

From (A.3),

$$\begin{aligned} &\sin 2\pi\left\{[f_0 + \mu(n-1)](n-1)\right\} \\ &= \frac{\cos 2\pi\left\{[f_0 + \mu(n-2)](n-2)\right\}}{\sin 2\pi(f_0 + 2\mu n - 3\mu)} \\ &\quad - \frac{\cos 2\pi\left\{[f_0 + \mu(n-1)](n-1)\right\}\cos 2\pi(f_0 + 2\mu n - 3\mu)}{\sin 2\pi(f_0 + 2\mu n - 3\mu)} \end{aligned} \tag{A.4}$$

Plugging (A.4) into (A.2),

$$
\begin{aligned}
x(n) &= \cos 2\pi\{[\, f_0 + \mu(n-1)](n-1)\} \\
&\cdot\left\{\cos 2\pi(\, f_0 + 2\mu n - \mu) + \frac{\sin 2\pi(\, f_0 + 2\mu n - \mu)\cos 2\pi(\, f_0 + 2\mu n - 3\mu)}{\sin 2\pi(\, f_0 + 2\mu n - 3\mu)}\right\} \\
&- \frac{\sin 2\pi(\, f_0 + 2\mu n - \mu)}{\sin 2\pi(\, f_0 + 2\mu n - 3\mu)}\cos 2\pi\big[(\, f_0 + \mu(n-2))(n-2)\big] \qquad , \qquad \text{(A.5)} \\
&= \frac{\sin 4\pi(\, f_0 + 2\mu n - 2\mu)}{\sin 2\pi(\, f_0 + 2\mu n - 3\mu)}\cos 2\pi\big[(\, f_0 + \mu(n-1))(n-1)\big] \\
&- \frac{\sin 2\pi(\, f_0 + 2\mu n - \mu)}{\sin 2\pi(\, f_0 + 2\mu n - 3\mu)}\cos 2\pi\big[(\, f_0 + \mu(n-2))(n-2)\big]
\end{aligned}
$$

where

$$
\begin{aligned}
c_1(n) &= -\frac{\sin 4\pi(\, f_0 + 2\mu n - 2\mu)}{\sin 2\pi(\, f_0 + 2\mu n - 3\mu)} \\
c_2(n) &= \frac{\sin 2\pi(\, f_0 + 2\mu n - \mu)}{\sin 2\pi(\, f_0 + 2\mu n - 3\mu)}
\end{aligned}
\quad . \qquad \text{(A.6)}
$$

For sufficiently small value of μ, we can have the approximations

$$
\begin{aligned}
c_1(n) &\approx -2\cos 2\pi\big[f_0 + 2\mu(n-1)\big] \\
c_2(n) &\approx 1
\end{aligned}
\quad . \qquad \text{(A.7)}
$$

Thus, $x(n)$ can be represented by the recursion as

$$
x(n) \approx 2\cos 2\pi\big[f_i(n-1)\big]x(n-1) - x(n-2)\,, \qquad \text{(A.8)}
$$

where the IF is

$$
f_i(n) = f_0 + 2\mu n\,. \qquad \text{(A.9)}
$$

A.2 Quadratic TV Frequency

The sinusoid signal with a quadratic TV frequency can be expressed as

$$\begin{aligned} x(n) &= \cos 2\pi(f_0 + \mu n^2)n \\ &= \cos 2\pi\left[f_0 + \mu(n-1+1)^2\right](n-1+1) \\ &= \cos 2\pi\left[f_0 + \mu(n-1)^2 + 2\mu(n-1) + \mu\right](n-1+1) \\ &= \cos 2\pi\left\{[f_0 + \mu(n-1)^2](n-1) + f_0 + \mu(n-1)^2 + 2\mu(n-1)n + \mu n\right\} \\ &= \cos 2\pi\left\{[f_0 + \mu(n-1)^2](n-1) + f_0 + 3\mu n^2 - 3\mu n + \mu\right\} \\ &= \cos 2\pi\left\{[f_0 + \mu(n-1)^2](n-1)\right\}\cos 2\pi(f_0 + 3\mu n^2 - 3\mu n + \mu) \\ &\quad - \sin 2\pi\left\{[f_0 + \mu(n-1)^2](n-1)\right\}\sin 2\pi(f_0 + 3\mu n^2 - 3\mu n + \mu) \end{aligned} \tag{A.10}$$

and

$$\begin{aligned} x(n-2) &= \cos 2\pi\left\{[f_0 + \mu(n-2)^2](n-2)\right\} \\ &= \cos 2\pi\left\{[f_0 + \mu(n-1-1)^2](n-1-1)\right\} \\ &= \cos 2\pi\left\{[f_0 + \mu(n-1)^2 - 2\mu(n-1) + \mu](n-1-1)\right\} \\ &= \cos 2\pi\left\{[f_0 + \mu(n-1)^2](n-1) - f_0 - \mu(n-1)^2 - 2\mu(n-1)(n-2) + \mu(n-2)\right\}. \\ &= \cos 2\pi\left\{[f_0 + \mu(n-1)^2](n-1) - f_0 - 3\mu n^2 + 9\mu n - 7\mu\right\} \\ &= \cos 2\pi\left\{[f_0 + \mu(n-1)^2](n-1)\right\}\cos 2\pi(f_0 + 3\mu n^2 - 9\mu n + 7\mu) \\ &\quad + \sin 2\pi\left\{[f_0 + \mu(n-1)^2](n-1)\right\}\sin 2\pi(f_0 + 3\mu n^2 - 9\mu n + 7\mu) \end{aligned} \tag{A.11}$$

From (A.11),

$$\begin{aligned} &\sin 2\pi\left\{[f_0 + \mu(n-1)^2](n-1)\right\} \\ &= \frac{\cos 2\pi\left\{[f_0 + \mu(n-2)^2](n-2)\right\}}{\sin 2\pi(f_0 + 3\mu n^2 - 9\mu n + 7\mu)} \\ &\quad - \frac{\cos 2\pi\left\{[f_0 + \mu(n-1)^2](n-1)\right\}\cos 2\pi(f_0 + 3\mu n^2 - 9\mu n + 7\mu)}{\sin 2\pi(f_0 + 3\mu n^2 - 9\mu n + 7\mu)} \end{aligned} \quad . \tag{A.12}$$

Plugging (A.12) into (A.10),

$$
\begin{aligned}
x(n) &= \cos 2\pi\left\{[\, f_0 + \mu(n-1)^2\,](n-1)\right\} \\
&\cdot\left\{\cos 2\pi(\, f_0 + 3\mu n^2 - 3\mu n + \mu) + \frac{\sin 2\pi(\, f_0 + 3\mu n^2 - 3\mu n + \mu)\cos 2\pi(\, f_0 + 3\mu n^2 - 9\mu n + 7\mu)}{\sin 2\pi(\, f_0 + 3\mu n^2 - 9\mu n + 7\mu)}\right\} \\
&- \frac{\sin 2\pi(\, f_0 + 3\mu n^2 - 3\mu n + \mu)}{\sin 2\pi(\, f_0 + 3\mu n^2 - 9\mu n + 7\mu)}\cos 2\pi\left\{[\, f_0 + \mu(n-2)^2\,](n-2)\right\} \\
&= \frac{\sin 4\pi(\, f_0 + 3\mu n^2 - 6\mu n + 4\mu)}{\sin 2\pi(\, f_0 + 3\mu n^2 - 9\mu n + 7\mu)}\cos 2\pi\left\{[\, f_0 + \mu(n-1)^2\,](n-1)\right\} \\
&- \frac{\sin 2\pi(\, f_0 + 3\mu n^2 - 3\mu n + \mu)}{\sin 2\pi(\, f_0 + 3\mu n^2 - 9\mu n + 7\mu)}\cos 2\pi\left\{[\, f_0 + \mu(n-2)^2\,](n-2)\right\}
\end{aligned}
\tag{A.13}
$$

For sufficiently small value of μ, we have the approximations

$$
\begin{aligned}
c_1(n) &\approx -2\cos 2\pi\left[f_0 + 3\mu(n-1)^2\right] \\
c_2(n) &\approx 1
\end{aligned}
. \tag{A.14}
$$

Thus, $x(n)$ can be represented by the recursion as

$$
x(n) \approx 2\cos 2\pi\left[f_i(n-1)\right]x(n-1) - x(n-2), \tag{A.15}
$$

where the IF is

$$
f_i(n) = f_0 + 3\mu n^2 . \tag{A.16}
$$

A.3 Periodic TV Frequency

The sinusoid signal with a periodic TV frequency can be represented as

$$
\begin{aligned}
x(n) &= \cos 2\pi\left\lfloor f_0 n - \mu_a \cos(\mu_f n)\right\rfloor \\
&= \cos 2\pi\left\{f_0(n-1+1) - \mu_a \cos[\mu_f(n-1+1)]\right\} \\
&= \cos 2\pi\left\{f_0(n-1) - \mu_a \cos[\mu_f(n-1)]\cos\mu_f + f_0 + \mu_a \sin[\mu_f(n-1)]\sin\mu_f\right\} \\
&= \cos 2\pi\left\{f_0(n-1) - \mu_a \cos[\mu_f(n-1)]\cos\mu_f\right\}\cos 2\pi\left\{f_0 + \mu_a \sin[\mu_f(n-1)]\sin\mu_f\right\} \\
&- \sin 2\pi\left\{f_0(n-1) - \mu_a \cos[\mu_f(n-1)]\cos\mu_f\right\}\sin 2\pi\left\{f_0 + \mu_a \sin[\mu_f(n-1)]\sin\mu_f\right\}
\end{aligned}
\tag{A.17}
$$

and

$$
\begin{aligned}
x(n-2) &= \cos 2\pi\{f_0(n-2) - \mu_a \cos[\mu_f (n-2)]\} \\
&= \cos 2\pi\{f_0(n-1-1) - \mu_a \cos[\mu_f (n-1-1)]\} \\
&= \cos 2\pi\{f_0(n-1) - \mu_a \cos[\mu_f (n-1)]\cos\mu_f - f_0 - \mu_a \sin[\mu_f (n-1)]\sin\mu_f\} \\
&= \cos 2\pi\{f_0(n-1) - \mu_a \cos[\mu_f (n-1)]\cos\mu_f\}\cos 2\pi\{f_0 + \mu_a \sin[\mu_f (n-1)]\sin\mu_f\} \\
&+ \sin 2\pi\{f_0(n-1) - \mu_a \cos[\mu_f (n-1)]\cos\mu_f\}\sin 2\pi\{f_0 + \mu_a \sin[\mu_f (n-1)]\sin\mu_f\}
\end{aligned}
\tag{A.18}
$$

Add (A.17) and (A.18), we get

$$
\begin{aligned}
&x(n) \\
&= 2\cos 2\pi\{f_0 + \mu_a \sin[\mu_f (n-1)]\sin\mu_f\}\cos 2\pi\{f_0(n-1) - \mu_a \cos[\mu_f (n-1)]\cos\mu_f\} - x(n-2)
\end{aligned}
\tag{A.19}
$$

For sufficiently small values of μ_a and μ_f, $\cos\mu_f \approx 1$ and $\sin\mu_f \approx \mu_f$. Thus, we have the approximations

$$
\begin{aligned}
c_1(n) &\approx -2\cos 2\pi\{f_0 + \mu_a\mu_f \sin[\mu_f (n-1)]\} \\
c_2(n) &= -1
\end{aligned}
. \tag{A.20}
$$

Thus, $x(n)$ can be represented by the recursion as

$$
x(n) \approx 2\cos 2\pi[f_i(n-1)]x(n-1) - x(n-2) \ , \tag{A.21}
$$

where the IF is

$$
f_i(n) \approx f_0 + \mu_a\mu_f \sin(\mu_f n) \, . \tag{A.22}
$$

B. A TVAR(p) process in additive white noise is equivalent to a TVARMA(p, p) process

$x(n)$ is the signal of a TVAR(p) process with the power spectral density (PSD)

$$
S_x(n, f) = \frac{1}{\left|1 + \sum_{i=1}^{p} c_i(n) e^{-j2\pi fi}\right|^2} \, . \tag{B.1}
$$

The observed signal $y(n)$ in additive white noise (AWN) is

$$y(n) = x(n) + w(n), \tag{B.2}$$

where $w(n)$ is the AWN with zero mean and variance σ_w^2.

The PSD of $y(n)$ can be calculated as

$$\begin{aligned} S_y(n, f) &= S_x(n, f) + \sigma_w^2 \\ &= \frac{1}{\left|1 + \sum_{i=1}^{p} c_i(n) e^{-j2\pi fi}\right|^2} + \sigma_w^2 \quad , \\ &= \frac{1 + \sigma_w^2 \left|1 + \sum_{i=1}^{p} c_i(n) e^{-j2\pi fi}\right|^2}{\left|1 + \sum_{i=1}^{p} c_i(n) e^{-j2\pi fi}\right|^2} \end{aligned} \tag{B.3}$$

which is actually the PSD of a TVARMA (p, p) process.

Therefore, a TVAR(p) process in AWN algebraically becomes a TVARMA(p, p) process. The coefficients in the numerator of the TVARMA transfer function depend on the PSD of the signal and noise variance.

C. A TVAR(∞) model validly represents a TVARMA(p, p) process

The transfer function of a TVARMA(p, p) process is

$$H_{ARMA}(n, z) = \frac{1 + \sum_{i=1}^{p} b_i(n) z^{-i}}{1 + \sum_{i=1}^{p} a_i(n) z^{-i}}, \tag{C.1}$$

and the transfer function of a TVAR(∞) process is

$$H_{AR}(n, z) = \frac{1}{1 + \sum_{i=1}^{\infty} c_i(n) z^{-i}}. \tag{C.2}$$

Let $H_{ARMA}(n,z) = H_{AR}(n,z)$, then

$$1+\sum_{i=1}^{\infty} c_i(n) z^{-i} = \frac{1+\sum_{i=1}^{p} a_i(n) z^{-i}}{1+\sum_{i=1}^{p} b_i(n) z^{-i}} = 1+\frac{\sum_{i=1}^{p} [a_i(n)-b_i(n)] z^{-i}}{1+\sum_{i=1}^{p} b_i(n) z^{-i}}, \tag{C.3}$$

thus

$$\sum_{i=1}^{\infty} c_i(n) z^{-i} = \frac{\sum_{i=1}^{p} [a_i(n)-b_i(n)] z^{-i}}{1+\sum_{i=1}^{p} b_i(n) z^{-i}}. \tag{C.4}$$

The parameters of the TVAR(∞) can be obtained through taking the inverse z-transform of (C.4) and solving the equation.

Take the TVARMA(1,1) process as a example, we have

$$1+\sum_{i=1}^{\infty} c_i(n) z^{-i} = \frac{1+a_1(n) z^{-1}}{1+b_1(n) z^{-1}} = 1+\frac{[a_1(n)-b_1(n)] z^{-1}}{1+b_1(n) z^{-1}}, \tag{C.5}$$

and the TVAR parameters can be obtained as

$$c_i(n) = [a_1(n)-b_1(n)][-b_1(n)]^{i-1}, i = 1,...,\infty. \tag{C.6}$$

Hence, a TVAR(∞) model validly represents a TVARMA(p, p) process.

VITA

Xiaolin Luo was born in Wuhan, Hubei, P. R. China on Nov. 5, 1975. She got her Bachelor degree from the Huazhong University of Sci. & Tech. in Wuhan, P.R. China in Jun. 1998. She came to study in the department of Electrical and Computer Engineering at the University of Tennessee, Knoxville in Aug. 2001.